UNIVERSITY OF TRENTO

DOCTORAL THESIS

Towards individualized TMS-EEG pipelines for stroke rehabilitation: the importance of individual structural and functional variability

---

Candidate:

Arianna Brancaccio

Supervisor:

Prof. Paolo Belardinelli

A thesis submitted in fulfilment of the requirements

for the degree of Doctor of Philosophy

in the

Doctorate in Cognitive and Brain Sciences

Academic Year 2022 – 2023

Declaration

I hereby declare that, the contents and organization of this dissertation constitute original work and do not compromise in any way the rights of third parties, including those relating to the security of personal data.

Arianna Brancaccio

December, 2022

Abstract

Doctorate in Cognitive and Brain Sciences

University of Trento

Doctor of Philosophy

Towards individualized TMS-EEG pipelines for stroke rehabilitation: the importance of individual structural and functional variability

Arianna Brancaccio

Stroke is the main cause of adult motor disability. Nevertheless, recent meta-analyses show that the theoretical models conceived to explain the post-stroke brain reorganization are inaccurate and therefore misleading in laying the theoretical foundation for rehabilitation protocols. Mixed results are reported especially in works investigating the excitability properties of the stroke injured brain. Shedding light on the reasons that brought to such mixed results is the central topic of this doctoral thesis. In particular, this confounding evidence is here discussed and tackled in the light of recent works employing brain-state dependent stimulation protocols. These works have been of paramount importance, as they showed that the effects of non-invasive stimulation (TMS and/or rTMS) on the hand knob of the motor cortex depend on the instantaneous sensorimotor state. This local state is largely determined by the phase of the mu-alpha oscillations, with the negative peak representing a high excitability condition. Brain-state dependent results show that controlling for the local state at the moment of stimulation is crucial in order to reduce variability in studies investigating cortical excitability: an approach that has never been employed in stroke literature, so far. In this doctoral thesis, new evidence is provided on affected and unaffected hemispheres' excitability properties

depending on the local state at the moment of stimulation. This previously uncontrolled state-dependent variability is here proposed as one of the factors at the basis of the mixed results in stroke literature. Furthermore, the current models aimed at explaining post-stroke brain reorganization do not take into account factors that recent works suggest might contribute to stroke recovery. In fact, it is here suggested that: interhemispheric inhibition should not be interpreted as competition, structural reserve should be assessed also at the level of the corpus callosum, diaschisis processes should be taken into account and structural and functional connectivity patterns should be included in patients' assessment. Finally, the excitability properties of the stroke brain have been often inferred comparing stroke patients' with young healthy controls'. In this regard, it is here proposed that only healthy peers should be included in the control groups, as brain structural changes due to healthy aging have an impact on corticospinal excitability. The aforementioned functional and structural issues are addressed in the following chapters by means of different techniques (i.e. TMS-EEG, MRI, MEG). In particular, in Chapter 1, a new framework of post-stroke brain reorganization is proposed, in which previously over-looked factors are suggested to be essential in the understanding of the potential plastic changes following stroke. Specifically, a new account where interhemispheric inhibition is interpreted in terms of integration and not competition, is supported. Moreover, the proposed framework includes recent pieces of evidence suggesting that structural reserve should be evaluated in the individual patient not only at the level of the cortex, but also in the different sections of the callosum. Finally, it is proposed that structural damage is not static, but rather dynamic as it continues also after the stroke episode through dischiasis processes. In Chapter 2, new knowledge is provided on the different excitability properties of the two hemispheres of stroke patients. In this chapter, TMS-EEG data of stimulation on both the affected and unaffected motor cortex in severe chronic strokes are analysed with a brain-state dependent approach. For the first time, it is shown that the excitability properties of the affected and unaffected hemispheres differ as the local state at the moment of stimulation influences the two hemispheres' response differently. In particular, the strong and simplified TMS-evoked response in the affected hemisphere, previously reported in severe patients,

is shown to depend on a disruption of the differentiation between the high and low excitability states of the motor cortex, determined by the instantaneous phase of alpha oscillations. This low differentiation between excitability states in the affected hemisphere should be systematically investigated, as it could be a potential feature of patients who experience poor recovery. Furthermore, in Chapter 3, connectivity at the individual alpha peak is investigated in a big cohort of healthy participants, in a resting state MEG dataset. This work was implemented because alpha connectivity networks have been shown to predict stroke recovery. For this reason, there is a necessity to reliably assess connectivity at alpha before and after rehabilitation, as this could be informative on the efficacy of rehabilitation. Specifically, it is shown that using complementary phase-coherence metrics is more effective to estimate connectivity patterns at source level. This compound approach is proposed as a tool to better control the modulatory effects of rehabilitation stimulation protocols, in order to identify which are the changes in activity patterns that are potentially responsible for recovery. Finally, in Chapter 4 brain structural changes associated with healthy aging are investigated in a big cohort of participants aged between 18 and 90 years old, both in terms of cortical thinning and cortical myelin concentration loss. In particular, given recent evidence on the relationship between cortical myelin content and corticospinal excitability, it is shown that age-dependent myelin loss occurs mostly at the level of the premotor, motor and sensory cortices. These structural changes need to be taken into account when stroke patients are compared with controls. In fact, since stroke patients are often in their elderly, these age-related structural changes need to be controlled by including only age-matched healthy participants in control groups, as this is not often a fulfilled criterion in stroke studies. To conclude, this doctoral thesis proposes that the current models' inaccuracy depends on **1**) patients' individual structural and functional factors that have not been taken into account in previous models of brain reorganization post-stroke (Chapter 1), **2**) brain-state dependent variability in stimulation effects that have not been controlled for in stroke literature (Chapter 2), **3**) a lack of a systematic method to assess the effects of stimulation rehabilitation protocols (Chapter 3) and **4**) structural brain changes due to healthy aging, that affect also the stroke brain, and that are not taken into account

when patients are compared with young controls in corticospinal excitability studies (Chapter 4). To the author's knowledge, this is the first work aimed at explaining mixed results in stroke literature from different perspectives and using different neuroimaging techniques for functional and structural anomalies, exploiting recent brain-state dependent approaches for the analysis of stroke patients' data.

Contents

Introduction

"Another error... is a conceit that of former opinions or sects, after variety and examination, the best hath still prevailed and suppressed the rest"

Francis Bacon, The Advancement Of Learning

Stroke is the second most common cause of death in developed countries and still represents one of the principal causes of adult motor disability, with its incidence having increased in recent years (Dobkin, 2005; Mergenthaler and Meisel, 2012;). The impact that this condition has on patients' lives is huge, given that more than half of the patients who experienced a stroke still show motor impairment after 3-6 months after the stroke episode (Dionisio et al., 2018). Despite the seriousness of this scenario, it remains very difficult to predict the goodness of recovery and the most certain notion in stroke rehabilitation remains that, especially in the acute and sub-acute stages, systematic motor physiotherapy predicts a better prognosis (Maulden et al., 2005; Horn et al., 2005). Nevertheless, standard physiotherapy practices have some limitations, with acute and subacute patients being unable to be involved in long physiotherapy sessions and also because, even when recovered in stroke units to receive rehabilitation treatment, stroke patients use their affected limbs less compared to healthy peers (Lang et al., 2007; Lang et al., 2009). Furthermore, even if patients in the chronic stage seem to benefit from physiotherapy too, the first months following stroke are crucial in terms of rehabilitation efficacy, and chronic patients tend to have less margin in terms of motor recovery (Ferrarello et al., 2009). For these reasons, alternative methods have been proposed to accomplish patients' motor assessment and rehabilitation. Among them, transcranial magnetic stimulation (TMS) and repetitive transcranial magnetic stimulation (rTMS) have been respectively proposed for motor assessment and rehabilitation purposes (Dionisio et al., 2018). This technique

makes use of a coil generating a magnetic field that, when placed on the scalp, can depolarize the superficial axons, inducing excitability changes in the cortex. While single pulse TMS is generally used to investigate the role of a given cortical area in a task or to assess corticospinal excitability when applied on the motor cortex, rTMS is thought to produce long-lasting changes in brain activity and therefore to induce plasticity (Klomjai et al., 2016; Thut et al., 2003). For example, when applied on the motor cortex, supratreshold single pulse TMS is used to induce descending volleys in the corticospinal tract eliciting the so called motor evoked potentials (MEPs) on the electromyography (EMG) electrodes applied on the hand contralateral to stimulation. In this way, single pulse TMS has been used to assess the state of potential disruption of the corticospinal tract (Klomjai et al., 2015). As for the repetitive TMS protocols instead, these are generally used in either the low-frequency (e.g. 1 Hz) or high-frequency (e.g. 10 Hz) forms in order to modulate cortical activity for a prolonged period of time after stimulation. For example, low-frequency and high-frequency rTMS can be applied on the motor cortex in order to produce, respectively, a long-lasting decrease or increase in the amplitude of MEPs later tested with single pulse TMS (Lefacheur et al., 2014). Given the non-invasive nature of these techniques and the relative ease with which these can be used on stroke patients, TMS has been used to assess the levels of disruption of the corticospinal tract in stroke patients, while rTMS' neuromodulatory properties have been exploited for rehabilitation purposes to induce plastic changes in the stroke brain (McDonnell and Stinear., 2017).

It is necessary to describe at this point which are the models of stroke brain reorganization that have inspired the different rTMS protocols so far used with the attempt to rehabilitate the patients. In fact, rTMS rehabilitation protocols change depending on the assumptions on the plastic properties of the stroke brain. The main two models of brain reorganization after stroke are *the interhemispheric competition model* and *the vicariation model* (Murase et al., 2004; Johansen-Berg et al., 2002). These two models differ in particular in the way they interpret the role of the contralesional hemisphere in stroke patients. While the interhemispheric competition model predicts that, after a stroke episode, the contralesional hemisphere exerts excessive inhibition over the ipsilesional hemisphere, preventing

it from recovering its functions, the vicariation model instead proposes that the over-activation of the contralesional hemisphere reflects vicarious contribution and support to the ipsilesional hemisphere. For an extensive review on this matter, the reader is invited to peruse chapter 1 of this thesis, consisting in a published review highlighting some of the mixed results in stroke literature that have possibly laid the foundations for the incorrect assumptions at the basis of the aforementioned models (Brancaccio et al., 2022).

Before proceeding with the introduction to each chapter of this thesis, it is necessary to state that currently there is no certainty on the efficacy of rehabilitation protocol for stroke patients and that this might depend on the aforementioned mixed results in stroke literature. This inconsistency has in fact influenced the theoretical assumptions at the basis of the *interhemispheric competition* and *vicariation* model. Therefore, the aim of this doctoral thesis is to highlight the presence of these mixed results, stressing their role in having wrongly informed the theoretical models of stroke brain reorganization. Furthermore, a new theoretical model of brain reorganization after stroke is proposed, where new factors are suggested to be relevant for stroke patients' assessment (chapter 1). Moreover, three studies are also presented that aim at proposing new functional and structural aspects that should be taken into account to evaluate the efficacy of rehabilitation stimulation protocols (chapter 2 and 3) and the potential recovery margin of an individual patient (chapter 4).

Specifically, the review presented in chapter 1 makes use of recent meta-analyses results showing the inefficacy of the rehabilitation stimulation protocols inspired by the *interhemispheric competition* and *vicariation* models (e.g. McDonnell and Stinear, 2017). The inefficacy of these protocols in rehabilitating stroke patients can be ascribed both to the mixed results in stroke TMS literature and to the fact that these models do not take into account some factors that should be considered in patients' assessment. As for the mixed results, McDonnell and Stinear (2017) highlight that, from the studies investigating interhemispheric inhibition (IHI) in strokes, no significant differences between the affected and unaffected hemispheres emerge when paired-pulse TMS

protocols are used to assess maladaptive interhemispheric imbalance. In this regard, paired-pulse studies are usually exploited to assess IHI by eliciting a so-called sub-threshold conditioning stimulus (CS) on one hemisphere and an above threshold test stimulus (TS) on the contralateral one. The activity elicited in the first hemisphere by the application of CS is thought to inhibit the contralateral one. This is because, when the TS is released on the hemisphere contralateral to the one receiving the CS, the MEPs are inhibited compared to the MEPs elicited by the TS alone. In some stroke studies, IHI from the contralesional hemisphere seems to elicit stronger IHI towards the ipsilesional one than viceversa and this has been interpreted in terms of interhemispheric imbalance (e.g. Duque et al., 2005). However, like McDonnell and Stinear (2019) point out in their meta-analysis, when considering stroke studies together, no real effect emerges in terms of different interhemispheric inhibitory properties between the two hemispheres in stroke patients. This result suggests that the assumption at the basis of the interhemispheric competition model of a stronger inhibition exerted by the unaffected hemisphere over the ipsilesional one is at the least incomplete. Moreover, these meta-analyses' results on the excitability properties of the two hemispheres in stroke patients, suggest that there is no clear evidence for a hyper-excitability of the contralesional hemisphere compared to the ipsilesional one. This means that the mixed results in stroke literature not only laid the foundation for wrong assumptions at the basis of the interhemispheric competition model, but also that the vicariation model might be incomplete. In fact, the vicariation model also assumes a hyper-excitability of the contralesional hemisphere which has been questioned as general feature of the stroke brain (McDonnell and Stinear, 2017). Finally, it is also important to stress that not only the work by McDonnell and Stinear has pointed at the mixed results in stroke literature, but that also previous meta-analyses have highlighted the mixed results on the efficacy of stimulation rehabilitation protocols currently used to rehabilitate patients. These protocols, exploiting mainly rTMS in either its low-frequency (inhibitory) or high-frequency (excitatory) application, are inspired either by the *interhemispheric competition* or the *vicariation* model, whose incorrect general assumptions explain the variability in their efficacy (e.g. McDonnell and Stinear, 2017; Klomjai et

al., 2015). Protocols inspired by the *interhemispheric competition* model generally aim at exciting the ipsilesional hemisphere and, most frequently, inhibiting the contralesional one. This, with the aim to "rebalance" the brain in terms of inhibitory interhemispheric properties. On the other hand, protocols inspired by the *vicariation* model aim at facilitating both the ipsilesional and contralesional hemisphere (Brancaccio et al., 2022).

The incorrect assumptions at the basis of the *interhemispheric competition* and *vicariation* model cannot only be ascribed to the mixed results in stroke literature. In fact, even though these mixed results have contributed to confusion in the interpretation of plastic processes after a stroke episode, it is here proposed that also other factors, that have not been considered before in stroke patients, should be taken into account in order to fully understand the plastic brain changes following a stroke episode. In the review presented in Chapter 1, some of these factors are proposed. In fact, in Brancaccio et al (2022), it is suggested that: 1. interhemispheric inhibitory processes are not to be necessarily interpreted as competition, but that inhibition as well can underlie integration (see Carson, 2020 for an extensive review), 2. the structural reserve needs to be evaluated not only at the level of the cortex, but also at the level of the callosum, 3. post-stroke diaschisis mechanisms need to be taken into account when evaluating stroke patients' reserve, 4. the role of the prefrontal cortex (PFC) in exerting high-level control in motor implementation needs to be evaluated individually. While the reader is invited to read chapter 1 for an extensive discussion on the matter, it is worth it to just mention here the reasons at the basis of these proposals. As for the first point, regarding the inhibition not to be considered in terms of competition, a recent work by Carson (2020) provides evidence in this direction. These pieces of evidence show that both excitation and inhibition are exploited by the brain to afford interhemispheric integration of both hemisphere's contributions to a given function. This mechanism is accomplished via "crossed surround inhibition", which involves both inhibitory and excitatory interhemispheric inputs, and is expressed by specular activations showing an excitatory centre and an inhibitory periphery aimed at focusing and amplifying the excited centre (Carson, 2020). This new interpretation of interhemispheric integration explains results in stroke patients

regarding the relationship between their recovery level and the callosal structural reserve. This is linked to the second factor proposed in Chapter 1 regarding the role of the callosum in stroke patients. In fact, different pieces of evidence support the view that the affected and unaffected hemispheres continuously contribute to behavioural outputs, showing an integration that appears to be fundamental especially in stroke patients (Carson, 2020). For example, it has been found that stroke patients show a negative relationship between the structural integrity of the callosum and their motor impairment (Dewanjee et al., 2015; Stewart et al., 2017; Chen et al., 2013; Hayward et al., 2017;). This suggests that the corpus callosum supports adaptive integration between the stroke patients' affected and unaffected hemispheres. In fact, if the interhemispheric competition model were correct, the opposite relation should have been found, where the less the integrity in the callosum, the better the motor function (Carson, 2020). This is because the corpus callosum constitutes the main pathway through which the two hemispheres communicate and therefore the main pathway through which the contralesional over-inhibition could have been exerted. Therefore, these findings contradicting the interhemispheric competition assumption strongly suggest that, again, this model needs revision and that the callosal integrity is a factor that needs to be considered when evaluating stroke patients.

As for the third factor proposed in the review paper presented in chapter 1, this consists in diaschisis mechanisms. In this regard, a recent work by Cheng and colleagues (2020) shows that, in stroke patients, sections of the callosum connected to the lesioned site in the ipsilesional hemisphere tend to degenerate much faster compared to the callosal sections not connected to the lesion. As shown in their work, this callosal degeneration in turns lead to structural damage also in contralesional areas homotopic to the lesioned site. Again, none of the previously mentioned models of brain reorganization after stroke takes into account the dynamic nature of the stroke brain also in terms of structural damage.

Finally, regarding the fourth factor, the functional role of PFC should be considered both to interpret differences with healthy controls in motor implementation and to understand stroke possible plastic reorganization outcomes. To mention an example on the importance of PFC in stroke patients,

a work by Sharma and colleagues (2009) found that minimally affected stroke patients show an increase in connectivity between the PFC and sensorimotor sector of the ipsilesional hemisphere compared to age-matched controls, suggesting that, just like in the elderly, an increase in communication between these sectors might have a compensatory role (Sharma et al., 2009; Michely et al., 2018). All the pieces of evidence in favour of a need to consider the aforementioned factors in stroke assessment will be discussed in detail in the work presented in Chapter 1, where the need for a revision of previous models emerges.

Nevertheless, in this thesis it is further proposed that taking into account the factors discussed in Chapter 1 may still be not sufficient to lay the foundation for correct assumptions at the basis of new brain models of the stroke brain. In fact, including the aforementioned new factors would only partially be of help, if other sources of variability in the results are not controlled for. In order to afford a more complete understanding of the stroke brain, future studies will need to control for factors that in previous literature have not been considered and that have led to more variability in the results, contributing to the mixed results in the literature.

Therefore, Chapters 2, 3 and 4 will be focused on which further factors should be taken into account in order to 1) better control the results' variability in TMS studies on stroke patients (Chapter 2); 2) better understand the neuromodulatory effects of rTMS protocols in healthy controls and stroke patients (Chapter 3); 3) control for age-related structural changes that affect stroke patients and that might have an impact on their margin of recovery and comparison with controls (Chapter 4).

Specifically, in chapter 2, the results of stroke TMS-EEG data analysed with a brain state-dependent approach are presented. Brain state-dependent literature has shown, in the very recent years, that the brain response to TMS stimulation changes depending on the brain-state at the moment of stimulation. In particular, with respect to brain-state dependent results of TMS stimulation in sensorimotor areas, it has been found that the phase of the mu alpha sensorimotor rhythm opens and closes windows of different motor cortex excitability. For example, Zrenner and colleagues (2018)

found that MEPs are larger in amplitude when the TMS pulse, applied on the motor cortex, is released at the trough of the sensory mu alpha rhythm, while they are smaller when the pulse is released at the positive peak. Therefore, the authors proposed that the trough of alpha oscillations constitutes a state of higher excitability of the motor cortex. Also the effects of rTMS stimulation have been investigated with a brain state-dependent approach, showing that the modulatory effects of rTMS protocols change depending on the phase of alpha at which the stimulation has occurred. For example, Baur et al (2019) have found that low frequency rTMS, previously thought to be only inhibitory, induces facilitatory modulation when it is systematically released over the motor cortex at the trough of the mu alpha sensory rhythm, while it induces a inhibitory effect when applied at the positive peak, demonstrating that by controlling for the phase, the variability in the effects of low frequency rTMS can be reduced. At the same time, Zrenner and colleagues (2018) have found that systematically applying high frequency rTMS in the motor cortex at the trough of the sensory mu alpha rhythm induces long-term potentiation, expressed in long-lasting larger MEPs amplitude, as compared with stimulation applied at the positive peak. Furthermore, high-frequency rTMS over the left dorsolateral prefrontal cortex (DLPFC) of patients with antidepressant-resistant depression has been found to induce long-term reduction in resting-state alpha activity in left DLPFC and increased TMS-induced beta oscillations only when consistently applied at the trough of the mu alpha rhythm, but not when applied at the random phase (Zrenner et al., 2020). Finally, it has been also shown that, depending on the phase of mu alpha at which the stimulation occurs, also the amplitude of TMS-evoked potentials (TEPs) recorded on the scalp change (Desideri et al., 2019). These findings explain why the effects of rTMS protocols are not as predictable as it would be expected: the mixed results in healthy subjects' rTMS studies can be explained by the fact that previous works have not taken into account the distribution of the phases at which the stimulation has fallen in each experimental session. At this point, the logic behind the study presented in chapter 2 is clear: given that the effect of the phase of the mu alpha rhythm accounts for some of the variability in the results of healthy studies, this factor needs to be taken into account also in stroke studies in order to reduce the mixed results in the literature. This

approach has never been attempted before in stroke patients, for which the only work in this direction purely focused on assessing whether alpha phase-targeting is possible in the affected hemisphere of stroke patients (Hussain et al., 2020). For these reasons, in Chapter 2, we investigate the effects of single pulse TMS on the M1 of both the affected and unaffected hemisphere separately, comparing the two hemispheres in TEPs, inter-trial phase coherence (ITC), time-frequency (TF) and post-pulse interhemispheric connectivity when the stimulation has happened at different phase states of the mu alpha sensorimotor oscillations. Our results show the different excitability properties of the affected and unaffected hemisphere, which react in different ways at the same phase state stimulation, showing differences in terms of excitability, latency and propagation properties. In particular, a lower differentiation between the high and low excitability states of the cortex is found in the affected hemisphere, which is suggested to be a potential feature at the basis of poor recovery. Therefore, the results presented in Chapter 2 suggest that brain-state dependent approaches need to be employed in stroke patients studies in order to understand how the stroke brain changes in terms of excitability properties with respect to controls. These results on the different excitability properties of the stroke brain also suggest that the effect of the mu alpha phase needs to be taken into account when evaluating the effects of rTMS stimulation protocols in strokes.

The effects of rTMS protocols, whether inhibitory or excitatory, need to be controlled in order to 1) understand their potential modulatory effects and 2) the reasons why in some cases they appear effective in stroke patients' motor rehabilitation and in others do not (e.g. Ovadia-Caro et al., 2019; Meidian et al., 2020; Salazar et al., 2018; Veldema et al., 2020; Olgiati et al., 2020). In this regard, a part from the need of controlling for the phase at which the stimulation falls (the local brain state), it is here proposed that a reliable way to predict and then to assess the modulatory effects of rTMS protocols would be to investigate how resting state connectivity patterns look before the application of the protocols and then how they get modulated by rTMS. The prediction of rTMS protocols' modulatory effects should in fact depend on the connectivity patterns observed at rest, as regions more strongly coherent with each other should also be modulated in coherence more compared to

regions that do not show strong connectivity. In fact, if the communication through coherence is correct (Fries et al., 2015), we expect that regions that show high coherence, will also be modulated in their "relationship" if one of them is targeted with rTMS. Therefore, assessing the patients' connectivity patterns before the application of rTMS might allow clinicians to predict which regions will be more strongly influenced by the protocol, depending on the target of stimulation. Moreover, comparing connectivity between pre- and post-stimulation measures would help confirm or disconfirm this prediction. In particular, the alpha frequency seems to be fundamental in terms of connectivity in stroke patients. In fact, resting state connectivity in this frequency seems to correlate with performance in motor and non-motor tasks (Westlake at al., 2012; Dubovik et al., 2012; Dubovik et al., 2013). Therefore, understanding how these connectivity patterns get modulated by rTMS protocols in the individual patient becomes essential to understand the potential beneficial effects of rehabilitation protocols. For this reason, in Chapter 3, we propose that a good measure of connectivity patterns in alpha should exploit complementary connectivity metrics. In particular, we show that the weighted pairwise phase consistency (WPPC) and weighted phase lag index (WPLI) can be used together to efficiently assess connectivity patterns in alpha at rest and control for potential spurious correlations in the results. In fact, these two connectivity metrics are complementary in their properties, since, when used to measure connectivity in the alpha frequency, the WPPC has a stronger sensitivity, compared to WPLI, allowing the assessment of stronger/weaker connectivity patterns between brain regions. However, the WPPC metric is still affected by spurious correlations for which it does not control for. Instead, the WPLI weights the cross-spectrum based on the magnitude of the imaginary part of the coherency, limiting the effects of artificial zero-lag correlations (Tabarelli et al., 2022). In the work proposed in Chapter 3, these two complementary metrics were exploited to assess connectivity at the individual alpha frequency (IAF) of 203 healthy controls, showing that making use of both metrics allows for a reliable assessment of connectivity patterns in alpha at rest. Connectivity was estimated at the source level using a Minimum Norm approach. This approach was chosen in order to be conservative with respect to potential cancelling effects arising from distant

strongly interacting sources. Indeed, beamformers can perform poorly in estimating coherence, especially when two or more distant sources are strongly coherent (Hincapié et al., 2017; Van Veen et al., 1997). The combination of connectivity metrics employed in Chapter 3 could be applied also to investigate connectivity patterns at rest in the stroke brain. In fact, since most of the available data in stroke patients are acquired with electroencephalography (EEG), whose inverse solution is more subjected to distortions due to the different conductivity properties of the damaged tissues, the combination of two connectivity metrics, where one of the two corrects for spurious correlations, is essential in order to assess connectivity patterns in a reliable way. In this way, resting state EEG data acquired in stroke patients before and after the applications of rTMS protocols would allow for the assessment of the modulatory effects of rTMS.

Finally, in chapter 4, we propose another factor that should be considered when evaluating stroke patients in corticospinal excitability studies. In this regard, it has been recently shown that myelin has an effect on corticospinal excitability. For example, Kwon et al (2020) found that sensorimotor myelin content correlates with participants' performance in an eye-hand coordination motor task. Furthermore, cortical myelin content and corticospinal tract integrity have been shown to correlate with MEPs latency (Dubbioso et al., 2021; Betti et al., 2022). Given that stroke patients are usually in their elderly, it stands to reason that, apart from being affected by the stroke lesion, they also suffer from normal age-related brain structural changes, which include degeneration of cortical myelin content. In this regard, only a few studies have investigated how the aging process impacts on the myeloarchitectonic properties of the cortex and most of them have not investigated how this process evolves over the entire life-span. In fact, most of these studies have explored age-related changes in cortical myelin content only up to childhood, young adolescence or young adulthood (Deoni et al., 2015; Kwon et al., 2020; Shafee et al., 2015). Only few studies investigated age-related myelin changes in later stages of life, in limited cohorts of healthy participants, with age groups of uncomparable sample sizes, showing processes of age-related myelin degeneration (Grydeland et al., 2013; Wu et al., 2016; Karolis et al., 2019). This limited information available on brain structural

changes over the entire life-span was the reason at the basis of the study presented in Chapter 4. In this section, analyses on the age-related cortical thickness and cortical myelin content changes are implemented on a big cohort of healthy participants (N = 608) aged between 18 up to 89 years old for which T1-weighted, T2-weighted and magnetization transfer (MT) sequences were available. In particular, cortical myelin content was assessed with both T1/T2 ratio and magnetization transfer ratio (MTR). Apart from showing the higher reliability of the MTR compared to the T1/T2 ratio, our results show that the healthy brain undergoes important age-related changes in terms of cortical myelin content that especially affect sensory and motor areas in different ways, showing a dissociation between these regions that was previously reported only in works investigating the micro-level laminar features of the cortex (Wagstyl et al., 2020). This evidence suggests that stroke patients should also be assessed in terms of cortical myelin content, given that, being in their elderly, they will also show different extent of myelin degeneration. Therefore, given that myelin content impacts on corticospinal excitability, stroke patients' assessment should include cortical myelin content measures, as assessed with the more reliable MTR proxy, in order to potentially improve the prediction of recovery.

In conclusion, it is proposed that new factors should be considered when evaluating a stroke patient, in terms of assessment, definition of an individualized rehabilitation protocol and prognosis. In Chapter 1, the interhemispheric competition and vicariation model are criticized given the recent evidence on the mixed results present in stroke literature, that wrongfully constitute the basis of the two models' theoretical assumptions. Furthermore, it is suggested that a complete model of brain reorganization after stroke should take into account not only the structural reserve of the cortex, but also the callosal integrity and potential diaschisis following the stroke, together with the individual connectivity patterns with respect to controls. In Chapters 2 and 3 the focus goes to two functional factors that should further be considered in order to predict the excitability properties of the stroke brain and its reaction to modulatory rTMS protocols.

In particular, in Chapter 2, brain state-dependent approaches are proposed to be useful to 1) control variability and avoid mixed results and 2) understand the stroke brain plastic reorganization. In fact, brain state-dependent TMS assessment should be used to evaluate how the excitability properties of the two hemispheres change with respect to controls. In this scenario, the results presented in the second chapter show that stroke patients deviate from controls as the affected and unaffected hemispheres react differently depending on the brain state at the moment of stimulation. The proposal is that, once this assessment of brain-state dependent excitability is accomplished, rTMS protocols aimed at rehabilitation should be developed on the basis of the individual excitability properties of the two hemispheres. However, coming up with a theoretically well formulated rTMS protocol is not enough to understand if and why this has been effective in patient's rehabilitation. Therefore, in Chapter 3, it is proposed that to further assess the mechanisms behind a potential efficacy of rTMS protocols in stroke patients, it is necessary to 1) predict which regions can potentially be modulated in terms of coherence by the applied protocol and 2) confirm/disconfirm this prediction by assessing connectivity patterns changes before and after the application of these protocols. For this purpose, a combination of two connectivity metrics is proposed to be necessary in order to efficiently assess connectivity patterns at rest before the application of the protocols. The combined connectivity analysis is in Chapter 3 used to assess connectivity patterns at rest at the IAF of healthy participants, showing that the combination of the two connectivity metrics is reliable in assessing connectivity in the alpha band. The reason why these metrics were tested in their reliability to assess connectivity in alpha at rest lies in the fact that, as previously anticipated in the introduction to Chapter 3, alpha connectivity patterns at rest are predictive of stroke patients' performance in motor tasks.

Finally, in Chapter 4, the reader is invited to consider stroke patients not only as affected by the stroke lesion, but also by healthy age-related changes in brain structure. The results in Chapter 4 in fact show that the aging process not only impacts on cortical thickness but, most importantly, on cortical myelin content. In this regard, cortical myelin has an effect on corticospinal excitability and

it should be therefore assessed individually in both hemispheres in order to efficiently predict recovery (Betti et al., 2022; Dubbioso et al., 2021).

This thesis constitutes a work in which new factors for patients' assessment and prognosis are proposed. Given the difficulties that clinicians meet when assessing a patient and predicting their prognosis (Stinear, 2010), it is proposed here that the factors considered should be more and more assessed individually. Importantly, future works should show the applicability of normative data approaches to stroke patients' assessment and rehabilitation, using individual information from the patient, the factors investigated in this dissertation, to be compared with standard healthy peers' information. This would ease the primary care physicians' task in patients' assessment, rehabilitation protocols' choice and prognosis by providing clinicians with tools that take into account the patients' individual information. This should include 1) EEG measures for connectivity assessment before and after the application of rTMS protocols, 2) brain-state dependent results on the excitability of the individual patient's affected and unaffected hemispheres and 3) structural MRI images from different sequences (for both cortical and callosal integrity and cortical myelin content assessment). In the course of this thesis, these factors will be shown to be essential in understanding the individual brain reorganization after the stroke. Only by moving in this direction of individualization and personalization of the assessment and treatment, physicians will be provided with an efficient tool to define for each patient individualized standards of care and, therefore, effective personalized rehabilitation protocols.

Notes:

Bibliography

1. Baur, D.; Galevska, D.; Hussain, S.; Cohen, L.G.; Ziemann, U.; Zrenner, C. Induction of LTD-like corticospinal plasticity by low-frequency rTMS depends on pre-stimulus phase of sensorimotor μ-rhythm. *Brain Stimul.* **2020**, *13*, 1580–1587.

2. Betti, S., Fedele, M., Castiello, U., Sartori, L., & Budisavljević, S. (2022). Corticospinal excitability and conductivity are related to the anatomy of the corticospinal tract. *Brain Structure and Function*, *227*(3), 1155-1164.

3. Brancaccio, A., Tabarelli, D., & Belardinelli, P. (2022). A new framework to interpret individual interhemispheric compensatory communication after stroke. *Journal of Personalized Medicine*, *12*(1), 59.

4. Carson, R.G. Interhemispheric inhibition sculpts the output of neural circuits by co-opting the two cerebral hemispheres. *J. Physiol.* **2020**, *598*, 4781–4802.

5. Chen, J.L.; Schlaug, G. Resting State Interhemispheric Motor Connectivity and White Matter Integrity Correlate with Motor Impairment in Chronic Stroke. *Front. Neurol.* **2013**, *4*, 178.

6. Cheng, B.; Dietzmann, P.; Schulz, R.; Boenstrup, M.; Krawinkel, L.; Fiehler, J.; Gerloff, C.; Thomalla, G. Cortical atrophy and transcallosal diaschisis following isolated subcortical stroke. *Br. J. Pharmacol.* **2020**, *40*, 611–621.

8. Deoni, S. C., Dean III, D. C., Remer, J., Dirks, H., & O'Muircheartaigh, J. (2015). Cortical maturation and myelination in healthy toddlers and young children. *Neuroimage*, *115*, 147-161.

9. Desideri, D., Zrenner, C., Gordon, P. C., Ziemann, U., & Belardinelli, P. (2018). Nil effects of μ-rhythm phase-dependent burst-rTMS on cortical excitability in humans: A resting-state EEG and TMS-EEG study. *PLoS One*, *13*(12), e0208747.

10. Dewanjee, P.; Tran, G.; Stewart, J.C.; Quinlan, E.B.; Dodakian, L.; McKenzie, A.; See, J.; Cramer, S.C. Structural Integrity of the Corpus Callosum Correlates with Sensorimotor Impairment after Stroke. *Stroke* **2015**, *46* (Suppl. 1), A2.

11. Dionisio, A., Duarte, I. C., Patricio, M., & Castelo-Branco, M. (2018). The use of repetitive transcranial magnetic stimulation for stroke rehabilitation: a systematic review. *Journal of Stroke and Cerebrovascular Diseases*, *27*(1), 1-31.

12. Dobkin, B.H. Rehabilitation after stroke. *N. Engl. J. Med.* **2005**, *352*, 1677–1684.

13. Dubbioso, R., Madsen, K. H., Thielscher, A., & Siebner, H. R. (2021). The myelin content of the human precentral hand knob reflects interindividual differences in manual motor control at the physiological and behavioral level. Journal of Neuroscience, 41(14), 3163-3179.

14. Dubovik, S., Pignat, J. M., Ptak, R., Aboulafia, T., Allet, L., Gillabert, N., ... & Guggisberg, A. G. (2012). The behavioral significance of coherent resting-state oscillations after stroke. *Neuroimage*, *61*(1), 249-257.

15. Dubovik, S., Ptak, R., Aboulafia, T., Magnin, C., Gillabert, N., Allet, L., ... & Guggisberg, A. G. (2013). EEG alpha band synchrony predicts cognitive and motor performance in patients with ischemic stroke. *Behavioural Neurology*, *26*(3), 187-189.

16. Ferrarello, F., Baccini, M., Rinaldi, L. A., Cavallini, M. C., Mossello, E., Masotti, G., ... & Di Bari, M. (2011). Efficacy of physiotherapy interventions late after stroke: a meta-analysis. *Journal of Neurology, Neurosurgery & Psychiatry*, *82*(2), 136-143.

17. Fries, P. (2015). Rhythms for cognition: communication through coherence. *Neuron*, *88*(1), 220-235.

18. Grydeland, H., Walhovd, K. B., Tamnes, C. K., Westlye, L. T., & Fjell, A. M. (2013). Intracortical myelin links with performance variability across the human lifespan: results from T1-and T2-weighted MRI myelin mapping and diffusion tensor imaging. Journal of Neuroscience, 33(47), 18618-18630.

19. Hayward, K.S.; Neva, J.; Mang, C.S.; Peters, S.; Wadden, K.P.; Ferris, J.K.; Boyd, L.A. Interhemispheric Pathways Are Important for Motor Outcome in Individuals with Chronic and Severe Upper Limb Impairment Post Stroke. *Neural Plast.* **2017**, *2017*, 1–12.

20. Hincapie, A. S., Kujala, J., Mattout, J., Pascarella, A., Daligault, S., Delpuech, C., ... & Jerbi, K. (2017). The impact of MEG source reconstruction method on source-space connectivity estimation: a comparison between minimum-norm solution and beamforming. Neuroimage, 156, 29-42.

21. Horn, S. D., DeJong, G., Smout, R. J., Gassaway, J., James, R., & Conroy, B. (2005). Stroke rehabilitation patients, practice, and outcomes: is earlier and more aggressive therapy better?. *Archives of physical medicine and rehabilitation*, *86*(12), 101-114.

22. Hussain, S. J., Hayward, W., Fourcand, F., Zrenner, C., Ziemann, U., Buch, E. R., ... & Cohen, L. G. (2020). Phase-dependent transcranial magnetic stimulation of the lesioned hemisphere is accurate after stroke. *Brain Stimulation: Basic, Translational, and Clinical Research in Neuromodulation*, *13*(5), 1354-1357.

23. Johansen-Berg, H.; Rushworth, M.; Bogdanovic, M.D.; Kischka, U.; Wimalaratna, S.; Matthews, P.M. The role of ipsilateral premotor cortex in hand movement after stroke. *Proc. Natl. Acad. Sci. USA* **2002**, *99*, 14518–14523.

24. Karolis, V. R., Callaghan, M. F., Tseng, C. E. J., Hope, T., Weiskopf, N., Rees, G., & Cappelletti, M. (2019). Spatial gradients of healthy aging: a study of myelin-sensitive maps. *Neurobiology of Aging*, *79*, 83-92.

25. Klomjai, W., Katz, R., & Lackmy-Vallée, A. (2015). Basic principles of transcranial magnetic stimulation (TMS) and repetitive TMS (rTMS). *Annals of physical and rehabilitation medicine*, *58*(4), 208-213.

26. Klomjai, W.; Lackmy-Vallée, A.; Roche, N.; Pradat-Diehl, P.; Marchand-Pauvert, V.; Katz, R. Repetitive transcranial magnetic stimulation and transcranial direct current stimulation in motor rehabilitation after stroke: An update. *Ann. Phys. Rehabil. Med.* **2015**, *58*, 220–224.

27. Kwon, D., Pfefferbaum, A., Sullivan, E. V., & Pohl, K. M. (2020). Regional growth trajectories of cortical myelination in adolescents and young adults: longitudinal validation and functional correlates. *Brain imaging and behavior*, *14*(1), 242-266.

28. Lang, C. E., MacDonald, J. R., Reisman, D. S., Boyd, L., Kimberley, T. J., Schindler-Ivens, S. M., ... & Scheets, P. L. (2009). Observation of amounts of movement practice provided during stroke rehabilitation. *Archives of physical medicine and rehabilitation*, *90*(10), 1692-1698.

29. Lang, C. E., Wagner, J. M., Edwards, D. F., & Dromerick, A. W. (2007). Upper extremity use in people with hemiparesis in the first few weeks after stroke. *Journal of Neurologic Physical Therapy*, *31*(2), 56-63.

30. Lefaucheur, J. P., André-Obadia, N., Antal, A., Ayache, S. S., Baeken, C., Benninger, D. H., ... & Garcia-Larrea, L. (2014). Evidence-based guidelines on the therapeutic use of repetitive transcranial magnetic stimulation (rTMS). *Clinical Neurophysiology*, *125*(11), 2150-2206.

31. Maulden, S. A., Gassaway, J., Horn, S. D., Smout, R. J., & DeJong, G. (2005). Timing of initiation of rehabilitation after stroke. Archives of physical medicine and rehabilitation, 86(12), 34-40.

32. McDonnell, M.N.; Stinear, C.M. TMS measures of motor cortex function after stroke: A meta-analysis. *Brain Stimul.* **2017**, *10*, 721–734.

33. Meidian, A.C.; Wahyuddin; Amimoto, K. Rehabilitation interventions of unilateral spatial neglect based on the functional outcome measure: A systematic review and meta-analysis. *Neuropsychol. Rehabil.* **2020**, 1–30.

34. Mergenthaler, P., & Meisel, A. (2012). Do stroke models model stroke?. *Disease models & mechanisms*, *5*(6), 718-725.

35. Michely, J.; Volz, L.; Hoffstaedter, F.; Tittgemeyer, M.; Eickhoff, S.; Fink, G.; Grefkes, C. Network connectivity of motor control in the ageing brain. *NeuroImage Clin.* **2018**, *18*, 443–455.

36. Murase, N., Duque, J., Mazzocchio, R., & Cohen, L. G. (2004). Influence of interhemispheric interactions on motor function in chronic stroke. Annals of Neurology: Official Journal of the American Neurological Association and the Child Neurology Society, 55(3), 400-409.

37. Olgiati, E.; Malhotra, P.A. Using non-invasive transcranial direct current stimulation for neglect and associated attentional deficits following stroke. *Neuropsychol. Rehabil.* **2020**, 1–32.

38. Ovadia-Caro, S.; Khalil, A.A.; Sehm, B.; Villringer, A.; Nikulin, V.V.; Nazarova, M. Predicting the Response to Non-invasive Brain Stimulation in Stroke. *Front. Neurol.* **2019**, *10*, 302.

39. Salazar, A.P.S.; Vaz, P.G.; Marchese, R.R.; Stein, C.; Pinto, C.; Pagnussat, A. Noninvasive Brain Stimulation Improves Hemispatial Neglect After Stroke: A Systematic Review and Meta-Analysis. *Arch. Phys. Med. Rehabil.* **2018**, *99*, 355–366.

40. Shafee, R., Buckner, R. L., & Fischl, B. (2015). Gray matter myelination of 1555 human brains using partial volume corrected MRI images. *Neuroimage*, *105*, 473-485.

41. Sharma, N.; Baron, J.-C.; Rowe, J. Motor imagery after stroke: Relating outcome to motor network connectivity. *Ann. Neurol. Off. J. Am. Neurol. Assoc. Child Neurol. Soc.* **2009**, *66*, 604–616.

42. Stewart, J.C.; Dewanjee, P.; Tran, G.; Quinlan, E.B.; Dodakian, L.; McKenzie, A.; See, J.; Cramer, S.C. Role of corpus callosum integrity in arm function differs based on motor severity after stroke. *NeuroImage Clin.* **2017**, *14*, 641–647.

43. Tabarelli, D., Brancaccio, A., Zrenner, C., & Belardinelli, P. (2022). Functional Connectivity States of Alpha Rhythm Sources in the Human Cortex at Rest: Implications for Real-Time Brain State Dependent EEG-TMS. *Brain Sciences*, *12*(3), 348.

44. Thut, G., Northoff, G., Ives, J. R., Kamitani, Y., Pfennig, A., Kampmann, F., ... & Pascual-Leone, A. (2003). Effects of single-pulse transcranial magnetic stimulation (TMS) on functional brain activity: a combined event-related TMS and evoked potential study. *Clinical neurophysiology*, *114*(11), 2071-2080.

45. Van Veen, B. D., Van Drongelen, W., Yuchtman, M., & Suzuki, A. (1997). Localization of brain electrical activity via linearly constrained minimum variance spatial filtering. IEEE Transactions on biomedical engineering, 44(9), 867-880.

46. Veldema, J.; Bösl, K.; Neumann, G.; Verheyden, G.; Nowak, D.A. Noninvasive brain stimulation in rehabilitation of hemispatial neglect after stroke. *CNS Spectr.* **2020**, *25*, 38–49.

47. Wagstyl, K., Larocque, S., Cucurull, G., Lepage, C., Cohen, J. P., Bludau, S., ... & Evans, A. C. (2020). BigBrain 3D atlas of cortical layers: cortical and laminar thickness gradients diverge in sensory and motor cortices. PLoS biology, 18(4), e3000678.

48. Westlake, K.P.; Hinkley, L.B.; Bucci, M.; Guggisberg, A.G.; Findlay, A.M.; Henry, R.G.; Nagarajan, S.S.; Byl, N. Resting state alpha-band functional connectivity and recovery after stroke. *Exp. Neurol.* **2012**, *237*, 160–169.

49. Wu, M., Kumar, A., & Yang, S. (2016). Development and aging of superficial white matter myelin from young adulthood to old age: Mapping by vertex-based surface statistics (VBSS). Human brain mapping, 37(5), 1759-1769.

50. Zrenner C, Desideri D, Belardinelli P, Ziemann U (2018) Real-time EEG defined excitability states determine efficacy of TMS-induced plasticity in human motor cortex. Brain Stimul 11:374 –389.

51. Zrenner, B., Zrenner, C., Gordon, P. C., Belardinelli, P., McDermott, E. J., Soekadar, S. R., ... & Müller-Dahlhaus, F. (2020). Brain oscillation-synchronized stimulation of the left dorsolateral prefrontal cortex in depression using real-time EEG-triggered TMS. Brain stimulation, 13(1), 197-205.

Chapter 1

A new framework to interpret individual interhemispheric compensatory communication after stroke

This Chapter consists in the proposal of a new framework to interpret brain plastic changes following a stroke. The novelty of the presented framework consists in taking into account previously overlooked factors in the assessment of stroke patients' recovery. The lack of consideration of these factors has wrongfully informed the theoretical assumptions of the models of brain reorganization after stroke that, in turn, have inspired the currently available rehabilitation protocols whose inefficacy has been recently stressed in meta-analyses works. This Chapter is adapted from "Brancaccio, A., Tabarelli, D., & Belardinelli, P. (2022). A new framework to interpret individual interhemispheric compensatory communication after stroke. *Journal of Personalized Medicine*, 12(1), 59" licensed under an open access Creative Commons CC BY 4.0 license. The copyright of this work is retained by the authors. All authors agreed on redistributing the following material for the purpose of this doctoral thesis.

1.1 Introduction

Stroke incidence is increasing in developing countries and young populations (Brainin et al., 2007; Katan et al., 2018). Despite its widespread occurrence, stroke still represents the principal condition leading to adult disability and motor impairment, even after the application of rehabilitation protocols (Dobkin et al., 2005). Two main types of strokes are usually reported: ischemic and haemorrhagic stroke, with ischemic stroke constituting the 80% of the cases (Sekerdag et al., 2018). In most cases, strokes are associated with damage at the level of the middle cerebral artery (Nogles et al., 2020). This structure consists of branches of vessels that provide blood supply to both cortical and subcortical structures. For this reason, strokes are further distinguished between cortical and

subcortical ones, according to the mostly damaged areas. In general, a sudden arrest in blood supply to neuronal cells which die from oxygen deprivation is at the basis of the stroke syndrome (Sekerdag et al., 2018). In the clinical practice, different brain stimulation protocols, together with standard physical rehabilitation practices, are delivered to the patient in order to increase the level of recovery after the stroke. However, in a remarkable number of cases, the patients still show impairment, even following the rehabilitation treatment. In this context, results reported in literature are still inconsistent since key factors have thus far not been considered in modelling post-stroke brain re-organization. This review proposes a new theoretical framework to better account for results in stroke literature, with a particular focus on the effectiveness of the different stimulation rehabilitation protocols proposed thus far.

Non-invasive brain stimulation (NIBS) protocols have been mainly inspired by currently available models of interhemispheric communication in strokes. The three main models are the *interhemispheric competition* model, the *vicariation* model, and the *bimodal balance–recovery* model. We think that, at present, these models need a critical revision. From a purely anatomical perspective, none of these models takes into account diaschisis processes that occur in response to the lesion. In particular, we hereby refer to transcallosal and contralesional diaschisis. In this context, diaschisis refers to structural changes in regions that have not been directly affected by the lesion but which degenerate because indirectly connected to the lesioned site (Cheng et al., 2020). Therefore, a revision explaining how both hemispheres cope with the lesion is required, since the evidence of such significant anatomical changes as a response to the lesion is recent and was not available at the time when these models were proposed. On the other hand, functional changes in brain network re-organization need to be included as well. In particular, the role of prefrontal cortices should be considered, given that most stroke patients show differences in terms of functional connectivity, especially in the fronto-parietal network (e.g. Sharma et al., 2009; Lam et al., 2018).

The role of structural reserve was first proposed by Di Pino and colleagues (2014) who tried to encompass the mixed results obtained by stimulation protocols inspired by the previous models in a

more general framework. Here, we stress the importance of the concept of structural reserve and propose to look at stroke severity on a continuous range, from the least to the most affected patients, with the mildly affected ones showing types of functional reorganization more similar to the minimally or the severely affected ones, depending on the kind of offence suffered. We believe that the allocation of a patient on a continuum of severity depends on the structural damage as well as on diaschisis processes of tissues connected to the lesion. Critically, depending on the spared tissue, functional reorganization of cortical networks will either afford to resolve compensation within the ipsilesional or contralesional hemisphere. Crucially, we propose that the structural reserve in the corpus callosum (CC) has to be considered to understand which type of reorganization the patient will possibly undertake. Furthermore, we suggest that functional brain network reorganization does not exclusively encompass sensorimotor areas, but the prefrontal network may also access a higher-level control over motor planning and execution. Importantly, while collecting pieces of evidence necessary to develop a more complete framework of stroke recovery, we also stress the epistemological mistakes that have been committed in interpreting stroke results. In fact, classic literature of stroke recovery has associated bad motor recovery to specific reorganization patterns that were reported in severely affected patients and thus thought to be maladaptive. Differently, we propose to look at these cases as the expression of the best possible reorganization the brain can undertake in order to gain some degree of recovery.

This review is focused on motor impairment and motor rehabilitation in stroke patients. The choice to focus only on the motor aspects of post-stroke deficits depends on two reasons. First, the most common impairment after stroke consists in motor deficits of the affected side of the body, with more than 80% of patients showing motor impairment in the acute stage and more than 40% in the chronic stage (e.g. Hatem et al., 2016). The second reason as to why we chose to focus on motor recovery, neglecting the cognitive aspects of stroke impairment, depends on the fact that the literature abounds in works investigating the relationship between motor scores on the assessment scales and connectivity patterns. Differently, few works are available on the relationship between scores on

cognitive assessment scales and connectivity patterns in stroke patients. For this reason, a comprehensive systematization on the relationship between cognitive impairment and connectivity patterns would have been inevitably incomplete.

This review is organized as follows. In the second section, we discuss the main stroke recovery models that have inspired recent rehabilitation protocols. In the third section, we report a recent explanatory model of interhemispheric interplay according to which the two hemispheres do not compete, but rather constantly integrate information via both facilitation and inhibition. In the fourth section, we critically analyse the current status of literature, showing the relevance of late discoveries regarding the role of corpus callosum and prefrontal cortices in sustaining stroke recovery. In the fifth section, we describe our new framework that delineates the different possibilities in stroke reorganization patterns.

1.2 Stroke Recovery Models and Efficacy of Non-invasive Rehabilitation Protocols

Transcranial magnetic stimulation (TMS) and transcranial direct current stimulation (tDCS) techniques have been used in the past years to improve motor recovery in stroke patients, often jointly with standard physiotherapy practice. However, while at the single study level the administration of TMS and tDCS treatments sometimes appear beneficial to patients, meta-analysis results have shown that these effects are rather limited or, in some cases, even non-existent (Meidian et al., 2020; Salazar et al., 2018; Veldema et al., 2020; Klomjai et al., 2015; McDonnell and Stinear, 2017). It should be noticed that these stimulation protocols have been developed on the basis of the conviction that either the interhemispheric competition or the vicariation model might be the one that best predicts recovery (McDonnell and Stinear, 2017).

The interhemispheric competition model finds its roots in a study by Murase and colleagues (2004). It assumes that the two hemispheres are in a continuous rivalry condition, by which they constantly

inhibit each other via transcallosal connections. This hypothesis of interhemispheric competitive interplay has led to the view that, when a stroke lesion damages one hemisphere, the unaffected one takes the lead by exercising excessive inhibition over the damaged one, because of the reduced and insufficient inhibition received from the lesioned side; this would then lead to an excessive depression of the spared activity in the affected region. Therefore, the affected hemisphere would suffer from both damage and excessive inhibition exerted by the non-lesioned hemisphere. TMS and tDCS rehabilitative protocols inspired by the interhemispheric competition model hence focused on limiting the inhibition exerted by the unaffected hemisphere and/or enhancing excitability of the affected one (e.g. Takeuchi et al., 2012; Dodd et al., 2017). Contralesional inhibition is supposed to decrease the inhibitory action of the spared hemisphere on one hand, while ipsilesional facilitation is thought to facilitate the inhibitory influence from the affected one (Klomjai et al., 2015). Evidence in support of this model stems from studies showing that (1) stroke patients attempting to produce a movement with the paretic hand fail because the unaffected hemisphere keeps inhibiting the affected one and does not switch to the facilitation mode at the time of movement onset (Duque et al., 2005); (2) anaesthesia reducing somatosensory input from one hand leads to an improvement in tactile spatial acuity for the contralateral hand (Werhahn et al., 2002); and (3) inhibitory repetitive TMS (rTMS) protocols applied on the contralesional motor cortex in some cases lead to an improvement in the paretic hand motor control (Grefkes et al., 2010). However, the evidence regarding the effectiveness of rTMS and tDCS rehabilitative protocols based on the competition model are inconclusive when results are evaluated at meta-analysis level. A review by Klomjai and colleagues (2015) has collected results from four meta-analyses on rTMS and tDCS protocols for stroke rehabilitation. Of these four meta-analyses, one focused on the use of tDCS applications and the other three on the use of rTMS in strokes: while one of them did not find any evidence of a successful application of rTMS protocols for stroke rehabilitation, two meta-analyses suggested a mild positive effect for subcortical strokes when inhibitive, low-frequency (1 Hz) rTMS was applied over the contralesional hemisphere (Ayache et al., 2012; Hsu et al., 2012; Hao et al., 2013; Elsner et al., 2013). Another recent and comprehensive

review (McDonnell and Stinear, 2017), including 112 TMS studies, evidenced the need of revising protocols inspired by the competition model. Indeed, the authors did not find (1) any evidence for a hyper-excitability of the unaffected hemisphere in stroke patients nor (2) any proof in favor of an interhemispheric, maladaptive imbalance. If the interhemispheric competition model were correct, the unaffected hemisphere should show hyper-excitability, given the impossibility for the affected hemisphere to participate in the process of mutual inhibition.

The vicariation model represents the alternative to the competition model and has been proposed in the attempt to explain how the brain might be coping with a stroke lesion. This model suggests that the over-activation of the contralesional hemisphere may be not maladaptive, but rather a vicarious mechanism through which the non-lesioned hemisphere compensates for the affected one's functional and structural damage. In this regard, a study by Johansen-Berg and colleagues (2002) showed that when TMS is used to disrupt the activity in the premotor cortex of the contralsional hemisphere, ipsilateral reaction time was slowed down by 12% in stroke patients but not in the control group, indicating a role of the contralesional hemisphere in sustaining motor production of the ipsilateral limb. This effect was greatest in the most impaired patients, suggesting that the larger the damage, the more the contralesional hemisphere is necessary for functional compensation. Further evidence in support of the vicariation model reveals that well-recovered chronic stroke patients show contralesional recruitment during motor implementation (Lotze et al., 2006; Riecker et al., 2010). Furthermore, it has been shown that inhibitory cathodal tDCS over the contralesional hemisphere in mildly impaired patients led to an improvement in the ipsilateral motor functions, while the same stimulation applied on severe patients worsened the motor outcome (Bradnam et al, 2012). Taken together, these results were interpreted as supportive evidence that the vicariation process might intervene when the affected hemisphere is strongly damaged. Indeed, in case of less severe damage, the plastic reorganization supporting recovery is thought to be manageable within the lesioned hemisphere itself, with no necessity of a more radical reorganization involving the unaffected one (Werhahn et al., 2003). However, at the meta-analysis level, slightly positive experimental evidence

of stroke patients' recovery was found for protocols that facilitate either the affected hemisphere in mildly affected patients or the unaffected one in severely affected patients (McDonnell and Stinear, 2017). Moreover, the supportive role of the unaffected hemisphere has been reported for both moderate and severely affected chronic stroke patients (Bundy et al., 2017).

Prior to the evidence from meta-analyses on the ineffectiveness of protocols inspired by the competition model (McDonnell and Stinear, 2017), an attempt to explain and integrate the mixed results in favour of one or the other model was made with the bimodal balance-recovery model by Di Pino and colleagues (2014). This framework advocates both competition and vicariation models as explanatory depending on the level of structural damage in the individual patient, where structural integrity is described as "*the remaining function of the motor areas and corticospinal tract in the affected hemisphere*". The authors suggest that interhemispheric competition predicts recovery more accurately in cases where the structural reserve is high. In a nutshell, less interhemispheric imbalance predicts better recovery for patients with limited damage. Differently, when the damage in the affected hemisphere is too spread out to attempt a local effective recovery, the over-recruitment of the unaffected hemisphere reflects its vicarious contribution. Even though this model was never directly tested, some works have shown that patients can be distinguished into sub-groups according to the level of damage. Moreover, this distinction predicts better recovery either after inhibitory tDCS over the affected hemisphere or excitatory stimulation of the unaffected one, suggesting that the mechanisms at the basis of an improvement after the lesion might change according to the amount of damage (Di Pino et al., 2014; Lindenberg et al., 2010).

However, the effort of Di Pino and colleagues to encompass different recovery models in one operative framework appears faulty in light of recent meta-analyses reporting no evidence in support of the competition model (McDonnell and Stinear, 2017). Moreover, Di Pino and colleagues did not consider the high-level control from prefrontal cortices, the extent of which can help to distinguish between different types of patients on the basis of their respective reorganization patterns. The

interhemispheric competition model constitutes an attempt at understanding the general mechanism of interaction between the hemispheres. The vicariation model, on the other hand, cannot be considered as a general model of brain functioning but rather as an endeavour to explain plastic changes unburdening stroke damage. The attempt of simply comprising both competition and vicariation model in the biphasic model reflects a knowledge gap and can be considered as a by-product of the fact that the general mechanism of interhemispheric communication is thus far still unclear. In particular, the question as to whether the two hemispheres are in an inhibitory or facilitatory relationship and to what extent one mechanism takes over the other is still an open matter. For the sake of completeness, we report two further attempts at improving stroke patients' stratification. Differently from the interhemispheric competition, vicariation, and biphasic models, these pipelines represent empirical models not focused on explanation of post-stroke interhemispheric interplay (i.e., inhibition or vicariation), but rather on finding a sensitive way to organize information from the individual patient in order to predict recovery and stimulation protocol outcomes. These two algorithms are the Predicting REcovery Potential (PREP) and the Structural reserve, Task Attributes, Connectivity (STAC). The PREP was introduced prior to the biphasic model, while STAC is the most recent one. For this reason, the main difference between the two models lies in the fact that STAC explicitly integrates the idea by Di Pino and colleagues, according to which the level of damage constitutes a weighting factor to choose the best stimulation protocol, and not only to assess the level of recovery (Harris-Love et al, 2017). In this sense, the bimodal balance-recovery model can be considered as a watershed in stroke literature.

The PREP algorithm (Stinear et al, 2018) stratifies patients in four categories: those who will go towards a "complete", "notable", "limited", or "none" recovery. The evaluation of a patient's potential recovery involves different steps, from the motor evaluation to the use of diffusion-weighted MRI to assess structural reserve in patients who show poor scores and no MEPs in TMS trials. PREP showed a predictive power of 88% and hence was proposed as an efficient method for predicting

recovery. However, as previously mentioned, this algorithm is not informative about the type of NIBS protocol that would best suit a specific patient.

On the other hand, STAC takes its acronym from the weighting factors that the authors propose as relevant when choosing for the best stimulation rehabilitative protocol. According to the authors, the structural reserve in the cortico-spinal tract (CST) needs to be used as a weighting factor to decide the best rehabilitative protocol. The innovation of their proposal lies in the criterion for choosing the best stimulation site: structural integrity needs to be considered jointly with two further factors, namely, (1) the task attributes and (2) the structural/functional connectivity of the candidate sites. As for the task attributes, the authors stress that different rehabilitative tasks involve different neural networks. Specifically, each task recruits different limbs' segments, and therefore the structural and functional features of, e.g., proximal and distal muscles can differ. Hence, different stimulation sites should be chosen according to the task. To intervene on structural and functional intra/interhemispheric connections (last considered factor), a precise stimulation over circumscribed cortical areas is recommended. To assess connectivity patterns of a region, structural connectivity analyses (e.g., DW-MRI) and functional techniques (e.g., non-invasive priming) are recommended.

Differently from previous pipelines, STAC does not rely on a general model explaining plastic changes in stroke patients but is rather a data-driven approach focused on finding a protocol that depends on patient's status, lesion site, and task specific factors. Furthermore, STAC considers interhemispheric structural connectivity only with the aim to better target a specific stimulation site. This approach is expanded in this work, proposing a new general model that could also be efficiently employed in a clinical environment. Individual interhemispheric structural connections should be used not only to understand whether a specific area needs to be stimulated, but most importantly to assess the spared callosal pathways which can be exploited to support interhemispheric integration.

1.3 Inhibition and Facilitation Used to Integrate Information between Hemispheres

As reported in the previous section, the model by Di Pino and colleagues is questionable in the light of relevant findings of the last few years (Di Pino et al, 2014). First, it does not consider diaschisis processes, nor the role of the callosum into sustaining interhemispheric communication in strokes. Secondly, the bimodal balance–recovery model does not include a potential role of the prefrontal cortices into sustaining motor implementation with high-level control. Finally, in their model, the authors consider the competition model as correct when the structural reserve of the individual patient is sufficient for the unaffected hemisphere to not serve a vicarious role. In this regard, a new framework on callosal function has been proposed by Carson (Carson, 2020). Carson's hypothesis helps clarify the role of the contralesional hemisphere in recovery. Carson supports the notion that the two hemispheres do not use either excitation or inhibition in interhemispheric transmission but rather that both mechanisms are employed to continuously sculpt each hemisphere's contribution to a specific behaviour. This occurs via "crossed surround inhibition", which implies both excitatory and inhibitory processes. This mechanism would explain results from works showing that stroke patients not only suffer from a motor impairment in the limb contralateral to the side of the lesion, but also that the "unaffected" hand shows an impairment compared to healthy controls (Desrosiers et al., 1996; Sunderland et al., 1999; Schaefer et al., 2007). Furthermore, it would explain results from studies showing a negative relationship between integrity of the callosum and impairment levels in stroke patients (Dewanjee et al., 2015; Stewart et al., 2017; Chen et al., 2013; Hayward et al., 2017). This is because a greater structural integrity of CC would allow for more interhemispheric integration. If the interhemispheric competition model were correct, it should be found that less integrity in the callosum leads to less over-inhibitory power by the unaffected hemisphere, which in turn would support a better motor status in the paretic side. However, experimental evidence shows the opposite: the higher the structural integrity of the CC, the better the motor recovery, suggesting a cooperative relationship. Moreover, Carson suggests that it is not correct to generally assume that the two

hemispheres are in mutual competition from the outcome of TMS-derived measures such as interhemispheric inhibition and ipsilateral silent period. In fact, the account supported by Carson is that TMS stimulates the cortical sites at intensities that are typically above the natural physiological activity levels, thus potentially masking other physiological mechanisms (Carson, 2020). A part from providing an explanation for the pieces of evidence on the relationship between callosal integrity and recovery, Carson's framework also accounts for better recovery outcomes that have been reported after facilitatory stimulation over the contralesional side (e.g. Ameli et al., 2009; Schlaug et al., 2008; Wang et al., 2020). In this regard, it must be noticed that stroke literature should in the future take into account that the effects of rTMS (inhibitory vs facilitatory) change depending on the excitability state of the cortex at the moment of stimulation (e.g. Baur et al., 2020).

Therefore, Carson's hypothesis reconsiders inhibitory processes in a novel view: inhibition does not mean competition, but it can rather be leveraged cooperatively with excitation for sculpting each hemisphere's contribution to a function. This conception of interhemispheric communication explains why the unaffected hemisphere in both mildly and severely stroke patients has been found crucial for rehabilitation (Bundy et al., 2017). Finally, the competition framework does not account for all the crossed-facilitation evidence in which the activation of one motor cortex leads to facilitation in the contralateral one (e.g. Hortobágyi et al., 2003). All these pieces of evidence, together with meta-analysis results regarding the incorrectness of the competition model's assumptions, suggest that a new model where the two hemispheres are not considered as purely competing should be formulated.

1.4 Critical Review of Current Models and the Need of a More Comprehensive Framework

Our new framework was conceived in light of the latest medical evidence regarding (1) the role of the CC in sustaining interhemispheric functional transfer in stroke patients, considering diaschisis

processes, and (2) the effects of tissue disruption leading to functional network reorganization, with a particular focus on the compensatory role of the prefrontal cortices in high-level control.

Regarding the first point, we propose that the structural reserve of CC represents an essential factor for assessing recovery in patients. Current stroke literature has mainly focused on white matter tracts different from CC, such as the internal capsule, because these were thought to be more directly affected by a stroke (Borich et al., 2012). Nevertheless, in recent years, the damage in CC was found to lead towards altered interhemispheric communication, providing a disturbance to the plastic changes that both hemispheres undergo to endure the damage (Wang et al., 2012). Three other pieces of evidence should be underlined: (1) a stroke lesion not only leads to neuronal death in the affected tissue, but the damage also spreads to neighboring areas and white matter tracts connected to the lesion. As a consequence of this process, a degeneration of homotopic contralesional sites has been observed (Cheng et al., 2020). (2) Recent works have evidenced the fact that white matter disconnection can be a good predictor of brain malfunctioning and recovery (De Schotten et al., 2020; Corbetta et al., 2015; Rizzo et al., 2008). Cheng and colleagues (2020) have demonstrated that degenerative processes in stroke patients occur progressively after the stroke, affecting not only the ipsilesional hemisphere but also the contralesional one by means of transcallosal fiber degeneration. The authors observed that the ipsilesional cortex connected to the lesion site showed a significant decrease in cortical thickness compared to the unconnected cortex. Cortical thinning of the ipsilesional cortex connected to the lesion was also accompanied by contralesional homotopic thinning. This degeneration was ascribed to a reduction in the integrity of the transcallosal tracts connecting the homotopic sites (Cheng et al., 2020). (3) It has been recently shown that the levels of structural integrity in the CC correlate with the motor status of patients depending on the severity of their symptoms. In fact, fractional anisotropy (FA) levels of CC motor section correlate with the motor status of mildly affected patients, while this is not the case in severely affected patients. Conversely, FA levels in the prefrontal section of the callosum correlate with the motor status of severely affected patients, while the same is not true for mildly affected individuals (Stewart et al.,

2017; Chen et al., 2013; Hayward et al., 2017). These pieces of evidence regarding the role of the CC suggest that this structure needs to be included in the clinical picture when evaluating patients and that structural reserve assessments should be implemented at multiple time points post stroke. Furthermore, this evidence also suggests that the CC might have an integrative function in the interhemispheric interplay. In this regard, despite the evidence in support of inhibitory mechanisms supported by the callosum, it has been claimed that transcallosal pathways mediate both inhibition and excitation between the hemispheres, and that both mechanisms are employed to sculpt hemispheres' contributions to a given function (Carson, 2020). In this context, given the evident relevance of different sections of the callosum in the recovery of differently affected patients, we propose that the unaffected hemisphere generally sustains an integrative function in favour of the contralateral one, and this contribution will occur via different transcallosal pathways, depending on the spared callosal tracts. In this regard, interpreting the interhemispheric imbalance in terms of competition between the hemispheres does not hold up: meta-analyses results do not justify the administration of stimulation protocols inspired by the competition model, while improvements after protocols facilitating either the affected hemisphere or the unaffected one have been found (McDonnell and Stinear, 2017; Wang et al., 2020). Moreover, the competition model would predict that interhemispheric imbalance dominates communication after the lesion. However, no evidence of interhemispheric imbalance has been found in stroke patients at the meta-analysis level (McDonnell and Stinear, 2017). Furthermore, interpreting the role of the contralesional hemisphere in a competitive manner does not explain how the non-paretic hand in strokes shows slight impairments compared to controls (e.g. Desrosiers et al., 1996). Finally, the negative relationship found between integrity in the CC and motor status of the patients suggests that the better the interhemispheric communication, the better the recovery (Carson, 2020; Stewart et al., 2017; Chen et al., 2013; Hayward et al., 2017).

This relationship between the integrity in different sections of the CC and the motor status of patients indicates that different compensatory mechanisms take place depending on stroke severity. This

distinction between highly and moderately affected patients was first proposed by Di Pino and colleagues (2014). However, the latest negative evidence about the competition model's assumptions suggests that their model is inaccurate. Furthermore, the bimodal balance–recovery model is currently incomplete because it does not consider (1) the CC in the estimation of structural reserve and its inhibition function, as Carson does (Carson, 2020); (2) diaschisis processes after stroke, which progressively occur after the stroke and interfere with plastic reorganization; and (3) the role of the prefrontal cortices in network re-organization.

Anticipating the new framework that will be extensively described later, we describe the relevance of the CC in mildly and severely affected patients' recovery, at this stage of this review, as follows: since motor impairment also depends on the level of structural damage, less affected patients will suffer from less degeneration in the motor system compared to more severely affected patients (damage levels as assessed via DWI techniques and not mere lesion volume assessment: Horn et al, 2016). Therefore, the motor section of CC might be sufficiently intact to support integrative functions between the two motor cortices in the mildly compared to the severely affected patients. Differently, in severely affected patients, motor transcallosal fibers are largely damaged, and, since prefrontal areas are generally the most spared ones after a stroke (Plow et al., 2015), compensatory mechanisms between hemispheres likely occur via prefrontal transcallosal connections. For this group of patients, the genu of the CC indeed positively correlates in terms of structural reserve with the patients' motor status (see Hayward et al., 2017). Liu and colleagues (2015) additionally found in contralesional frontal cortices of stroke patients the following pieces of evidence: (1) increased FA levels in the white matter tracts in the contralesional medial frontal gyrus, and (2) thalamocortical connections including projections to somatosensory, primary motor, and premotor areas were positively correlated with motor recovery (Liu et al., 2015). Furthermore, cortical thickness of frontal cortex in the contralesional hemisphere shows an increase already three months after the stroke (Brodtmann et al., 2012).

While the role of CC is essential for reorganization in mildly and more severely affected patients, it might play a minor role in the recovery of the minimally affected patients—a further, often overlooked category. These patients show minimal impairment, associated with an increased connectivity between the ipsilesional prefrontal area and the sensorimotor cortex compared to controls (see Sharma et al., 2009). Therefore, for the minimally affected patients, it might be the prefrontal cortex of the ipsilesional hemisphere to exert a compensatory role.

As previously mentioned, the prefrontal cortices generally exert a functional role in strokes' recovery, regardless of the level of impairment. Mildly affected patients show different patterns of reorganization processes, depending on the degree to which they can resolve the reorganization within the ipsilesional hemisphere. Nevertheless, regardless of their degree of reliance on the ipsilesional or contralesional hemisphere, the importance of the prefrontal cortices' role in mildly affected patients' recovery has also been assessed. In fact, in mildly affected patients, it has been found that the stronger the connectivity between prefrontal and motor cortices at rest, the better the motor production (e.g. Lam et al., 2018). Finally, also in severely affected patients, the prefrontal cortices seem to have a role in patients' recovery. This is not only inferred by the role of the prefrontal CC in the recovery of this group of patients (Hayward et al., 2017). In fact, severely affected patients also show a correlation between the level of prefrontal–sensorimotor cortices connectivity at rest and their level of motor recovery (e.g. Yin et al., 2012). These different patterns of support and compensation provided by the prefrontal cortices have not been considered thus far, neither in the stratification of stroke patients nor in any of the previous models. Interestingly, prefrontal areas seem to exert a different grade of high-level control over motor planning and production depending on the level of impairment of the patient (e.g. Sharma et al., 2009; Lam et al., 2018; Grefkes et al., 2011; Liu et al., 2016). In this regard, it is interesting to note that a potential compensatory role of the prefrontal cortices has been observed also in elderly healthy subjects. In fact, an increase in the coupling between prefrontal areas and areas involved in a task predicts their performance in the task (Cabeza et al., 2012; Fleck et al., 2016;). In particular, a prefrontal–premotor–M1 coupling predicts psychomotor speed in the elderly during

motor execution (Michely et al., 2018). The evidence reported in this section is essential to stress the gaps in previous models attempted at explaining stroke interhemispheric communication. In particular, we hope it is now clear to the reader that the roles of the CC and prefrontal cortices cannot be neglected when investigating stroke patients' recovery. All these pieces of evidence will be integrated and synthetized in a new, more comprehensive framework.

1.5 A New Framework for Predicting Rehabilitation Protocols Effects

Since the first studies on stroke patients, epistemological mistakes have been made in interpreting the relationship between brain re-organization and recovery. J. Williamson recently stressed how clinical medicine is full of examples where causal relationships between phenomena are inferred only on the basis of correlations, while the mechanism behind them cannot be explained, making it difficult to assess the real direction of the relationship (Williamson et al., 2019). In the case of stroke literature, full recovery has been associated to a return to brain patterns more similar to controls', while the impossibility to reach full recovery in severe patients has been interpreted as a by-product of functional imbalance between hemispheres. This interpretation might be the product of a spuriously inferred causal relationship: the recruitment of the contralesional hemisphere can in fact also be interpreted as a result of a larger damage in severe patients. In these patients, stronger interhemispheric integration might be the most efficient strategy to compensate for damage and not the by-product of a maladaptive reorganization. Di Pino and colleagues (2014) proposed that severely affected patients might benefit from such re-organization. However, their model lacks of an explanation of how brain networks re-adapt according to the level of damage.

In our theoretical framework, patients are allocated on a continuum of motor impairment (see Figure 1.1). Depending on their position on the severity scale, they will probably undergo one re-configuration of brain networks rather than another. Such re-configurations differ from two functional

aspects: (1) the role of the prefrontal cortices in exerting high-level motor planning and execution and (2) the relevance that a given portion of the callosum (e.g. genu or midbody) gets into sustaining interhemispheric integration.

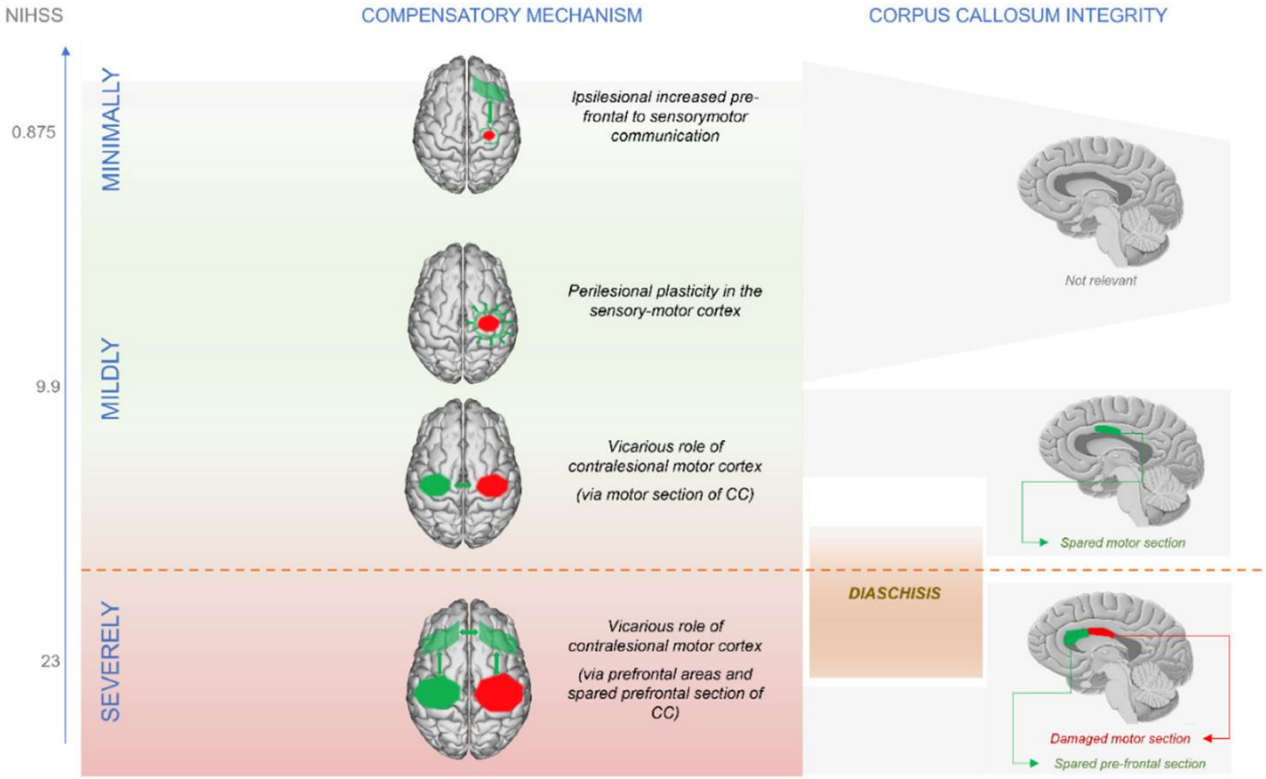

Figure 1.1: Patients lay on a continuum of severity. Minimally affected patients resolve the competition within the ipsilesional hemisphere. Going towards the more affected patients, the contralesional hemisphere becomes more and more relevant in compensatory processes. The process of diaschisis start playing role in more severe-like mildly affected patients.

Minimally affected patients, who show scores very close to controls during the chronic stage, do not rely on the contralesional hemisphere as more affected patients do. In fact, minimally affected patients should have sufficient structural reserve in the ipsilesional hemisphere, and this resource should allow them to accomplish recovery by relying on increased connectivity between ipsilesional sensorimotor and prefrontal cortex. Contralesional over-recruitment has been proposed to be adaptive in the first days after stroke occurrence (Calautti et al., 2003; Grefkes et al., 2014). After the acute stage, patients

with a good recovery (as the minimally affected ones) return to normal patterns, and the neurophysiological difference remaining between them and age-matched controls is detected in a connectivity increase between prefrontal and sensorimotor areas (Sharma et al, 2009). For these minimally affected patients, high-level control of motor planning seems sufficient for regaining motor functions (see Figure 1.1 and Figure 1.2). Sharma and colleagues show that the increase in connectivity between ipsilesional prefrontal and sensorimotor cortices emerges in the contrast between minimally affected strokes and age-matched controls only in a task of motor imagery, while this difference does not show up in the motor execution condition. In this regard, it should be noticed that, in Sharma and colleagues' work (2009), healthy controls were selected on the basis of the "age-matched" criterion. Since stroke patients were in their elderly, age-matched controls will show compensatory mechanisms that are typical of older participants. In fact, elderly healthy subjects show an increase in connectivity between prefrontal and sensorimotor cortices too, and the level of this increase predicts their psychomotor speed (e.g. Michely et al., 2018). At the same time, healthy participants usually show lower levels of connectivity between prefrontal and sensorimotor cortices in imagery tasks compared to actual motor execution (Obayashi et al., 2017; Kim et al., 2018). For this reason, the compensatory mechanism in minimally affected strokes emerges only in the imagery condition and not in the executed movement, since their age-matched controls use a similar compensatory strategy that involves prefrontal cortices in the motor execution condition. In this regard, it should be also noticed that becoming an expert through training in a certain motor task is associated with a decrease of cross-regional connectivity in alpha. In fact, novices need to "train" communication between regions involved in a task before being able to implement a trained behavior in an automatic way (Gallicchio et al., 2017). Stroke might be working in the same way: because the compensatory increase in connectivity between ipsilesional prefrontal and sensorimotor areas needs to be trained, the patients show a greater in inter-regional communication compared to controls.

Figure 1.2: List of references describing patients with different functional and structural connectivity reorganization depending on the level of impairment. Mildly affected patients, in the middle, can either develop in a more "minimally affected" fashion or, on the contrary, can develop towards patterns more similar to severely affected patients.

Mildly affected patients are the most difficult to classify in terms of recovery during the acute stage. They lie in the middle section of the continuum (see Figure 1.1) and thus might develop their recovery course either by getting close to the "minimally" affected reorganization or towards the "severely affected" one. In the first scenario, some patients might leverage peri-lesional plastic changes and increased connectivity between ipsilesional prefrontal and sensorimotor areas, coming to resemble minimally affected patients. In this case, just as in minimally affected patients, a positive relationship was found between ipsilesional increase in connectivity of the prefrontal cortex and motor status of patients (Westlake et al., 2012). Plastic processes appear to peak during the acute stage and slowdown at the dawn of the chronic phase (Xerri et al., 2014). Therefore, especially in the evaluation of mildly affected patients, time elapsed from stroke is crucial. During the chronic phase, mildly affected patients who did not manage to resolve compensation within the ipsilesional hemisphere need to evolve according to a second type of reorganization. This scenario involves a larger relay on the contralesional hemisphere, turning the status of the motor CC into a key factor for patients' recovery. For these patients, indeed, it might be safely assumed that (1) the extension of the lesion is limited, (2) the degeneration in the motor section of the CC is also consequently lower, and (3) this major preservation of CC might be associated with an analogous preservation of homologous contralesional areas (Cheng et al, 2020). In this context, the positive correlation between structural reserve in the CC motor section and their motor status provides evidence that interhemispheric integration occurs

via the CC motor section. This hypothesis is further corroborated by other contributions investigating functional changes in strokes and showing that mildly affected patients in their chronic phase show a positive relationship between increased interhemispheric sensorimotor communication and motor recovery (e.g. Chen et al., 2013; Carter et al., 2010; Cramer et al., 1997; Park et al., 2011; Kawano et al., 2017). This suggests that these patients manage to cope with the lesion by relying on interhemispheric integration to compensate for the ipsilesional damaged ones (see Figure 1.1). Additionally, high-level control of the motor outcome through prefrontal areas still seems to play a role in mildly affected patients, since increased connectivity at rest within the attention network correlates with their motor recovery (Carter et al., 2010).

In severely impaired patients, FA in the motor section of the CC does not correlate with motor status, but FA in the prefrontal section of the CC does (Hayward et al., 2017), together with FA in the CST (Stewart et al., 2017). Therefore, interhemispheric communication does not apparently occur via the motor section of CC but finds rather a less damaged pathway. In this regard, there is evidence that cortical prefrontal areas are more likely preserved from stroke than motor regions (Plow et al., 2015), and hence the prefrontal section of CC should also be more likely spared since this section of white matter would not connect to any lesioned site. For this reason, the positive correlation between prefrontal CC and motor status in these patients can be interpreted as evidence that the contribution from the spared hemisphere is mediated via the prefrontal tract of the CC, reaching the spared neuronal population of the CST. In fact, the CST is the other structure whose structural integrity correlates with the motor status of highly affected patients (Stewart et al., 2017). Moreover, there is evidence from “in vivo” studies in monkeys and TMS trials in humans that prefrontal areas communicate with both premotor and motor regions (Hayward et al., 2017; Barbas et al., 2987; Yeterian et al., 2012). From a functional point of view, prefrontal and sensorimotor connectivity of the contralesional hemisphere at rest correlates with motor status in severely affected patients (Lam et al., 2018). Finally, Rehme and colleagues (2011) have reported an over-recruitment of the contralesional hemisphere both at the level of the prefrontal areas and sensorimotor areas. This over-

recruitment correlates with better motor outcomes in severe patients compared to less impaired ones. This suggests that the more the damage, the more the patient will rely on the contralesional hemisphere, which will communicate with the affected one via prefrontal connections (Hayward et al., 2017) (see Figure 1.1 and Figure 1.2).

To summarize, we propose that minimally affected patients will rely on a reorganization more similar to healthy controls, where the prefrontal cortex' increased communication with ipsilesional sensorimotor areas suggests a compensatory role. Mildly affected patients lie in between minimally and severely affected ones, and their reorganization patterns can either tend towards peri-lesional plastic changes in the ipsilesional hemisphere (thus resembling minimally affected patients) or, in case of moderately severe damage, increased interhemispheric connectivity within the sensorimotor network (sustained by the motor CC). Finally, severe patients will rely on the contralesional hemisphere, both at the level of the sensorimotor areas and prefrontal cortex. Importantly, the vicarious contribution of the contralesional hemisphere is not interpreted here strictly in terms of over-recruitment, but primarily in terms of structural and functional connectivity patterns that, depending on the individual patient's structural reserve, can be exploited to accomplish interhemispheric integration.

1.6 Conclusions

In this work, a new framework for a stratification of stroke patients was proposed. After discussing the limits of models currently available for choosing rehabilitation strategy, we showed how some relevant structural and functional aspects have been disregarded thus far. For this reason, we propose a new classification of stroke patients, based on both impairment severity and structural/functional outcomes. Stroke patients should be considered over a continuum of impairment severity. Depending on the impairment level, the patient might undergo different compensatory routes. These options

differ depending on the role of the callosum into sustaining interhemispheric integration and on the role of prefrontal cortices high level control on motor planning and implementation. The convention that well-recovered patients resemble healthy controls in brain reorganization and consequently all patients should be pushed towards the same, healthy-like state does not hold up. Patients should be supported in their individual re-organization, which critically depends on the available structural resources. The new framework proposed in this work needs to be systematically validated, given that it has been formulated from a review of the literature results. One way to do so would lay in the analysis of connectivity patterns of stroke patients, at different times from stroke, to be correlated with their current and future motor scores. Moreover, measures of structural reserve both at the cortical, corticospinal and callosal level should be implemented. If this model will be proven to be successful at predicting general patterns of recovery, new stimulation protocols should be formulated in order to meet the need to support a more individualized plastic reorganization of the brain.

Bibliography

1. Ameli, M.; Grefkes, C.; Kemper, F.; Riegg, F.P.; Rehme, A.K.; Karbe, H.; Fink, G.R.; Nowak, D.A. Differential effects of high-frequency repetitive transcranial magnetic stimulation over ipsilesional primary motor cortex in cortical and subcortical middle cerebral artery stroke. *Ann. Neurol. Off. J. Am. Neurol. Assoc. Child Neurol. Soc.* **2009**, *66*, 298–309.

2. Ayache, S.; Farhat, W.H.; Zouari, H.; Hosseini, H.; Mylius, V.; Lefaucheur, J.-P. Stroke rehabilitation using noninvasive cortical stimulation: Motor deficit. *Expert Rev. Neurother.* **2012**, *12*, 949–972.

3. Barbas, H.; Pandya, D.N. Architecture and frontal cortical connections of the premotor cortex (area 6) in the rhesus monkey. *J. Comp. Neurol.* **1987**, *256*, 211–228.

4. Baur, D.; Galevska, D.; Hussain, S.; Cohen, L.G.; Ziemann, U.; Zrenner, C. Induction of LTD-like corticospinal plasticity by low-frequency rTMS depends on pre-stimulus phase of sensorimotor μ-rhythm. *Brain Stimul.* **2020**, *13*, 1580–1587.

5. Bernhardt, J.; Hayward, K.; Kwakkel, G.; Ward, N.; Wolf, S.L.; Borschmann, K.; Krakauer, J.W.; A Boyd, L.; Carmichael, S.T.; Corbett, D.; et al. Agreed definitions and a shared vision for new standards in stroke recovery research: The Stroke Recovery and Rehabilitation Roundtable taskforce. *Int. J. Stroke* **2017**, *12*, 444–450.

6. Bloom, J.S.; Hynd, G.W. The Role of the Corpus Callosum in Interhemispheric Transfer of Information: Excitation or Inhibition? *Neuropsychol. Rev.* **2005**, *15*, 59–71.

7. Borich, M.R.; Wadden, K.P.; Boyd, L.A. Establishing the reproducibility of two approaches to quantify white matter tract integrity in stroke. *NeuroImage* **2012**, *59*, 2393–2400.

8. Bradnam, L.V.; Stinear, C.M.; Barber, P.A.; Byblow, W.D. Contralesional hemisphere control of the proximal paretic upper limb following stroke. *Cereb. Cortex* **2012**, *22*, 2662–2671.

9. Brainin, M.; Teuschl, Y.; Kalra, L. Acute treatment and long-term management of stroke in developing countries. *Lancet Neurol.* **2007**, *6*, 553–561.

10. Brodtmann, A.; Pardoe, H.; Li, Q.; Lichter, R.; Østergaard, L.; Cumming, T. Changes in regional brain volume three months after stroke. *J. Neurol. Sci.* **2012**, *322*, 122–128.

11. Bundy, D.T.; Souders, L.; Baranyai, K.; Leonard, L.; Schalk, G.; Coker, R.; Moran, D.W.; Huskey, T.; Leuthardt, E.C. Contralesional Brain–Computer Interface Control of a Powered Exoskeleton for Motor Recovery in Chronic Stroke Survivors. *Stroke* **2017**, *48*, 1908–1915.

12. Cabeza, R.; Dennis, N.A. Frontal lobes and aging: Deterioration and compensation. *Princ. Front. Lobe Funct.* **2012**, *2*, 628–652.

13. Calautti, C.; Baron, J.C. Functional neuroimaging studies of motor recovery after stroke in adults: A review. *Stroke* **2003**, *34*, 1553–1566.

14. Carson, R.G. Interhemispheric inhibition sculpts the output of neural circuits by co-opting the two cerebral hemispheres. *J. Physiol.* **2020**, *598*, 4781–4802.

15. Carter, A.R.; Astafiev, S.V.; Lang, C.E.; Connor, L.T.; Rengachary, J.; Strube, M.J.; Pope, D.L.; Shulman, G.L.; Corbetta, M. Resting interhemispheric functional magnetic resonance imaging connectivity predicts performance after stroke. *Ann. Neurol.* **2010**, *67*, 365–375.

16. Chen, J.L.; Schlaug, G. Resting State Interhemispheric Motor Connectivity and White Matter Integrity Correlate with Motor Impairment in Chronic Stroke. *Front. Neurol.* **2013**, *4*, 178.

17. Cheng, B.; Dietzmann, P.; Schulz, R.; Boenstrup, M.; Krawinkel, L.; Fiehler, J.; Gerloff, C.; Thomalla, G. Cortical atrophy and transcallosal diaschisis following isolated subcortical stroke. *Br. J. Pharmacol.* **2020**, *40*, 611–621.

18. Corbetta, M.; Ramsey, L.; Callejas, A.; Baldassarre, A.; Hacker, C.D.; Siegel, J.; Astafiev, S.; Rengachary, J.; Zinn, K.; Lang, C.; et al. Common Behavioral Clusters and Subcortical Anatomy in Stroke. *Neuron* **2015**, *85*, 927–941.

19. Cramer, S.C.; Nelles, G.; Benson, R.R.; Kaplan, J.D.; Parker, R.A.; Kwong, K.K.; Kennedy, D.N.; Finklestein, S.P.; Rosen, B.R. A Functional MRI Study of Subjects Recovered From Hemiparetic Stroke. *Stroke* **1997**, *28*, 2518–2527.

20. De Schotten, M.T.; Foulon, C.; Nachev, P. Brain disconnections link structural connectivity with function and behaviour. *Nat. Commun.* **2020**, *11*, 1–8.

21. Desrosiers, J.; Bourbonnais, D.; Bravo, G.; Roy, P.M.; Guay, M. Performance of the 'unaffected' upper extremity of elderly stroke patients. *Stroke* **1996**, *27*, 1564–1570.

22. Dewanjee, P.; Tran, G.; Stewart, J.C.; Quinlan, E.B.; Dodakian, L.; McKenzie, A.; See, J.; Cramer, S.C. Structural Integrity of the Corpus Callosum Correlates with Sensorimotor Impairment after Stroke. *Stroke* **2015**, *46* (Suppl. 1), A2.

23. Di Pino, G.; Pellegrino, G.; Assenza, G.; Capone, F.; Ferreri, F.; Formica, D.; Ranieri, F.; Tombini, M.; Ziemann, U.; Rothwell, J.; et al. Modulation of brain plasticity in stroke: A novel model for neurorehabilitation. *Nat. Rev. Neurol.* **2014**, *10*, 597–608.

24. Dobkin, B.H. Rehabilitation after stroke. *N. Engl. J. Med.* **2005**, *352*, 1677–1684.

25. Dodd, K.C.; Nair, V.; Prabhakaran, V. Role of the Contralesional vs. Ipsilesional Hemisphere in Stroke Recovery. *Front. Hum. Neurosci.* **2017**, *11*, 469.

26. Duque, J.; Hummel, F.; Celnik, P.; Murase, N.; Mazzocchio, R.; Cohen, L.G. Transcallosal inhibition in chronic subcortical stroke. *NeuroImage* **2005**, *28*, 940–946.

27. Elsner, B.; Kugler, J.; Pohl, M.; Mehrholz, J. Transcranial direct current stimulation (tDCS) for improving function and activities of daily living in patients after stroke. *Cochrane Database Syst. Rev.* **2013**, CD009645.

28. Fleck, J.I.; Kuti, J.; Brown, J.; Mahon, J.R.; Gayda-Chelder, C. Frontal-posterior coherence and cognitive function in older adults. *Int. J. Psychophysiol.* **2016**, *110*, 217–230.

29. Fries, P. A mechanism for cognitive dynamics: Neuronal communication through neuronal coherence. *Trends Cogn. Sci.* **2005**, *9*, 474–480.

30. Gallicchio, G.; Cooke, A.; Ring, C. Practice makes efficient: Cortical alpha oscillations are associated with improved golf putting performance. *Sport, Exerc. Perform. Psychol.* **2017**, *6*, 89–102.

31. Grefkes, C.; Fink, G.R. Connectivity-based approaches in stroke and recovery of function. *Lancet Neurol.* **2014**, *13*, 206–216.

32. Grefkes, C.; Fink, G.R. Reorganization of cerebral networks after stroke: New insights from neuroimaging with connectivity approaches. *Brain* **2011**, *134*, 1264–1276.

33. Grefkes, C.; Nowak, D.A.; Wang, L.; Dafotakis, M.; Eickhoff, S.B.; Fink, G.R. Modulating cortical connectivity in stroke patients by rTMS assessed with fMRI and dynamic causal modeling. *NeuroImage* **2010**, *50*, 233–242.

34. Hao, Z.; Wang, D.; Zeng, Y.; Liu, M. Repetitive transcranial magnetic stimulation for improving function after stroke. *Cochrane Database Syst. Rev.* **2013**, *2013*, CD008862.

35. Harris-Love, M.L.; Harrington, R.M. Non-Invasive Brain Stimulation to Enhance Upper Limb Motor Practice Poststroke: A Model for Selection of Cortical Site. *Front. Neurol.* **2017**, *8*, 224.

36. Hatem, S.M.; Saussez, G.; Della Faille, M.; Prist, V.; Zhang, X.; Dispa, D.; Bleyenheuft, Y. Rehabilitation of Motor Function after Stroke: A Multiple Systematic Review Focused on Techniques to Stimulate Upper Extremity Recovery. *Front. Hum. Neurosci.* **2016**, *10*, 442.

37. Hayward, K.S.; Neva, J.; Mang, C.S.; Peters, S.; Wadden, K.P.; Ferris, J.K.; Boyd, L.A. Interhemispheric Pathways Are Important for Motor Outcome in Individuals with Chronic and Severe Upper Limb Impairment Post Stroke. *Neural Plast.* **2017**, *2017*, 1–12.

38. Horn, U.; Grothe, M.; Lotze, M. MRI Biomarkers for Hand-Motor Outcome Prediction and Therapy Monitoring following Stroke. *Neural Plast.* **2016**, *2016*, 1–12.

39. Hortobágyi, T.; Taylor, J.; Petersen, N.C.; Russell, G.; Gandevia, S. Changes in Segmental and Motor Cortical Output With Contralateral Muscle Contractions and Altered Sensory Inputs in Humans. *J. Neurophysiol.* **2003**, *90*, 2451–2459.

40. Hsu, W.Y.; Cheng, C.H.; Liao, K.K.; Lee, I.H.; Lin, Y.Y. Effects of repetitive transcranial magnetic stimulation on motor functions in patients with stroke: A meta-analysis. *Stroke* **2012**, *43*, 1849–1857.

41. Johansen-Berg, H.; Rushworth, M.; Bogdanovic, M.D.; Kischka, U.; Wimalaratna, S.; Matthews, P.M. The role of ipsilateral premotor cortex in hand movement after stroke. *Proc. Natl. Acad. Sci. USA* **2002**, *99*, 14518–14523.

42. Katan, M.; Luft, A. Global Burden of Stroke. In *Seminars in Neurology*; Georg Thieme Verlag: New York, NY, USA, 2018; Volume 38, pp. 208–211.

43. Kawano, T.; Hattori, N.; Uno, Y.; Kitajo, K.; Hatakenaka, M.; Yagura, H.; Fujimoto, H.; Yoshioka, T.; Nagasako, M.; Otomune, H.; et al. Large-scale phase synchrony reflects clinical status after stroke: An EEG study. *Neurorehabilit. Neural Repair* **2017**, *31*, 561–570.

44. Kim, Y.K.; Park, E.; Lee, A.; Im, C.-H.; Kim, Y.-H. Changes in network connectivity during motor imagery and execution. *PLoS ONE* **2018**, *13*, e0190715.

45. Klomjai, W.; Lackmy-Vallée, A.; Roche, N.; Pradat-Diehl, P.; Marchand-Pauvert, V.; Katz, R. Repetitive transcranial magnetic stimulation and transcranial direct current stimulation in motor rehabilitation after stroke: An update. *Ann. Phys. Rehabil. Med.* **2015**, *58*, 220–224.

46. Koganemaru, S.; Mima, T.; Nakatsuka, M.; Ueki, Y.; Fukuyama, H.; Domen, K. Human motor associative plasticity induced by paired bihemispheric stimulation. *J. Physiol.* **2009**, *587*, 4629–4644.

47. Lam, T.K.; Dawson, D.R.; Honjo, K.; Ross, B.; Binns, M.A.; Stuss, D.T.; Black, S.E.; Chen, J.J.; Levine, B.T.; Fujioka, T. Neural coupling between contralesional motor and frontoparietal networks correlates with motor ability in individuals with chronic stroke. *J. Neurol. Sci.* **2018**, *384*, 21–29.

48. Lindenberg, R.; Renga, V.; Zhu, L.L.; Betzler, F.; Alsop, D.; Schlaug, G. Structural integrity of corticospinal motor fibers predicts motor impairment in chronic stroke. *Neurology* **2010**, *74*, 280–287.

49. Liu, G.; Dang, C.; Chen, X.; Xing, S.; Dani, K.; Xie, C.; Peng, K.; Zhang, J.; Li, J.; Zhang, J.; et al. Structural remodeling of white matter in the contralesional hemisphere is correlated with early motor recovery in patients with subcortical infarction. *Restor. Neurol. Neurosci.* **2015**, *33*, 309–319.

50. Liu, H.; Tian, T.; Qin, W.; Li, K.; Yu, C. Contrasting Evolutionary Patterns of Functional Connectivity in Sensorimotor and Cognitive Regions after Stroke. *Front. Behav. Neurosci.* **2016**, *10*, 72.

51. Lotze, M.; Markert, J.; Sauseng, P.; Hoppe, J.; Plewnia, C.; Gerloff, C. The Role of Multiple Contralesional Motor Areas for Complex Hand Movements after Internal Capsular Lesion. *J. Neurosci.* **2006**, *26*, 6096–6102.

52. McDonnell, M.N.; Stinear, C.M. TMS measures of motor cortex function after stroke: A meta-analysis. *Brain Stimul.* **2017**, *10*, 721–734.

53. Meidian, A.C.; Wahyuddin; Amimoto, K. Rehabilitation interventions of unilateral spatial neglect based on the functional outcome measure: A systematic review and meta-analysis. *Neuropsychol. Rehabil.* **2020**, 1–30.

54. Michely, J.; Volz, L.; Hoffstaedter, F.; Tittgemeyer, M.; Eickhoff, S.; Fink, G.; Grefkes, C. Network connectivity of motor control in the ageing brain. *NeuroImage Clin.* **2018**, *18*, 443–455.

55. Murase, N., Duque, J., Mazzocchio, R., & Cohen, L. G. (2004). Influence of interhemispheric interactions on motor function in chronic stroke. *Annals of Neurology: Official Journal of the American Neurological Association and the Child Neurology Society*, *55*(3), 400-409.

56. Nogles, T.E.; Galuska, M.A. *Middle Cerebral Artery Stroke*; StatPearls: Treasure Island, FL, USA, 2020.

57. Obayashi, Y.; Uemura, J.-I.; Hoshiyama, M. Functional inter-cortical connectivity among motor-related cortices during motor imagery: A magnetoencephalographic study. *Somatosens. Mot. Res.* **2017**, *34*, 1–8.

58. Olgiati, E.; Malhotra, P.A. Using non-invasive transcranial direct current stimulation for neglect and associated attentional deficits following stroke. *Neuropsychol. Rehabil.* **2020**, 1–32.

59. Ovadia-Caro, S.; Khalil, A.A.; Sehm, B.; Villringer, A.; Nikulin, V.V.; Nazarova, M. Predicting the Response to Non-invasive Brain Stimulation in Stroke. *Front. Neurol.* **2019**, *10*, 302.

60. Park, C.-H.; Chang, W.H.; Ohn, S.H.; Kim, S.T.; Bang, O.Y.; Pascual-Leone, A.; Kim, Y.-H. Longitudinal Changes of Resting-State Functional Connectivity during Motor Recovery after Stroke. *Stroke* **2011**, *42*, 1357–1362.

61. Park, J.-W.; Oh, J.C.; Lee, J.-W.; Yeo, J.-S.; Ryu, K.H. The effect of 5Hz high-frequency rTMS over contralesional pharyngeal motor cortex in post-stroke oropharyngeal dysphagia: A randomized controlled study. *Neurogastroenterol. Motil.* **2012**, *25*, 324-e250.

62. Plewnia, C.; Rilk, A.J.; Soekadar, S.R.; Arfeller, C.; Huber, H.S.; Sauseng, P.; Hummel, F.; Gerloff, C. Enhancement of long-range EEG coherence by synchronous bifocal transcranial magnetic stimulation. *Eur. J. Neurosci.* **2008**, *27*, 1577–1583.

63. Plow, E.B.; Cunningham, D.A.; Varnerin, N.; Machado, A. Rethinking stimulation of the brain in stroke rehabilitation: Why higher motor areas might be better alternatives for patients with greater impairments. *Neuroscientist* **2015**, *21*, 225–240.

64. Rehme, A.K.; Fink, G.R.; Von Cramon, D.Y.; Grefkes, C. The Role of the Contralesional Motor Cortex for Motor Recovery in the Early Days after Stroke Assessed with Longitudinal fMRI. *Cereb. Cortex* **2011**, *21*, 756–768.

65. Riecker, A.; Gröschel, K.; Ackermann, H.; Schnaudigel, S.; Kassubek, J.; Kastrup, A. The role of the unaffected hemisphere in motor recovery after stroke. *Hum. Brain Mapp.* **2010**, *31*, 1017–1029.

66. Rizzo, G.; Martinelli, P.; Manners, D.; Scaglione, C.; Tonon, C.; Cortelli, P.; Malucelli, E.; Capellari, S.; Testa, C.; Parchi, P.; et al. Diffusion-weighted brain imaging study of patients with clinical diagnosis of corticobasal degeneration, progressive supranuclear palsy and Parkinson's disease. *Brain* **2008**, *131*, 2690–2700.

67. Salazar, A.P.S.; Vaz, P.G.; Marchese, R.R.; Stein, C.; Pinto, C.; Pagnussat, A. Noninvasive Brain Stimulation Improves Hemispatial Neglect After Stroke: A Systematic Review and Meta-Analysis. *Arch. Phys. Med. Rehabil.* **2018**, *99*, 355–366.

68. Sauseng, P.; Hoppe, J.; Klimesch, W.; Gerloff, C.; Hummel, F.C. Dissociation of sustained attention from central executive functions: Local activity and interregional connectivity in the theta range. *Eur. J. Neurosci.* **2007**, *25*, 587–593.

69. Schaefer, S.Y.; Haaland, K.Y.; Sainburg, R.L. Ipsilesional motor deficits following stroke reflect hemispheric specializations for movement control. *Brain* **2007**, *130*, 2146–2158.

70. Schlaug, G.; Renga, V.; Nair, D. Transcranial direct current stimulation in stroke recovery. *Arch. Neurol.* **2008**, *65*, 1571–1576.

71. Sekerdag, E.; Solaroglu, I.; Gursoy-Ozdemir, Y. Cell death mechanisms in stroke and novel molecular and cellular treatment options. *Curr. Neuropharmacol.* **2018**, *16*, 1396–1415.

72. Sharma, N.; Baron, J.-C.; Rowe, J. Motor imagery after stroke: Relating outcome to motor network connectivity. *Ann. Neurol. Off. J. Am. Neurol. Assoc. Child Neurol. Soc.* **2009**, *66*, 604–616.

73. Stefanou, M. I., Desideri, D., Belardinelli, P., Zrenner, C., & Ziemann, U. (2018). Phase synchronicity of μ-rhythm determines efficacy of interhemispheric communication between human motor cortices. Journal of Neuroscience, 38(49), 10525-10534.

74. Stewart, J.C.; Dewanjee, P.; Tran, G.; Quinlan, E.B.; Dodakian, L.; McKenzie, A.; See, J.; Cramer, S.C. Role of corpus callosum integrity in arm function differs based on motor severity after stroke. *NeuroImage Clin.* **2017**, *14*, 641–647.

75. Stinear, C.M.; Barber, P.A.; Petoe, M.; Anwar, S.; Byblow, W.D. The PREP algorithm predicts potential for upper limb recovery after stroke. *Brain* **2012**, *135*, 2527–2535.

76. Sunderland, A.; Bowers, M.P.; Sluman, S.-M.; Wilcock, D.J.; Ardron, M.E. Impaired dexterity of the ipsilateral hand after stroke and the relationship to cognitive deficit. *Stroke* **1999**, *30*, 949–955.

77. Takeuchi, N.; Tada, T.; Matsuo, Y.; Ikoma, K. Low-Frequency Repetitive TMS Plus Anodal Transcranial DCS Prevents Transient Decline in Bimanual Movement Induced by Contralesional Inhibitory rTMS After Stroke. *Neurorehabilit. Neural Repair* **2012**, *26*, 988–998.

78. Veldema, J.; Bösl, K.; Neumann, G.; Verheyden, G.; Nowak, D.A. Noninvasive brain stimulation in rehabilitation of hemispatial neglect after stroke. *CNS Spectr.* **2020**, *25*, 38–49.

79. Veniero, D., Ponzo, V., & Koch, G. (2013). Paired associative stimulation enforces the communication between interconnected areas. Journal of Neuroscience, 33(34), 13773-13783.

80. Wang, L.E.; Tittgemeyer, M.; Imperati, D.; Diekhoff, S.; Ameli, M.; Fink, G.R.; Grefkes, C. Degeneration of corpus callosum and recovery of motor function after stroke: A multimodal magnetic resonance imaging study. *Hum. Brain Mapp.* **2012**, *33*, 2941–2956.

81. Wang, Q.; Zhang, D.; Zhao, Y.-Y.; Hai, H.; Ma, Y.-W. Effects of high-frequency repetitive transcranial magnetic stimulation over the contralesional motor cortex on motor recovery in severe hemiplegic stroke: A randomized clinical trial. *Brain Stimul.* **2020**, *13*, 979–986.

82. Werhahn, K.J.; Conforto, A.B.; Kadom, N.; Hallett, M.; Cohen, L.G. Contribution of the ipsilateral motor cortex to recovery after chronic stroke. *Ann. Neurol. Off. J. Am. Neurol. Assoc. Child Neurol. Soc.* **2003**, *54*, 464–472.

83. Werhahn, K.J.; Mortensen, J.; Van Boven, R.W.; Zeuner, K.E.; Cohen, L.G. Enhanced tactile spatial acuity and cortical processing during acute hand deafferentation. *Nat. Neurosci.* **2002**, *5*, 936–938.

84. Westlake, K.P.; Hinkley, L.B.; Bucci, M.; Guggisberg, A.G.; Findlay, A.M.; Henry, R.G.; Nagarajan, S.S.; Byl, N. Resting state alpha-band functional connectivity and recovery after stroke. *Exp. Neurol.* **2012**, *237*, 160–169.

85. Williamson, J. Establishing Causal Claims in Medicine. *Int. Stud. Philos. Sci.* **2019**, *32*, 33–61.

86. Xerri, C.; Zennou-Azogui, Y.; Sadlaoud, K.; Sauvajon, D. Interplay between intra- and interhemispheric remodeling of neural networks as a substrate of functional recovery after stroke: Adaptive versus maladaptive reorganization. *Neuroscience* **2014**, *283*, 178–201.

87. Yeterian, E.H.; Pandya, D.N.; Tomaiuolo, F.; Petrides, M. The cortical connectivity of the prefrontal cortex in the monkey brain. *Cortex* **2012**, *48*, 58–81.

88. Zibman, S., Daniel, E., Alyagon, U., Etkin, A., & Zangen, A. (2019). Interhemispheric cortico-cortical paired associative stimulation of the prefrontal cortex jointly modulates frontal asymmetry and emotional reactivity. Brain Stimulation, 12(1), 139-147.

Chapter 2

Instantaneous EEG Excitability States of Stroke Affected and Unaffected Hemispheres probed by TMS

This Chapter is aimed at investigating the different excitability properties of the affected and unaffected hemisphere in chronic stroke patients employing a phase-dependent approach in the analysis of TMS-EEG data. In particular, it is here shown for the first time that, depending on the brain-state at the moment of stimulation, the two hemispheres react differently to TMS. The affected hemisphere's strong and simplified TMS-evoked response, a feature of severe stroke patients previously reported, is here shown to depend on a low degree of differentiation between the low and high excitability states in the motor cortex. The differentiation between the excitability states of the motor cortex is proposed to be a condition that might need to be restored in order for recovery to be successful.

2.1 Introduction

Stroke occurrence in humans has been raising in recent years (Brainin et al., 2007; Katan et al., 2018). Although this disease is one of the most affecting in terms of motor disability, rehabilitation protocols currently used are inconsistently effective (McDonnell and Stinear, 2018). These protocols are based either on the interhemispheric competition (Murase et al., 2004) or the vicariation model (Johansen-Berg et al., 2002) which describe brain plastic changes after stroke. The interhemispheric competition model assumes that the healthy brain's hemispheres are in equilibrium, determined by a continuous and mutual inhibition. After a stroke, the *affected* hemisphere (AH) is predicted to suffer from both the lesion and excessive inhibition exercised by the *unaffected* hemisphere (UH), which would prevent the AH from recovering (Meyer et al., 1995; Murase et al., 2004; Duque et al., 2005). On the contrary, the vicariation model, specifically developed to explain how the

brain copes with a stroke lesion, interprets the hyperexcitability of the UH as due to the unaffected side trying to compensate for the damage (e.g. Lotze et al., 2006; Johansen-Berg et al., 2002).

However, current literature reports mixed results on the correctness of both models (see Brancaccio et al., 2022 for a review) with no certainty regarding the efficacy of the protocols inspired by either. Importantly, the most recent and complete meta-analysis by McDonnell and Stinear (2018) reports no evidence for a general law of UH hyperexcitability or maladaptive interhemispheric imbalance in stroke. This latter result points out the limitations of both models, as they rely on UH hyperexcitability, even though this eventuality is interpreted differently in the two frameworks.

TMS-EEG studies investigating both the AH and UH' excitability properties in stroke found no evidence for UH hyperexcitability. In fact, Casula et al. (2021) showed a smaller cortical response in UH to single-pulse TMS compared to healthy brain. Differently, the AH showed smaller EEG responses to TMS compared to both UH and healthy brain. Therefore, the UH does not appear inherently 'hyperexcitable', but rather exhibits stronger responses compared to AH and weaker responses compared to healthy controls. Tscherpel and colleagues (2020) also evaluated TMS-evoked EEG responses in the AH of stroke patients. Differently from Casula and colleagues (2021), they found simplified, high-amplitude biphasic EEG responses to TMS in the AH of severe patients. This latter finding was reproduced by Sarasso and colleagues (2020) who found that TMS stimulation over the perilesional site, but not over the UH, evoked a simplified and large response especially in multifocal severely affected patients.

No UH hyperexcitability emerged from these studies; rather, the TMS-evoked response in AH appeared either large and hypersimplified, as reported by (Tscherpel et al., 2020; Sarasso et al., 2020) or characterized by hypoexcitability (Casula et al., 2021) compared to healthy controls.

With the aim to present an approach to reduce variability in stroke studies, we resume here evidences from brain-state dependent stimulation experiments. In healthy participants, real-time EEG-TMS has been

shown to reduce 1) inter-trial variability of motor-evoked potentials (MEPs, Zrenner et al., 2018), a metric employed to assess corticospinal excitability in stroke patients and 2) inter- and intra- individual variability in the effects of repetitive TMS (Zrenner et al., 2020; Baur et al., 2020). Zrenner and colleagues (2018) report two relevant findings on corticospinal excitability determined by the instantaneous alpha phase of somatosensory mu rhythm at the time of TMS stimulation. First, MEPs are larger on average when the TMS pulse is released over the motor cortex at the mu-alpha negative peak (*trough*) than in other phase-states. Secondly, high frequency rTMS triplets applied over the hand-knob of the motor cortex systematically at mu-alpha *trough* induced long-term potentiation, while the same stimuli at the positive peak induced no different effects from random mu-alpha phase stimulation. In fact, the mu-alpha *trough* has been considered as a state in which the dendrites of pyramidal neurons are close to their firing threshold (Zrenner et al., 2018). The authors concluded that intra- and inter-individual variability as well as low effect-sizes found both in excitability and rTMS plasticity interventions depend on "*blind to the ever and rapidly changing instantaneous brain state*" approaches (Zrenner et al., 2018). The relevance of local mu-alpha phase to TMS stimulation effects on the motor hand-knob was also confirmed by Baur et al. (2020) who found low-frequency rTMS systematically at the positive peak provided long-term depression. Differently, the same intervention synchronized with the negative peak induced a tendency towards long-term potentiation. For this reason, results were interpreted as a proof of concept that intra- and inter-individual variability in low-frequency rTMS studies can be explained with brain-state dependent approaches considering the instantaneous excitability state of the motor cortex at stimulation time.

Here we analysed TMS-EEG data in a cohort of severe stroke patients who were stimulated on both AH and UH motor cortex, separately. We applied a post-hoc phase-bin sorting on the basis of the mu alpha oscillation phase recorded over the left and right motor cortex at the moment of stimulation. This was accomplished by computing the signal over C3 and C4 Hjorth filtered at IAF. Hussain et al. (2020) provided evidence of mu-alpha phase detection accuracy also in the affected motor cortex of stroke patients.

On the basis of previous findings (Casula et al., 2021; Tscherpel et al., 2020; Sarasso et al., 2020), we expected to find either an hypoexcitability or a high-amplitude and simplified response of the AH. Since TEPs change depending on the local state at the moment of stimulation in healthy controls (e.g. Desideri et al., 2020), the

phase-dependent approach employed in this work was intended to investigate phase-dependently the excitability properties of both the AH and UH. The aim was to understand if their differences in excitability can be ascribed to the mu alpha phase-states at the instant of TMS stimulus. The effects of phase-states on TMS-EEG responses are assessed in this work by computing different metrics from data: TMS-evoked potentials (TEPs), inter-trial phase coherence (ITPC), time-frequency spectrograms (TF) and interhemispheric phase-coupling. In the next section, the reasons behind the choice of these metrics are discussed.

2.2 TEPs, ITPC, TF and Connectivity to assess phase-dependent cortical excitability properties

In this section, we discuss the choice of different metrics to investigate brain activity changes following phase-dependent TMS stimulation.

The TEPs consist in a series of positive and negative deflections at different latencies evoked by the TMS stimulus in the cortical activity recorded with EEG. When TMS stimulation is given in the motor cortex, the TEP components evoked are the P25, N45, P70, N100 and P180. P and N refer to the polarity (positive or negative) of the deflection, while the numbers refer to the typical latency, with respect to the TMS stimulus, at which the component is usually recorded (Desideri, 2020). TEPs metric have been already proposed as a possible proxy of the excitatory/inhibitory properties of the cortex. For example, pharmaco-TMS-EEG with GABAergic and glutamatergic drugs has provided converging evidence about the N45 TEP: 1. It was enhanced by Benzodiazepines (Alprazolam and Diazepam, GABAA-R agonists) (Premoli et al., 2014) 2. It was enhanced in an analogous way by an NMDA-R antagonist (Dextromethorphan) (Belardinelli et al., 2021) 3. It was attenuated by a GABAA-R antagonist in a dosage-dependent fashion (Darmani et al., 2016). Thus, it can be reasonably considered as a reliable biomarker for the Excitation-Inhibition balance in the human brain. Moreover, Casula et al. (2014) showed low-frequency rTMS to increase P70 and N100 TEPs and proposed these results as reflecting inhibitory processes. Therefore, TEPs are an interesting measure as they reflect modulation of inhibitory and excitatory properties of the cortex. In general, only few studies have investigated TEPs in strokes. Hordacre et al. (2019) have reported that TEPs elicited with single pulse TMS applied over

ipsilesional M1 are stronger compared to controls and more frontal responses in the P30 component in stroke patients were found compared to healthy controls during a motor task. Also, Gray and colleagues (2017) confirmed that the P30 (a TEP which correlated with MEP amplitude in (Mäki & Ilmoniemi 2009)) shows anomalies in stroke patients and that differences can be found in TEPs between patients and controls up to 300 ms after the pulse. These pieces of evidence point toward an alteration of TEPs in stroke patients compared to controls. Nevertheless, mixed results have been found also in stroke literature investigating TEPs. Like previously mentioned, Casula and colleagues (2021) have shown that the AH is characterized by an hypoexcitability in terms of elicited TEPs, while Tscherpel et al. (2020) and Sarasso et al. (2020) found different results. Only two works have investigated TEPs sorted on the basis of the mu-phase at time of the stimulus in healthy participants (Desideri et al., 2017, 2018). It has been shown that stimulation falling at *trough* of the sensorimotor mu alpha rhythm leads to greater P70 and N100 components than same stimulation at the positive mu-alpha peak. Therefore, these TEPs were proposed to be representative of cortical excitability at the moment of stimulation, as stimulating at mu-alpha *trough* seem to recruit larger neuronal populations compared to the same stimulation at the positive mu-alpha peak (Desideri et al., 2018). To our knowledge, our work is the first to investigate the excitability of the two stroke hemispheres using TEPs analysed with a phase-dependent approach.

With respect to ITPC, this is a measure of phase consistency across trials rarely investigated in stroke patients. Gyulai et al., 2021 showed delta and theta ITPC increases over ipsilesional parietal areas possibly reflecting improvement in motor impairment. Importantly, ITPC can be considered as a metric of intra-individual variability in a given stimulation condition (e.g. Papenberg et al., 2013). Therefore, we investigated ITPC of mu-alpha phase-dependent EEG-TMS responses in order to ascertain whether stimulation provided at determined phase-state influences ITPC in the AH and UH and whether this modulation occurs differently in the two hemispheres when they are stimulated at the same phase-state.

We also computed time-frequency resolved spectrograms from EEG activity in both the AH and UH as a function of local mu-alpha phase-state. TF analyses in stroke patients TMS-EEG studies have shown post-

pulse alpha power increases to correlate with motor improvement, suggesting a role of alpha in stroke plastic reorganization underlying functional recovery (e.g. Pellicciari et al., 2018). Therefore, given this role of alpha in reflecting cortical plastic changes, we predicted alpha to be selectively modulated by the local phase state at the moment of the pulse and that this would occur differently in the AH and UH stimulation.

Finally, brain-state dependent literature has rarely focused on the effects of spTMS on the cortico-cortical connectivity (FC) between homologous regions. Momi et al. (2022) have shown mu-alpha *trough* to elicit stronger interhemispheric synchronization at the Individual Alpha frequency (IAF) between the two motor cortices compared to stimulation at positive peak in healthy subjects. In particular, they showed that post-pulse interhemispheric coherence between homotopic regions is larger than pre-pulse coherence when the pulse is given at the *trough* compared to the positive peak of local mu-alpha. Understanding whether this pattern changes in stroke patients might therefore highlight differences in terms of induced interhemispheric synchrony in stroke patients which depend on 1). stimulated hemisphere and 2). mu-alpha phase. For these reasons, we investigated whether interhemispheric coherence between sensorimotor regions changes depending on mu-alpha local phase and stimulated hemisphere in strokes and controls.

In conclusion, the presented quantities were computed in both stroke patients and healthy controls to understand how the instantaneous local phase at stimulation time influences 1) post-pulse elicited cortical activity (TEPs, TF) 2) propagation across hemispheres of the effects of stimulation (TEPs and TF) 3) phase-dependent intra-individual variability to stimulation (ITPC) 4) post pulse interhemispheric connectivity (FC, phase-coupling).

2.3 Methods

2.3.1 Participants

Recruitment and testing were carried out by the Brain Networks and Plasticity Group in Tubingen (lab head: Dr. Ulf Ziemann; at the Center of Neurology of the The Hertie Institute for Clinical Brain Research (HIH) and the Clinic of Neurology at University Hospital Tübingen). A total of 20 unilateral chronic strokes and 11 healthy controls in the same age range were included in this experiment. All participants gave their written informed consent to take part into the experiment. Because of data quality issues, data from 3 stroke patients had to be discarded, while only one healthy control had to be discarded for the same reason. Furthermore, because our experimental conditions depended on a post-hoc determination of the mu alpha oscillation phase at the moment of stimulation, the number of trials in a given condition was a variable fraction of the overall number of trials available for the individual patient. For this reason, not all of the 17 stroke patients with good data quality had enough trials in all conditions (>30) and 6 of them had to be discarded from the analysis on TEPs, ITPC, TF and connectivity (see Suppl. Table 2.1 for further details on the number of trials in each patient). Therefore, the final sample included 11 stroke patients and 10 matched controls (for demographic characteristics of the final stroke and control sample, see Table 2.1 and 2.2, respectively).

	Age	**Gender**	**Lesion Site**	**TPS (years)**	**FM**	**SH**	**RMT iM1**	**RMT cM1**
S1	63	M	basal ganglia	2	22/66	left	63%	60%
S2	51	F	MCA	9	44/66	right	48%	48%
S3	60	M	MCA	6	NA	left	54%	65%
S4	79	F	MCA	2	7/66	right	67%	48%
S5	62	M	MCA	6	31/66	left	67%	57%
S6	61	M	MCA	3	37/66	right	66%	73%
S7	66	M	MCA	3	24/66	left	66%	42%
S8	57	F	basal ganglia	2	59/66	right	72%	54%

S9	69	M	basal ganglia	11	19/66	right	73%	40%
S10	60	F	basal ganglia	2	21/66	left	60%	47%
S11	53	F	Fronto-temporal	15	16/66	right	59%	56%
	62 ± 8	F = 5		5 ± 4				

Table 2.1: Stroke patients' characteristics; TPS is time from stroke; FM is Fugl-Meyer score; SH is stroke hemisphere; RMT is resting motor treshold; iM1 and cM1 are affected and unaffected M1 respectively. MCA (middle cerebral artery) patients suffered an ischemic stroke, while the patients with basal ganglia and fronto-temporal lesions suffered from haemorrhagic strokes.

	Age	**Gender**	**RMT lM1**	**RMT rM1**
C1	43	M	56%	60%
C2	60	F	69%	69%
C3	70	M	52%	48%
C4	53	F	76%	70%
C5	47	F	81%	75%
C6	64	F	58%	60%
C7	NA	M	85%	82%
C8	50	M	62%	63%
C9	64	F	54%	64%
C10	61	M	49%	47%
		F=5		

Table 2.2: Healthy controls' characteristics. RMT is resting motor threshold; lM1 and rM1 are left and right M1 respectively.

2.3.2 TMS-EEG Recordings

All participants were seated on a comfortable chair for the whole duration of the TMS-EEG experiment. TMS was delivered using a biphasic stimulator (MagPro R30) connected to a 75 mm hand-held coil (MCF-B65, MagVenture) positioned on the participant's M1. The location of the individual M1 and resting motor threshold

(RMT) was accomplished by using standard protocols on both hemispheres in both strokes and controls. The coil orientation in both stroke and controls was set as the position that elicited the biggest and most constant MEPs in the motor hotspot search (5 out of 10 > 50 μV) in normal posterior-anterior orientation orthogonal to the central sulcus. Pulses at 115% of the individual RMT were delivered on both hemispheres of healthy controls and stroke patients. In healthy controls a total of 800 pulses per hemisphere was delivered, while in stroke patients the number of pulses depended on the tolerance of the individual patient. In stroke patients, EEG recording of cortical responses to TMS were recorded using a 64-channels cap, while in healthy controls a 128-channels cap was used. EEG data were collected continuously (sampling frequency: 5000 Hz). In order to make the stroke patients and healthy controls data comparable (i.e. same number of electrodes), the healthy controls' number of channels was reduced from a 128 channels cap to 64 channels, comparable with the stroke cap both in terms of number and positions of the electrodes.

2.3.3 Preprocessing

Data preprocessing was performed using MATLAB (The Mathworks, Natick, MA, USA) custom code partially based on functions of the open-source toolboxes EEGLAB and TESA (Delorme and Makeig, 2004; Rogasch et al., 2016;). EEG recordings were first visually inspected in order to exclude bad-channels and continuous recordings were then epoched between -1.4 and +1.6 around the pulse. TMS artefacts were removed from each epoch and interpolated between – 5 and 20 ms around the pulse (with cubic interpolation on data 50 ms before and after pulse). Epochs were then visually inspected again to discard bad trials. After, SOUND algorithm, as implemented in TESA, was used to attenuate each channel's noise level due to TMS stimulation and interpolate previously discarded bad-channels (Mutanen et al., 2020). As TESA-SOUND requires a forward head model, we used a standard three-layer spherical head model based on the cap channels' position registered for data recording. Data were then high-pass filtered at 0.5 Hz and data from -5 to 40 ms were removed before using the Fast-ICA TESA implementation for ocular artefacts removal. Epoched data were then baseline corrected (- 500 to -50 ms). Finally, SSP-SIR (Mutanen et al., 2016) algorithm was used to clean EEG data from TMS-induced muscular artefacts. After this, a stopband of 48 – 52 Hz and of the

respective harmonics up to 500 Hz was applied for filtering out the power line noise. Finally, an anti-aliasing filter at 225 Hz was applied before resampling at 500 Hz.

2.3.4 Data Analysis and Statistics

All the following analyses were performed using MATLAB (The Mathworks, Natick, MA, USA) custom code, partially based on functions of the open-source toolbox Fieldtrip (Oostenveld et al., 2011). In order to achieve a phase-dependent analysis of TEPs, ITPC, TF and connectivity in both strokes and controls, we first computed a post-hoc estimate of the phase at which stimulation had occurred in each subject's trial. Right strokes were flipped to the left side in order to be group-consistent in lesion location. Then, individual alpha peak (IAF) was detected for each subject pooling together activity recorded over the sensorimotor Hjorth of both hemispheres (left/*affected* Hjorth: C3, C1, C5, FC3, CP3; right/*unaffected* Hjorth: C4, C2, C6, FC4, CP4). Then, left and right hemisphere Hjorth filters were computed, for each time point, by subtracting from the reference channel of each Hjorth (C3 for left Hjorth and C4 for right Hjorth) the average value across the remaining four channels of the respective hemisphere (C1, C5, FC3, CP3 for left Hjorth and C2, C6, FC4, CP4 for the right Hjorth). Data from each participant's trial was then filtered between +/- 1 Hz around the IAF and an autoregressive model was used to predict the phase at IAF in Hjorth-C3 and Hjorth-C4 separately, depending on the side of stimulation and for both healthy and stroke patients (in our stroke datasets we flipped the layout so as the UH was always the right one). In this way, for both strokes and controls, we defined four stimulation conditions, depending on the stimulated hemisphere and targeted IAF phase: *unaffected*/right at *trough*, *unaffected*/right at no-*trough*, *affected*/left at *trough*, *affected*/left at *no-trough*, where the *trough* condition refers to trials in which the pulse was delivered when the phase of the IAF oscillation was between 150 and 210 degrees, and the *no-trough* condition refers to trials at the remaining phases. The reason we choose this scheme for defining phase dependent conditions is twofold. First of all, our classification of the trials is based on a post-hoc phase estimation. The number of trials in a certain condition depends on how many stimuli were delivered (by chance) within a certain phase interval at IAF in the experimental session. In this selection process a reasonable requirement is that a subject can be included in the analysis if there are at least 30 trials for both conditions (*trough* and *no-trough*). The number of trials for each condition depends on the phase interval (the larger the

interval the higher the number of trials) while its variability depends on the total number of trials in a given subject. In this framework, it is clear that defining conditions on the basis of small intervals (e.g: considering *trough* and *peaks*) will result in discarding more subjects, because the variability affects the number of trials for both the phase conditions together. On the other hand, there is robust evidence, so far, that mainly the *trough* is a high-excitability state, while the effect of stimulating at the positive peak does not dramatically differ from random phases (e.g. Zrenner et al., 2018). For these reasons, we decided to compare the trials in which the stimulation fell at *trough* with the trials at which stimulation fell at all the other phases (*no-trough*). For each of these conditions and separately for the healthy and controls, TEPs ITPC and TF analyses were performed. Since, as frequent in clinical research, stroke patients could not stay as long as controls in the experiment, only 11 out of the original 19 strokes sample were found to have enough trials (>30) in the *trough* condition and therefore were kept for further statistical analysis (see Table 2.1 for final sample characteristics).

Specifically, TEPs were computed between -0.5 and 0.75 s around the pulse and rectified after computing the grand-averages of each subject in each condition. After this, group statistical clustering between TEPs conditions was achieved using a bootstrap non-parametric paired-samples t-tests (N randomizations = 1000). For multiple comparisons correction, a cluster approach was used and the channel neighbours' structure was determined by the distribution of the 64 channels in the cap (minimum number of neighbouring channels = 2; alpha = 0.05). The cluster statistics comparing the TEPs in the contrasts of interest were computed over the following time windows of interest, in order to be sensitive to the latencies of the typical M1 TEPs peaks (P25, N45, P70, N100): 0.02 - 0.04; 0.04 - 0.055; 0.055 - 0.075; 0.089 - 0.129 (Desideri et al., 2019).

Furthermore, for each condition, the ITPC and its time modulation was computed using a Hanning taper between 4 and 36 Hz on sliding windows of step (interval -0.15 s to 0.3 s from the stimulation trigger). The size of the sliding time window for the Fourier analysis was set to 3 cycles of the frequency of interest. ITPC values were computed from Fourier coefficients and then Fisher-regularized with the inverse hyperbolic tangent. Statistical analysis was computed in the same way as for the TEPs statistics, but separately for the frequency bands theta (4 – 7 Hz) and beta (13 – 30 Hz), averaging ITPC values over each band. The alpha frequency was not investigated with ITPC because the two experimental conditions were determined on the basis of the pre-stimulus alpha phase. Indeed, we defined the two *trough*/ *no-trough* conditions by the phase

of the IAF oscillation at stimulation being in one of two intervals that differs in size (60° for the *trough*, 300° for the *no-trough*). This, in principle, will introduce a bias in the ITPC computation: in particular, we expect the ITPC in the *trough* condition being higher because the phases for this condition are bound in a smaller interval by design. For this reason, we did not analyse and interpret ITPC at the alpha frequency, being it impossible, in the current design, to disentangle genuine effects of the stimulation from the above mentioned bias effect.

Furthermore, for each condition, TF analysis was performed. TF coefficients were computed between 2 and 50 Hz and between 0.025 s to 0.8 s in steps of 0.025 ms using a multi-taper-method based on discrete prolate spherical sequences (DPSS). TF statistics between the conditions of interest was run in the same way as for TEPs and ITPC, but separately for the three frequency bands of interest theta (3 – 7 Hz), alpha (8 – 12 Hz) and beta (13 – 30 Hz) and on the continuous time rather than on specific TOIs (this in order to allow potential effects in the theta band to emerge).

Moreover, on the same 11 strokes and 10 controls, TEPs were also computed with no phase-dependent post-hoc sorting on left and right hemisphere (C3, CP3, CP5 for left and C4, CP4, CP6 for right) in order to compare our results with previous literature (Casula et al., 2021). Furthermore, TEPs computed without post-hoc sorting over all channels, were also used for statistical comparisons between hemispheres.

Finally, connectivity analyses were performed using two different connectivity metrics (weighted pairwise phase consistency (WPPC; Vinck et al., 2011) and phase-locking value (PLV, Lachaux et al., 1999)). Both WPPC and PLV were computed between 7 and 35 Hz starting from the Fourier coefficients of 1) the left and right Hjorths 2) the original Fourier coefficients of each single channel used for computing the Hjorth signals. The latter analysis has been performed in order to exploit peaks of coupling between Hjorth channels that could have been, in principle, masked by computing the Hjorth signals before connectivity analysis. These analyses were run in order to understand whether the phase-synchronization between the left and right hemisphers of both healthy and stroke patients changed depending on the stimulated hemisphere and the mu alpha phase at the moment of stimulation. In 1) the left and right Fourier transforms for each participant were computed (DPSS single taper with 1.67 Hz smoothing from 7 to 35 Hz) from Hjort transformed signals in the following time windows of interest: pre-pulse: - 650 ms to – 50 ms; post-pulse: 50 ms to 650 ms). Afterwards,

PLV and WPPC between the left and right hemispheres were computed and Fisher-regularized by means of the inverse hyperbolic tangent. As for the analysis 2) Fourier transforms were computed from each single channel of the left and right Hjorths and then interhemispheric PLV and WPPC connectivity was estimated and Fisher-regularized for each left/right combination, resulting in a 5 x 5 connectivity matrix. PLV and WPPC connectivity matrices were then reduced by taking the mean or the median of all matrix elements, resulting, as in 1), in a single PLV and WPPC value for the interhemispheric connectivity in each condition and matrix reduction method. Connectivity results for all subjects from 1) and 2) were then compared between the conditions of interest using a dependent sample t-test with a bootstrap approach (number of randomization: 2000; alpha: 0.05; cluster correction for multiple comparisons;). The contrasts of interest, in both strokes and controls, and for both types of connectivity analysis (Hjorth signals or single channels) were the following: (1) post-pulse period with stimulation at *trough* vs *no-trough*; (2) pre- vs post-pulse windows after stimulation at *trough*; (3) pre- vs post-pulse windows after stimulation at no *trough*; moreover, for the strokes: (4) post-pulse period stimulation at *trough* or *no-trough* in AH vs UH stimulation. Additionally, for both healthy and controls, the same connectivity analyses were implemented also in a non-phase-dependent manner, meaning without separating the trials on the basis of the mu alpha phase. In the PLV and WPPC analyses with no phase post-hoc sorting, conditions depended only on the stimulated hemisphere and the statistical test assessed potential differences between the interhemispheric coherence after stimulation in the left vs right hemisphere of controls and AH vs UH of stroke patients.

2.4 Results

2.4.1 TEPs and ITPC results with post-hoc sorting based on mu-alpha phase detection

As expected, TEPs elicited by stimulation at *trough* were larger in amplitude compared to stimulation at *no-trough* in healthy controls. In fact, in the 40 – 50 ms time window, stimulation at *trough* in the right hemisphere elicits stronger TEPs with a positive significant cluster ($p = 0.004$) compared to stimulation at *no-trough*. In the 55 – 75 ms time window, two positive significant clusters are found, both in the stimulated hemisphere and in the left hemisphere contralateral to stimulation ($p = 0.046$; $p= 0.051$, respectively). In the earliest time

window (20 – 40 ms) statistical results show a tendency for a positive significant cluster (p= 0.054) (see Suppl. Fig. 2.1). Statistical analyses on the ITPC results between the same conditions (healthy right hemisphere stimulation at *trough* vs *no-trough*), show that ITPC is larger in the beta band (13 – 30 Hz) when stimulation is given at *trough* compared to *no-trough* (p= 0.004). No difference was found between the two conditions when the statistical test on ITPC was run in the theta band (4 – 7 Hz). No significant differences were found between stimulation at *trough* and *no-trough* in left hemisphere of healthy controls, except for a tendency towards stronger TEPs in the left hemisphere when stimulated at *trough*, in the 55-75 ms time window.

Differences between left and right stimulation at mu-alpha *trough* were furthermore investigated comparing the two hemispheres of healthy controls. The logic behind this approach is the following: by comparing the two hemispheres when they are stimulated at the same excitability state (e.g. *trough*) should return specular positive and negative clusters if stimulation induces in the two hemispheres similar activations. Differently, the absence of specular positive and negative clusters suggests that the two hemispheres are reacting dissimilarly. Therefore, similar activation patterns are expected in the right and left hemisphere in healthy controls. Hence, we ran the cluster analysis between right vs left hemisphere stimulated at mu-alpha *trough*. Results show stimuli to provide for a similar activation (TEPs) in the stimulated hemisphere, revealing a tendency towards both specular positive and negative clusters in the 40 – 55 ms and 55 – 75 ms time windows (see Fig. 2.1 for all cluster p-values).

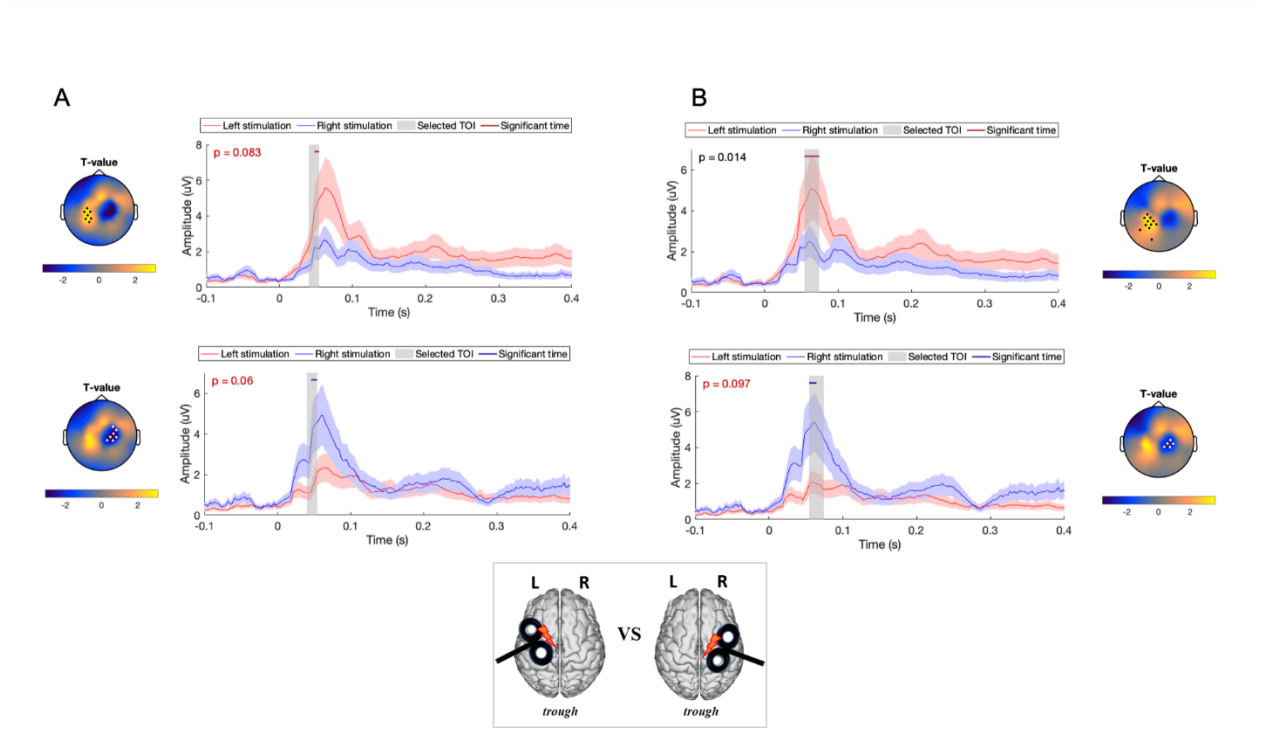

Figure 2.1: Significant clusters for rectified TEPs statistic comparing left vs right stimulation at trough in healthy controls. Time window of interest: A) 40 -55; B) 55 -75 ms.

In stroke patients, we first looked into differences between the AH stimulation at *trough* vs *no-trough*. We found stimulation at *trough* in the AH to elicit greater TEPs in both the AH and UH compared to stimulation at *no-trough*. This difference emerges already in the early time window post-pulse, showing a positive cluster in the *affected* stimulated hemisphere (p = 0.03, Fig. 2.2A). In the later time window (40 – 55 ms), stimulation at *trough* leads to significant positive clusters in both the UH and AH (p = 0.049; p = 0.014; p = 0.005, Fig. 2.2B). The TMS-evoked activity elicited by the AH stimulation at *trough*, compared to *no-trough*, propagates in the UH contralateral to stimulation where a significant positive cluster is present in the 55-75 ms time window (p = 0.011; Fig. 2.2C). Cluster statistics on ITPC results showed that, stimulation at *trough* elicits greater ITPC in beta compared to stimulation at *no-trough* for the entire time window also in the AH (p = 0.001; Fig. 2.2D). No differences in theta ITPC is found depending on the stimulation condition (*trough*/*no-trough*) in the AH (Fig. 2.2D).

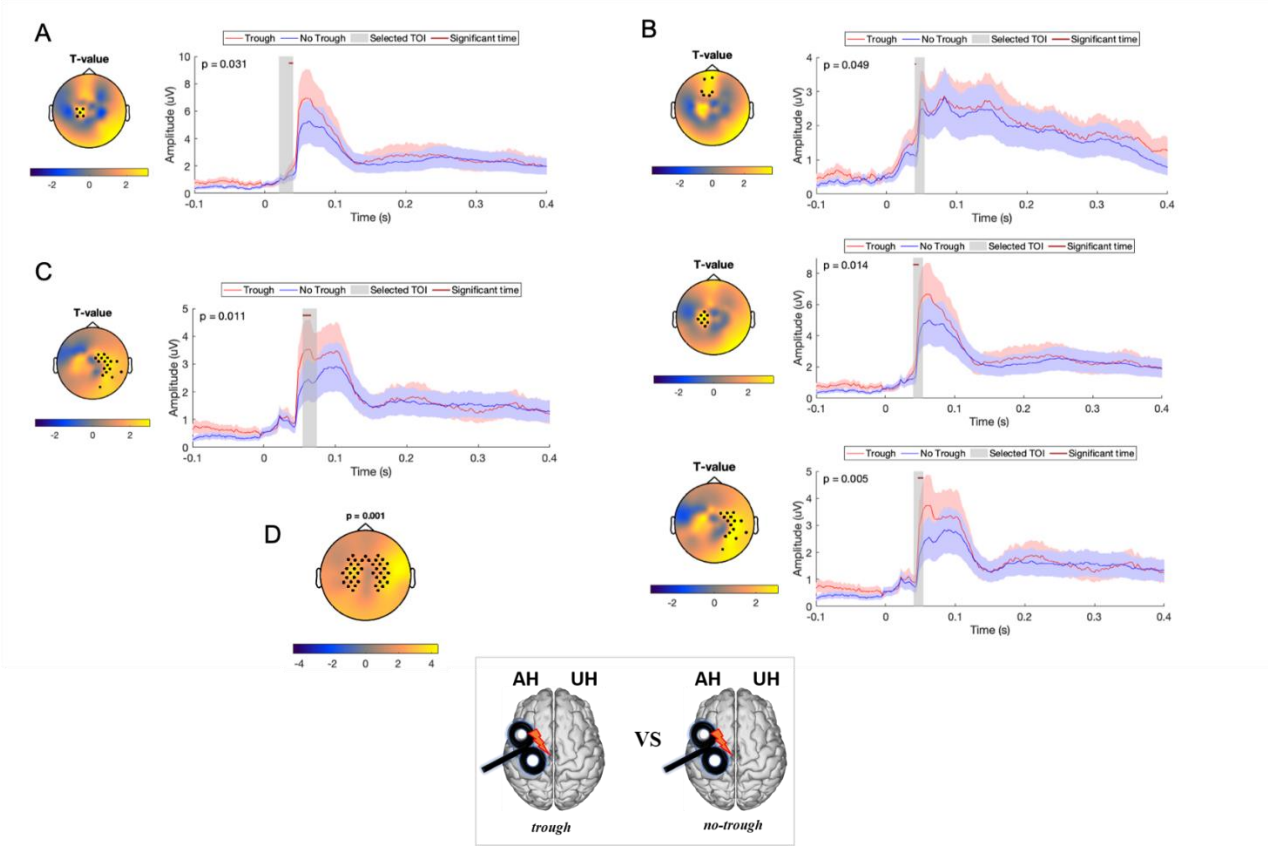

Figure 2.2: rectified TEP activity for significant clusters comparing trough vs no-trough for ipsilesional stimulation. Black/white dots in the topoplots refer to positive/negative clusters, respectively. Time window of interest: A) 20 -40 ms; B) 40 -55; C) 55 -75 ms. D) T value and cluster of significant electrodes in the comparison of ITPC between trough and no-trough for ipsilesional stimulation in the beta band.

The same comparisons were computed for the UH, contrasting the UH stimulation at *trough* vs *no-trough*. We found similar results as in the AH, with stimulation at *trough* eliciting stronger TEPs in both the stimulated UH and in the AH contralateral to stimulation. However, the difference between TEPs elicited by the *trough* stimulation emerges only later in the UH (40 – 55 ms; p = 0.03) compared to the difference in the AH that emerged already in the 20 - 40 ms time window (Fig. 2.3A to be compared with Fig. 2.2A). This indicates that no phase-dependent significant difference in TEPs is present in either hemisphere when UH is stimulated in the early time window (20-40 ms after stimulation). In the comparison between UH stimulation at *trough* vs *no-trough*, statistics on ITPC results shows that stimulation at *trough* compared to *no-trough* in the UH elicits stronger ITPC in both theta (p = 0.002) and beta (p= 0.004; p = 0.013) (Fig. 2.3D and 2.3E).

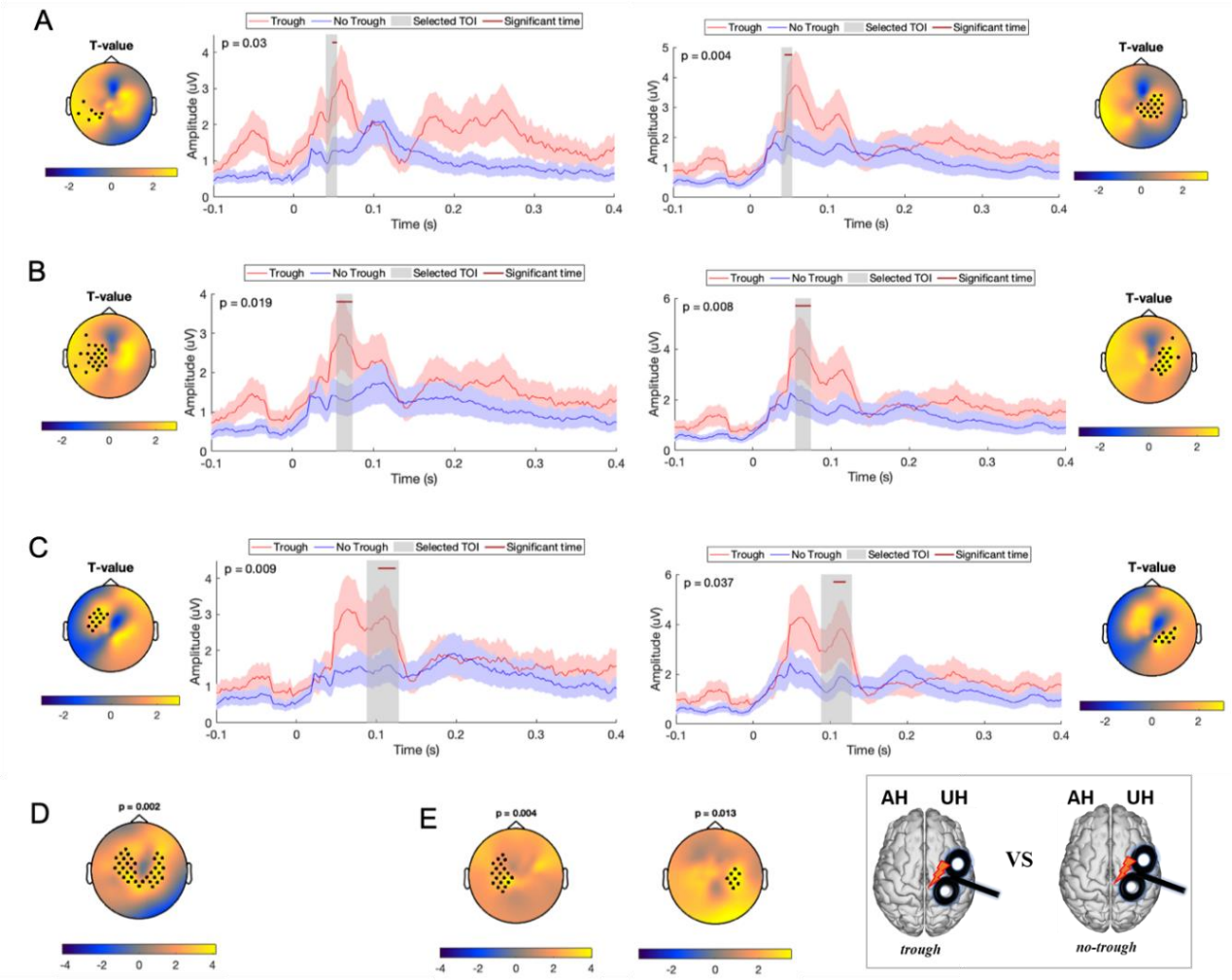

Figure 2.3: rectified TEP activity for significant clusters comparing trough vs no-trough for contralesional stimulation. Black/white dots in the topoplots refer to positive/negative clusters, respectively. Time window of interest: A) 40 -55 ms; B) 55 -75 ms; C) 89 - 129 ms. D) and E): T-value and clusters of significant electrodes in the comparison of ITPC between trough and no-trough for contralesional stimulation in the theta (D) and beta (E) band.

Furthermore, we contrasted the two hemispheres (AH vs UH), comparing them both when stimulation falls at the *trough* and at the *no-trough*, separately. The logic behind this contrast is the same used for healthy controls: if the two hemispheres are reacting analogously when stimulated either at *trough* or at *no-trough*, we should find opposite specular clusters as in healthy controls. Instead, we found that only a negative cluster emerges in the early 20 – 40 ms time window. This shows that the UH stimulation at *trough* elicits stronger early TEPs in the UH compared to the TEPs induced from the *affected* side stimulation at *trough* to the UH contralateral to stimulation ($p = 0.035$). Also, the absence of a positive specular cluster in the AH suggests that the TEPs elicited by the AH stimulation at *trough* in the AH itself are not significantly different from the TEPs conducted

to the AH when the UH one is stimulated at *trough* (Fig. 2.4A). Results from cluster statistics on ITPC between AH vs UH when stimulation falls at *trough* show stronger ITPC in theta in the AH when the AH itself is stimulated compared to when the UH is stimulated at *trough*. The absence of a specular negative cluster indicates that ITPC in theta does not change in the UH when stimulation falls at *trough* in the *affected* one compared to when it falls at *trough* in the UH itself (Fig. 2.4B).

In the later time windows the contrast between the AH stimulation vs UH stimulation at *trough* on TEPs shows a tendency towards two opposite specular clusters (p= 0.03; p = 0.069; Fig. 2.5A). Finally, in the time window 55 – 75 ms, the contrast between AH vs UH stimulation at *trough* shows a tendency only towards one positive cluster in the AH. This suggests that '*trough*' TEPs evoked in the AH, are greater compared to the same TEPs elicited by the UH stimulation in the *affected* one contralateral to stimulation (p = 0.049). The absence of a negative specular cluster suggests that there is no significant difference between the '*trough*' TEPs elicited in the UH compared to the same TEPs elicited by stimulation in the AH in the *unaffected* one contralateral to stimulation (Fig. 2.5B). Moreover, ITPC cluster statistics returns a positive cluster in theta ITPC in the AH (p = 0.028; Fig. 2.5C) in the contrast between the AH and UH stimulated at *trough*.

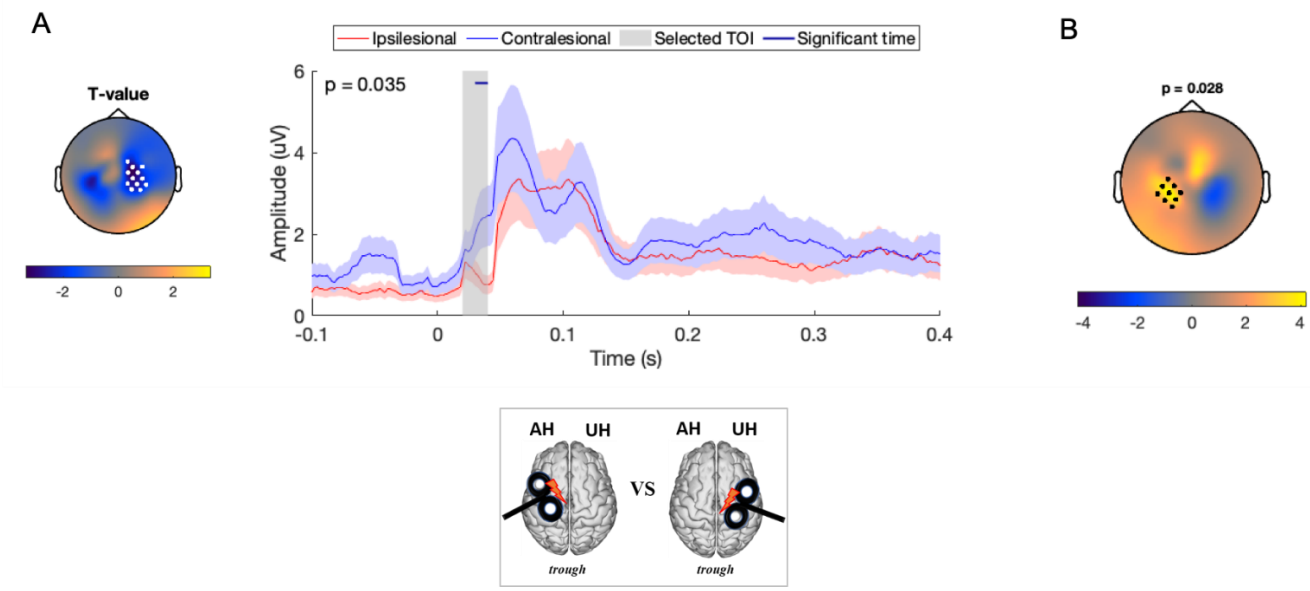

Figure 2.4: A) rectified TEP activity for significant clusters comparing ipsilesional vs contralesional stimulation at trough in the 20 – 40 ms time window. Black/white dots in the topoplots refer to positive/negative clusters, respectively. B) T-value and cluster of significant electrodes in the comparison of ITPC at trough between ipsilesional and contralesional stimulation in the theta band.

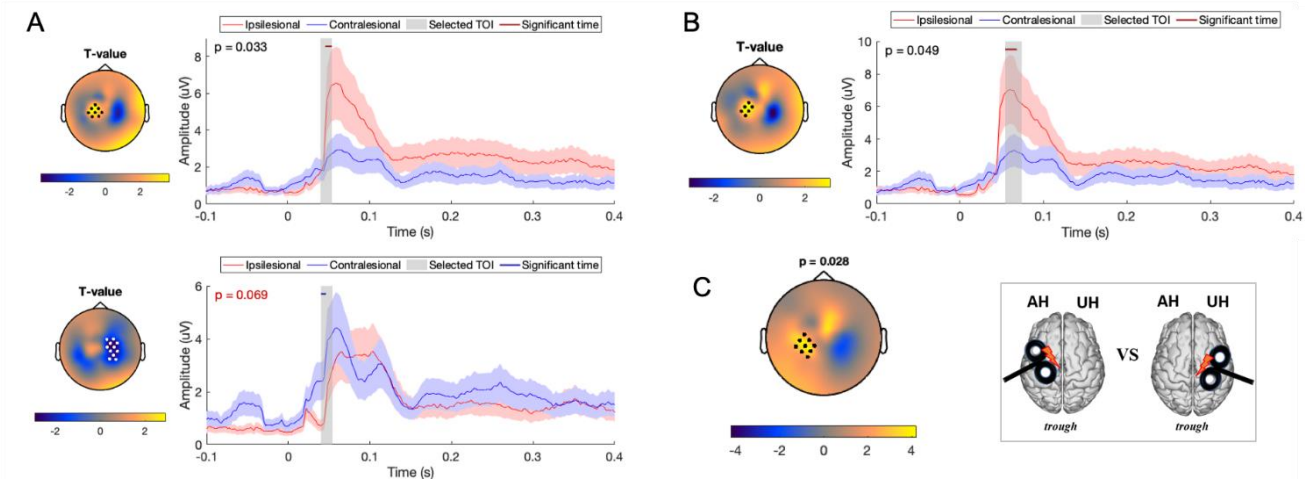

Figure 2.5: rectified TEP activity for significant clusters comparing ipsilesional vs contralesional stimulation at trough. Black/white dots in the topoplots refer to positive/negative clusters, respectively. Time window of interest: A) 40 -55 ms; B) 55 -75 ms. C) T-value and cluster of significant electrodes in the comparison of ITPC at trough between ipsilesional and contralesional stimulation in the theta band.

Furthermore, we investigated the contrast between the AH vs UH when they are stimulated at *no-trough*. While in healthy controls no difference is detected between the two hemispheres for stimulation at *no-trough*, in stroke patients two positive clusters emerge in the AH in the 40 – 55 and 55 -75 ms time windows respectively, showing greater TEPs in the AH when this has been stimulated at *no-trough* compared to the TEPs elicited in the AH from '*no-trough*' stimulation in the UH (p = 0.031, p = 0.019; Fig. 2.6). The absence of a specular negative cluster suggests that the '*no-trough*' TEPs elicited in the UH are not significantly different from the same TEPs elicited in the UH, contralateral to stimulation, by AH stimulation at the *no-trough* state (Fig. 2.6). Interestingly, in the ITPC analysis comparing the AH vs UH at the *no-trough* stimulation condition, a positive cluster emerges again in the AH in the theta band (p = 0.008, Fig. 2.6C). For a summary of the TEPs and ITPC results in stroke patients, see Suppl. Table 2.2 and Suppl. Table 2.3.

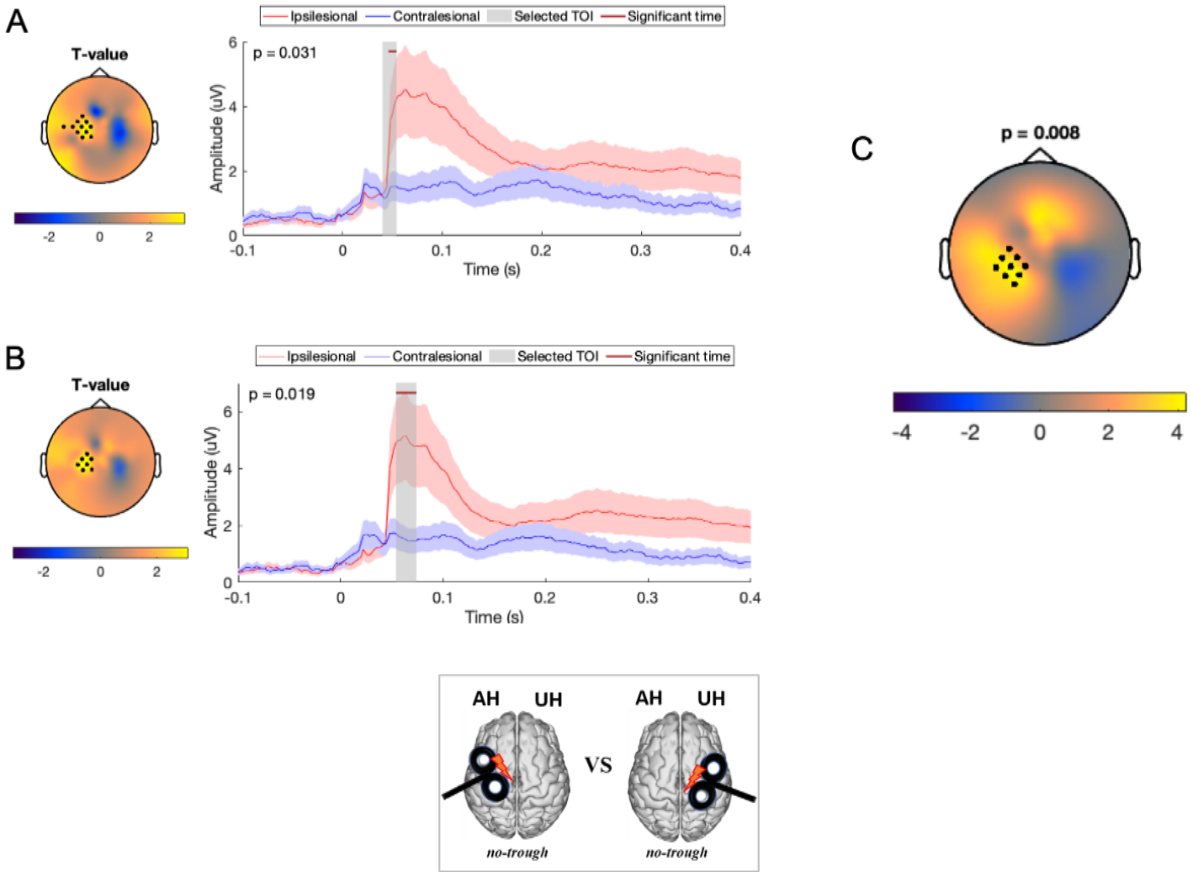

Figure 2.6: rectified TEP activity for significant clusters comparing ipsilesional vs contralesional stimulation at no-trough. Black/white dots in the topoplots refer to positive/negative clusters, respectively. Time window of interest: A) 40 -55 ms; B) 55 -75 ms. C) T-value and cluster of significant electrodes in the comparison of ITPC at no-trough between ipsilesional and contralesional stimulation in the theta band.

2.4.2 TEPs results with no post-hoc sorting

We also looked into the results obtained on the TEPs computed with no post-hoc sorting over the restricted C3- and C4- Hjorths in both strokes and controls. From this analysis, a general stronger response of the AH emerges, compared to both the UH and controls (Suppl. Fig. 2.2A). Also, an hypersimplified response of the AH can be appreciated, compared to both the UH and healthy controls (Suppl. Fig. 2.2B plot showing the grand-average TEPs time series). Furthermore, results from the cluster statistics on AH *vs* UH stimulation computed with no phase post-hoc sorting show an early (20-40 ms) tendency of the UH to be more excitable compared to the AH (Suppl. Figure 2.3). In fact, we do find a tendency for a negative cluster showing stronger TEPs in the UH ($p < 0.1$). We did not find a specular and opposite positive cluster in the AH suggesting that the activity evoked by the single TMS pulse over the AH in the 20-40 ms post-pulse time window is not

significantly different from the activity conducted from the UH to the AH when UH is stimulated (Suppl. Fig. 2.2). Differently, the strong and simplified evoked response of the AH emerges later, since the comparison between AH vs UH stimulation shows only positive clusters in all the three later time windows of interest (40 – 55 ms, p = 0.02; 55 – 75 ms, p = 0.023; 89 – 129 ms, p = 0.06) (Supp. Fig. 2.3).

2.4.3 TF results

We analysed the TF between-hemispheres comparison both in the healthy and stroke group. In healthy controls, stimulation at *trough* elicits stronger power, compared to the *no-trough* stimulation, immediately after stimulation in all frequency bands (theta, alpha and beta). However, we found stronger theta power when stimulation falls at *trough* vs *no-trough* only in the right hemisphere and at a very long latency with respect to the TMS pulse (right hemisphere *trough* vs *no-trough*, positive significant cluster with p-value: 0.006 from ~0.3; Supp. Fig. 2.4). This greater theta power is detected over both hemispheres when stimulation falls in the right hemisphere of healthy controls. Also, healthy controls show greater increase in alpha power after stimulation at *trough* compared to *no-trough* in both hemispheres and this difference is visible already immediately after stimulation. In the right hemisphere stimulation, the contrast between *trough* vs *no-trough*, shows a unique and continuous positive cluster in alpha. (p = 0.013) Differently, in the left hemisphere stimulation the contrast between *trough* vs *no-trough*, returns two significant positive clusters, an early one and a later one (p= 0.02; p = 0.002, respectively; Supp. Fig. 2.4). Despite this small difference between the left and right hemispheres changes in alpha power depending on the stimulation condition, they both show stronger alpha power in healthy controls when stimulation falls at *trough* compared to *no-trough*.

In the beta band, stimulation at *trough* elicits stronger beta power bilaterally immediately after the pulse, compared to *no-trough* stimulation. In this case, the contrast between left hemisphere stimulation at *trough* vs *no-trough* returns differences in the beta band earlier compared to the right hemisphere stimulation (p: 0.001; p = 0.002; Supp. Fig. 2.4).

Also in stroke patients we looked into TF differences between stimulation at *trough* vs *no-trough*, in the AH and UH, separately. We found no difference between stimulation at *trough* vs *no-trough* in theta in the

AH, except for a small positive cluster emerging around 700 ms post-pulse (p-value: 0.01; Fig. 2.7). Instead, stimulation at *trough* vs *no-trough* in the *UH* elicits larger theta power in both hemispheres already at 300 ms post pulse (p-value = 0.001; Fig. 2.7). Furthermore, stimulation at *trough* elicits stronger power in both alpha and beta band also in stroke patients. However, in the UH, stimulation at *trough* elicits stronger power in alpha compared to stimulation at *no-trough* bilaterally (p-value: 0.001; Fig. 2.7), while in healthy controls it is localized initially only in the stimulated hemisphere (Suppl. Fig. 2.4). Stimulation at *trough* in the AH elicits no differences in alpha power compared to stimulation at *no-trough* until 250 ms from the pulse and, only after that, a difference in alpha power is detected between stimulation at *trough* vs *no-trough* first in the hemisphere contralateral to stimulation (UH) and then in both hemispheres (p-value: 0.001). Importantly, the differences here described on the alpha power between stimulation at trough vs no-trough in the affected hemisphere (detectable only after 200 ms post pulse) demonstrates that, at group level, the alpha activity is detectable in the affected hemisphere. Nevertheless, a further sanity check was computed and the power spectrum of each subject, separately for the affected and unaffected Hjorths, is shown (Suppl. Fig. 2.5). From it, it can be seen that the two hemispheres show similar power spectra and that alpha is detectable in both.

In the beta band, power is also larger in both hemispheres of stroke patients when stimulation falls at the *trough* compared to *no-trough*. However, stimulation at *trough* in the UH elicits stronger beta power, compared to stimulation at *no-trough*, initially in the AH contralateral to stimulation (p-value: 0.0009) and then bilaterally from 250 ms (p-value = 0.001). The contrast between stimulation at *trough* vs *no-trough* in the AH, instead shows stronger beta at first in the stimulated AH and only later bilaterally (p = 0.001) (Fig. 2.7).

For a summary of the TF results in stroke patients, see Suppl. Table 2.4.

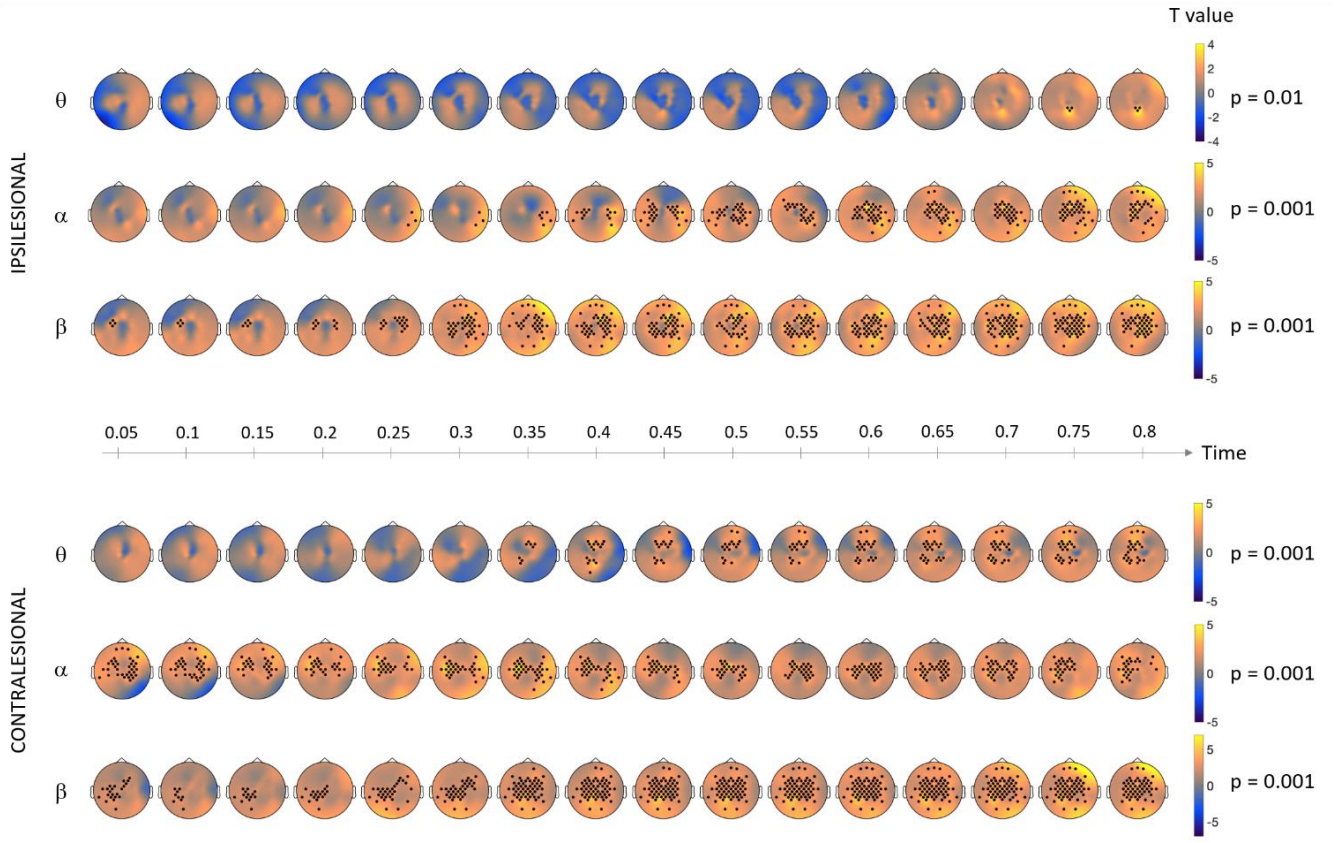

Figure 2.7: Cluster statistics on TF between stimulation at trough vs no-trough in contralesional and ipsilesional, separately in the theta, alpha and beta band. Black dots in the topoplots refer to positive cluster;

2.4.4 PLV and WPPC Connectivity

Connectivity analyses did not show significant results in any of the analyses performed and conditions tested. In fact, neither the PLV nor the WPPC analyses on both the Hjorths and reduced (mean or median based) channels coefficients led to significant results in strokes and controls. Furthermore, no significant result was found in the non-phase-dependent analysis of PLV and WPPC.

2.5 Discussion

This work aimed at understanding whether differences, in terms of TEPs, ITPC, TF spectrograms and connectivity between the AH and UH can be appreciated using a post-hoc phase-dependent approach in the analysis of TMS-EEG data. To test this, we implemented TEPs analysis both with and without (as in Casula et al., 2021; Tscherpel et al., 2020) a phase sorting. As expected, results show that the phase-dependent analyses allow to explore in greater detail the cortical responses to TMS in the two hemispheres of stroke patients, compared to the non-phase-dependent analyses. We only found a large and hypersimplified response of the AH with no phase-bin sorting (Suppl. Fig 2.2). This increased TMS-evoked EEG response of the AH in our sample of mostly severely impaired strokes, was expected. In fact, this pattern was previously described in moderately to severely affected patients (Tscherpel et al., 2020; Sarasso et al., 2020) but not in less affected patients (Casula et al., 2021).

Furthermore, averaging TEPs over long time-windows (e.g. Casula et al.: 20 – 150 ms; Tscherpel et al.: 10 – 100 ms) appears to mask effects that can be informative on the excitability properties of the two hemispheres in stroke. In fact, in Suppl. Fig. 2.2A and 2.2B we replicated the analysis of Casula et al. (2021) and Tscherpel et al. (2020), respectively. From these results, the AH strong evoked response can be appreciated as in Tscherpel et al. (2020) and Sarasso et al. (2020). At the same time, when the excitability of the two hemispheres was investigated with a cluster statistic on the non-phase-dependent TEPs computed over short time-windows centred around the main TEP latencies (like in Desideri et al., 2018 and differently from Casula et al., 2021 and Tscherpel et al., 2020), an initial tendency towards stronger TMS-evoked response and stronger propagation from the UH can be further appreciated. In fact, a negative cluster in the 20-30 ms window was detected in UH (Suppl. Fig. 2.3). The presence of a negative cluster, together with the absence of an opposite specular one in AH, indicates that the P25 component elicited in AH when AH is stimulated is not statistically different from the signal propagated to AH by UH stimulation in the 20-30 ms time window post-pulse. Therefore, from the non-phase dependent statistical contrasts on the TEPs of the AH vs UH stimulation over short time windows, we detected an initial (20 – 30 ms) tendency of UH towards a stronger evoked response

compared to AH, followed by the later AH strong cortical response already pointed out in the previous studies (Tscherpel et al., 2020; Sarasso et al., 2020).

Results from phase-dependent analyses revealed differences in the excitability properties of the two hemispheres (with the exception of connectivity metrics). Critically, these differences depend on local mu-alpha phase in TEPs, ITPC and TF spectrograms elicited by the TMS pulse.

We first analyse results obtained from the cluster statistics in the healthy group, comparing the two hemispheres when they are excited at the same local state. Fig. 2.1 shows the results from the cluster statistical contrasts on TEPs between left and right hemispheres after *trough* stimulation. A tendency towards specular clusters can be detected at N45 and P60 components, suggesting that the two hemispheres tend to respond in a similar way to the TMS stimulation in the healthy group when stimulated at the same local state. This result appears not surprising in healthy controls, as the two hemispheres in the control group are not supposed to show differences in their responses to the TMS pulse when they are stimulated in correspondence of the same local state. Differently, the cluster statistics comparing the AH vs UH for the *trough* stimulation shows that the two hemispheres do not respond in the same way to stimulation at the same local state in the stroke brain. In fact, in the early time window post-pulse (20 – 40 ms) we find one negative significant cluster, meaning that stimulation in UH' elicits a P25 response that is larger compared to the P25 elicited with stimulation in AH when the pulse falls at *trough* (Fig. 2.4). In later time windows, the opposite pattern is true, as only positive clusters can be found, suggesting that, after 40 ms from the pulse at *trough*, the AH generally exhibits larger TMS-evoked EEG responses compared to UH (Fig. 2.5). Finally, AH and UH were compared for the *no-trough* stimulation (low excitability state). From this analysis, only significant positive clusters emerged, indicating larger TMS-evoked EEG responses in AH also when stimulation falls at trough, compared to the UH which exhibits reduced evoked responses when stimulated at the *no-trough* compared to AH (Fig. 2.6). Therefore, while stimulation at the same phase state in healthy controls elicits similar activity patterns in the two hemispheres, in stroke patients this does not apply.

To better understand the excitability properties of the stroke brain, we performed statistical comparisons between TEPs elicited at *trough* vs *no-trough* state in the same hemisphere stimulation. These

analyses showed that targeting the *trough* elicits in general greater TMS-evoked EEG responses compared to stimulation at no *trough*, in both healthy controls and stroke patients. This result was expected, since targeting the *trough* of the mu alpha rhythm was found to elicit greater TEP (P70 and N100) components compared to stimulation at the positive peak in healthy subjects (Desideri et al., 2019; Desideri, 2020). Specifically, in our control group we found that, the N45 and P70 components showed greater amplitudes after stimulation at *trough* compared to no *trough* (Supp. Fig. 2.1).

In stroke patients, the AH stimulation elicited greater N45 and P70 components when stimulation had fallen at *trough* vs *no-trough*, as in controls (Fig. 2.2). The UH stimulation elicited greater amplitudes in the N45, P70 and N100 components when stimulation fell at *trough* compared to *no-trough* (Fig. 2.3).

Importantly, by comparing Fig. 2.2 with Fig. 2.3, it can be noticed that the phase-dependent differences in TEPs' time courses are strongly more evident in UH compared to AH stimulation. Also, the AH comparison between stimulation at *trough* vs *no-trough* (Fig. 2.2) shows no phase-dependent differences beyond 55 ms post-pulse. Differently, the UH stimulation at *trough* elicits stronger TEPs than at *no-trough* up to 130 ms after the pulse (Fig. 2.3). The lower differentiations between the two excitability states in AH vs UH is further confirmed by the contrast between the two hemispheres when stimulation falls at *no-trough* (the low excitability state) (Fig. 2.6). In Fig. 2.6, stimulating at the *no-trough* in AH leads to larger TEPs in AH compared to the TEPs elicited in AH by UH stimulation at *no-trough*. The absence of a specular negative cluster indicates that, when at *no-trough*, AH stimulation elicits TEPs in UH which are not significantly different from TEPs evoked in UH when this is stimulated at *no-trough* itself. For this reason, we can ascribe the lower differentiation between the excitability states in AH to a higher excitability of AH when stimulation falls at the *no-trough* state, compared to UH.

The low differentiation between the two excitability states in AH can be appreciated also from ITPC results. In fact, we found no phase-dependent modulation in the theta ITPC when the AH is stimulated. The only difference between the AH stimulation at *trough* vs *no-trough* is a stronger ITPC in beta after stimulation, suggesting less intra-individual (i.e. inter-trial) variability in beta when stimulation falls at the *trough* vs *no-trough* in the AH. Differently, we found no difference in theta intra-individual variability (theta ITPC)

depending on the local state at the moment of stimulation in the AH (Fig. 2.2). Instead, in the UH the cluster statistic comparing the ITPC after stimulation at *trough* vs *no-trough* shows greater ITPC in both theta and beta after stimulation at *trough* compared to no *trough* (Fig. 2.3). These results suggest no phase-dependent TMS modulation in theta ITPC in the AH. Furthermore, when the AH vs UH stimulations are compared at trough, only a greater theta ITPC in the AH is detected (Fig. 2.4 and Fig. 2.5). The same pattern emerges when the AH and UH' stimulations are compared at the no *trough* state (Fig. 2.6). The absence of a negative cluster in UH in the theta band ITPC suggests that the UH stimulation elicits the same theta ITPC in the UH as the stimulation in the AH. The peculiar role of theta phase consistency across trials when the AH is stimulated needs to be investigated in deep. In fact, only one other work had investigated theta ITPC in stroke patients, showing a first decrease, immediately after stroke, of theta ITPC in the AH, followed by a later increase in theta ITPC, which was interpreted by the authors as an effect of network remodelling (Gyulai et al., 2021). This interpretation of theta as involved in network remodelling might be in line with works showing that theta coherence is involved in cortico-subcortical communication, which might reasonably be altered by the lesion especially in the AH (e.g. van Wijk et al., 2022). Furthermore, theta connectivity alterations have been linked with cortico-cortical and cortico-subcortical alterations in the stroke brain and especially in the AH (Caliandro et al., 2016). However, the patients included in our sample are in their chronic stage, while the ones included in Gyulai et al. (2021) were tested twice (acute stage and three months' post stroke). Gyulai and colleagues (2021) explained the increase in theta ITPC during recovery in the AH as a by-product of network remodelling. However, given that our stroke patients are both severe and also more chronic (all of them at least >1 year from stroke), we wonder whether the less intra-individual variability in theta ITPC and its general increase in AH compared to UH might still be a by-product of network remodelling in our stroke sample or if its role might more likely be the product of disruptions in cortico-cortical and cortico-subcortical networks.

In the TF spectrograms of healthy controls, we found larger alpha and beta power increases when stimulation is given at *trough* vs *no-trough*. In the alpha band, the increase is initially localized in the stimulated hemisphere, while in the beta band it is more bilateral right after stimulation (Suppl. Fig. 2.4). Post-pulse power modulation (desynchronization and rebound) in alpha and beta after single pulse TMS was reported in healthy

subjects (e.g. Fecchio et al., 2017; Manganotti et al., 2012). Our results on a greater alpha power following stimulation at trough vs no-trough appear in line with previous evidence on the relationship between alpha power and the level of activation of the cortex (Veniero et al., 2011). Also, our phase-dependent results on modulation of alpha and beta power reminds of the results from works showing post-pulse alpha and beta lasting changes following rTMS intervention (Chung et al, 2015). rTMS interventions change the excitability of the cortex and lead to post-pulse modulation in alpha and beta power later tested with spTMS. This seems in line with our results on a phase-dependent modulation of alpha and beta power, as the phase of the mu alpha rhythm modulates the excitability of the cortex.

TF results further confirmed the low differentiation between the two excitability states in the AH. As expected, this occurred peculiarly in the alpha modulation. In fact, as for the alpha power phase-dependent modulation, the UH shows greater alpha power all over the brain after stimulation at *trough* compared to when stimulation falls at no *trough*. Differently, when stimulation falls in the AH, no phase-dependent modulation in the alpha band can be appreciated up to 200 ms after the pulse (Fig. 2.7). This suggests that in the AH, the stimulation at the two excitability states elicit similar modulations in the alpha power. The functional mechanism at the basis of this lack of differences in the modulation of alpha in the AH needs to be further addressed, given that TMS modulations in alpha power has been proposed to be a good predictor of stroke recovery (Pellicciari et al., 2018). Pellicciari and colleagues (2018) found that in the AH of stroke patients there is an increase in alpha power evoked by the TMS pulse. This latter result is in line with our findings, as we find that in the AH, stimulation elicits always the same modulation in alpha power, regardless the excitability state of the cortex. Instead, the UH shows stronger alpha power after TMS at *trough* compared to *no-trough*, leading to lower evoked power in alpha in the UH stimulation, compared to AH stimulation, when the effect of the local excitability state is not taken into account like in (Pellicciari et al., 2018).

Therefore, the hyperexcitability of the AH in our sample of mostly severely affected strokes confirms previous findings on severely impaired strokes (Tscherpel et al., 2020; Sarasso et al., 2020). We further show that the large and simplified response of the AH depends on a lower differentiation between the local excitability states of the motor cortex of AH vs UH. Importantly, the AH hyperexcitability seems to be mainly

a feature of severe stroke patients, given that both our patients and those included in Tscherpel et al. (2020) and Sarasso et al. (2020)' works were mostly severe. This might suggest that a feature of severe patients may be a lack of restoration of a functional differentiation between the local excitability states of the affected motor cortex, a lack of differentiation that, if not restored, can lead to a low degree of recovery. In this regard, it is interesting to report that a recent work by Potter-Baker and colleagues (2018) compared the inter-trial variability in MEPs elicited in the AH compared to the UH of stroke patients. They found that the MEPs elicited in the paretic-hand, with stimulation over the AH, showed in general less variability compared to the MEPs elicited in the non-paretic hand. This result is in line with our finding on a low differentiation between excitability states in the AH. In fact, as the recent brain-state dependent literature shows (e.g. Zrenner et al., 2018), variability in MEPs can be reduced by controlling for the brain-state at the moment of stimulation (phase of mu alpha rhythm). Therefore, our result on the low differentiation between the excitability states of the affected cortex explain these results on a low variability in MEPs elicited in the AH: the brain-state at the moment of stimulation is functionally less relevant in AH vs UH, hence MEPs elicited from AH stimulation will be less modulated by the brain-state at the moment of the pulse, resulting in less variability in the paretic-hand's MEPs compared to MEPs elicited over UH.

It must be noticed here that, despite the lower differentiation between the two excitability states in the AH compared to the UH, the *trough* still represents a state of slightly higher excitability than *no-trough*, also in the AH of the patients included in our sample. In fact, we found that, in the comparison between AH stimulation at *trough* vs *no-trough*, the stimulation at *trough* in the AH elicits greater activity in the UH contralateral to stimulation, compared to stimulation at no-*trough*. This suggests that the differentiation between the two excitability states is weaker in the AH vs UH, However, it is not completely lost and the AH propagates to UH more when the former is stimulated at *trough vs no trough*. Importantly, this result on the stronger propagation from AH towards UH when the AH is stimulated at *trough* vs *no-trough* further suggests that the AH of patients is not composed by inert material. This is in contrast with Casula et al. (2021)'findings according to which the AH stimulation of mildly affected patients would not propagate to the UH contralateral to stimulation.

Finally, it is essential here to discuss our nil findings in the coherence analysis. These negative findings might not be due to a real absence of difference in induced interhemispheric connectivity depending on the IAF phase at moment of stimulation and stimulated hemisphere, but could also be ascribed to spatial leakage, which is a confounding effect, especially in EEG at the sensor level. In this regard, connectivity analysis on EEG data between channels not spatially distant from each other is affected by spatial leakage: the effect of leakage, as it introduces common spurious activity on channels, is a general flattening of connectivity metrics towards its maximum. Therefore, when the contrast between two conditions is computed and statistically validated, no significant result can be returned, as spatial leakage affects both contrasted conditions in the same way, resulting in no differences in the contrast between the connectivity estimates. Due to this issue, and also considering the relatively small sample size (N strokes = 11; N controls = 10), connectivity effects might have been masked.

To conclude, we reported evidence in support of the fact that the AH shows a low degree of differentiation between the *trough* and *no-trough* excitability states as 1) stimulation in the AH leads to small differences between TEPs elicited at the two different excitability states; 2) after 55 ms, no difference in TEPs can be found in the contrast between AH stimulation at *trough* vs *no-trough* in either hemisphere; 3) the AH appears more excitable (greater TEPs) at the *no-trough* state compared to the UH; 4) theta ITPC appears increased in the AH compared to UH, but the contrast between AH stimulation at *trough* vs *no-trough* does not return any effect in theta ITPC, indicating that the same modulation of theta phase occurs when AH is stimulated at *trough* and *no-trough*; 5) there is no difference in alpha power modulation between AH stimulation at *trough* vs *no-trough*, indicating that the same alpha modulation happens when AH is stimulated, regardless of the excitability state at the moment of the pulse. This low differentiation between the excitability states in the affected motor cortex is not present in the UH as stimulation in the UH leads to greater differences in TEPs when stimulation at *trough* vs *no-trough are compared*. In fact, 1) the difference between TEPs elicited at *trough* vs *no-trough* is bigger for the UH stimulation compared to the AH stimulation; 2) in the comparison between UH stimulation at *trough* vs *no-trough*, differences in the TEPs are visible up to 130 ms after stimulation. 3) the UH is less excitable when stimulated at *no-trough* compared to the AH; 4) UH stimulation at *trough* increases ITPC in

both theta and beta compared to stimulation at *no-trough*, while in the AH, greater ITPC in theta does not emerge when AH stimulation is compared at *trough* vs *no-trough*. 5) the UH shows, like in healthy controls, a difference in the alpha power modulation between stimulation at *trough* and *no-trough*. This difference does not emerge in the AH up to 200 ms.

Therefore, it is here proposed that the strong and simplified TMS-evoked response of the AH, shown in the results presented so far, and also in previous works (Tscherpel et al., 2020; Sarasso et al., 2020), could be at least partially ascribed to the low differentiation between the cortical excitability states in the AH, which is instead preserved in the UH. Furthermore, given that our sample includes mainly moderately to severely impaired patients, it is here proposed that the lack of recovery might be due to a failure in the restoration of the differences between the local excitability states in the affected side.

2.6 Limitations and Future Directions

The study reported here presents some limitations. First of all, the samples here included are relatively small (stroke = 11; healthy controls = 10), with the potential consequence that some effects, especially in the connectivity analyses, might have been masked. Moreover, in this study, the mu alpha phase was estimated post-hoc by using an autoregressive model on the parietal Hjorths data filtered at IAF. Even though this approach has been employed in previous works (e.g. Mathewson et al., 2009; Duguè et al., 2011), it remains a less reliable procedure compared to approaches employing online EEG-TMS protocols, where the local state of the brain is itself the trigger to the TMS pulse (Zrenner et al., 2018; Baur et al., 2020; Stefanou et al., 2018; Hussain et al., 2020). Therefore, future studies should include larger samples of stroke patients and employ brain-state dependent stimulation approaches in order to further investigate differences in the excitability properties of the two hemispheres in stroke patients and the changes in interhemispheric connectivity that depend on the local excitability state at the moment of stimulation. This would in fact help bring new knowledge on the relationship between the local excitability state and the plastic processes occurring in the

stroke brain. Importantly, given our finding on a low differentiation between the different cortical excitability states in the affected hemisphere in severe patients, we propose that future studies should investigate phase-dependent cortical excitability changes in pre- vs post-rehabilitation stroke data.

2.7 Conclusions

In general, our results on stroke patients' show different cortical responses to TMS which depend on the stimulated hemisphere (AH or UH) and the local excitability state (mu alpha phase). The main emerging difference is that the local excitability state has a low influence on the AH excitability. In fact, the AH shows lower differences between TEPs, ITPC and TF in the *trough* vs *no-trough* comparisons compared to the UH stimulation. Previous models on stroke literature do not take into account the evidenced differences between the stroke patients' hemispheres, when evaluating the state of their interplay. Therefore, part of the variability that has contributed to the mixed findings in stroke literature might depend on the distribution of the mu alpha phases at the moment of stimulation in previous studies. Given the characteristics of the stroke patients investigated here and their high level of impairment, we propose that a feature of severe patients could lie in this weak difference between the different excitability states of the AH. For this reason, we propose that future works should assess phase-dependent excitability properties of the AH before and after rehabilitation paradigms in order to assess potential recovery.

Therefore, we propose that the phase-dependent investigation of the excitability properties of both the AH and UH need to be accomplished in relation with the assessment of the structural reserve in the individual patient. Understanding the effects of TMS stimulation at different phases in the both hemispheres, together with the effects of TMS stimulation given the phase relationship between the two M1s and describing how these depend on the structural reserve of the single patient would in fact bring light on the reasons at the basis of the mixed results in stroke literature. We believe that these are some of the lacking ingredients that would be essential to design successful individualized rehabilitation protocols. Finally, understanding the relationship between the restoration of the differentiation between the low and high excitability state in the affected hemisphere and the

recovery of the patient might become a standard procedure to assess the efficacy of the rehabilitation protocols, making the patients' assessment become, from only behaviour-dependent, both behaviour- and metric-dependent.

Bibliography

1. Baur, D., Galevska, D., Hussain, S., Cohen, L. G., Ziemann, U., & Zrenner, C. (2020). Induction of LTD-like corticospinal plasticity by low-frequency rTMS depends on pre-stimulus phase of sensorimotor μ-rhythm. Brain stimulation, 13(6), 1580-1587.

2. Belardinelli, P., König, F., Liang, C., Premoli, I., Desideri, D., Müller-Dahlhaus, F., ... & Ziemann, U. (2021). TMS-EEG signatures of glutamatergic neurotransmission in human cortex. *Scientific reports*, *11*(1), 1-14.

3. Brainin, M.; Teuschl, Y.; Kalra, L. Acute treatment and long-term management of stroke in developing countries. *Lancet Neurol.* **2007**, *6*, 553–561.

4. Brancaccio, A., Tabarelli, D., & Belardinelli, P. (2022). A new framework to interpret individual interhemispheric compensatory communication after stroke. Journal of Personalized Medicine, 12(1), 59.

5. Caliandro, P., Vecchio, F., Miraglia, F., Reale, G., Della Marca, G., La Torre, G., ... & Rossini, P. M. (2017). Small-world characteristics of cortical connectivity changes in acute stroke. Neurorehabilitation and neural repair, 31(1), 81-94.

6. Casula, E. P., Pellicciari, M. C., Bonnì, S., Spanò, B., Ponzo, V., Salsano, I., ... & Koch, G. (2021). Evidence for interhemispheric imbalance in stroke patients as revealed by combining transcranial magnetic stimulation and electroencephalography. Human Brain Mapping, 42(5), 1343-1358.

7. Casula, E. P., Tarantino, V., Basso, D., Arcara, G., Marino, G., Toffolo, G. M., ... & Bisiacchi, P. S. (2014). Low-frequency rTMS inhibitory effects in the primary motor cortex: Insights from TMS-evoked potentials. Neuroimage, 98, 225-232.

8. Chung, S. W., Rogasch, N. C., Hoy, K. E., & Fitzgerald, P. B. (2015). Measuring brain stimulation induced changes in cortical properties using TMS-EEG. *Brain stimulation*, *8*(6), 1010-1020.

9. Darmani, G., Zipser, C. M., Böhmer, G. M., Deschet, K., Müller-Dahlhaus, F., Belardinelli, P., ... & Ziemann, U. (2016). Effects of the selective α5-GABAAR antagonist S44819 on excitability in the human brain: a TMS–EMG and TMS–EEG phase I study. *Journal of Neuroscience*, *36*(49), 12312-12320.

10. Delorme, A., & Makeig, S. (2004). EEGLAB: an open source toolbox for analysis of single-trial EEG dynamics including independent component analysis. Journal of neuroscience methods, 134(1), 9-21.

11. Desideri, D. (2020). Dependency of non-invasive brain stimulation effects on real-time EEG-based measurements of instantaneous excitability in human motor cortex (Doctoral dissertation, Dissertation, Tübingen, Universität Tübingen, 2020).

12. Desideri, D., Zrenner, C., Ziemann, U., & Belardinelli, P. (2019). Phase of sensorimotor μ-oscillation modulates cortical responses to transcranial magnetic stimulation of the human motor cortex. The Journal of Physiology, 597(23), 5671-5686.

13. Dugué, L., Marque, P., & VanRullen, R. (2011). The phase of ongoing oscillations mediates the causal relation between brain excitation and visual perception. Journal of neuroscience, 31(33), 11889-11893.

14. Duque, J.; Hummel, F.; Celnik, P.; Murase, N.; Mazzocchio, R.; Cohen, L.G. Transcallosal inhibition in chronic subcortical stroke. NeuroImage 2005, 28, 940–946.

15. Fecchio, M., Pigorini, A., Comanducci, A., Sarasso, S., Casarotto, S., Premoli, I., ... & Rosanova, M. (2017). The spectral features of EEG responses to transcranial magnetic stimulation of the primary motor cortex depend on the amplitude of the motor evoked potentials. PloS one, 12(9), e0184910.

16. Gray, W. A., Palmer, J. A., Wolf, S. L., & Borich, M. R. (2017). Abnormal EEG responses to TMS during the cortical silent period are associated with hand function in chronic stroke. Neurorehabilitation and neural repair, 31(7), 666-676.

17. Gyulai, A., Körmendi, J., Juhasz, Z., & Nagy, Z. (2021). Inter trial coherence of low-frequency oscillations in the course of stroke recovery. Clinical Neurophysiology, 132(10), 2447-2455.

18. Hordacre, B., Ghosh, R., Goldsworthy, M. R., & Ridding, M. C. (2019). Transcranial magnetic stimulation-EEG biomarkers of poststroke upper-limb motor function. Journal of Stroke and Cerebrovascular Diseases, 28(12), 104452.

19. Hussain, S. J., Hayward, W., Fourcand, F., Zrenner, C., Ziemann, U., Buch, E. R., ... & Cohen, L. G. (2020). Phase-dependent transcranial magnetic stimulation of the lesioned hemisphere is accurate after stroke. Brain Stimulation: Basic, Translational, and Clinical Research in Neuromodulation, 13(5), 1354-1357.

20. Johansen-Berg, H.; Rushworth, M.; Bogdanovic, M.D.; Kischka, U.; Wimalaratna, S.; Matthews, P.M. The role of ipsilateral premotor cortex in hand movement after stroke. Proc. Natl. Acad. Sci. USA 2002, 99, 14518–14523.

21. Katan, M.; Luft, A. Global Burden of Stroke. In *Seminars in Neurology*; Georg Thieme Verlag: New York, NY, USA, 2018; Volume 38, pp. 208–211.

22. Lachaux, J. P., Rodriguez, E., Martinerie, J., & Varela, F. J. (1999). Measuring phase synchrony in brain signals. Human brain mapping, 8(4), 194-208.

23. Lotze, M.; Markert, J.; Sauseng, P.; Hoppe, J.; Plewnia, C.; Gerloff, C. The Role of Multiple Contralesional Motor Areas for Complex Hand Movements after Internal Capsular Lesion. J. Neurosci. 2006, 26, 6096–6102.

24. Mäki, H., & Ilmoniemi, R. J. (2010). The relationship between peripheral and early cortical activation induced by transcranial magnetic stimulation. *Neuroscience letters*, *478*(1), 24-28.

25. Manganotti, P., Formaggio, E., Storti, S. F., De Massari, D., Zamboni, A., Bertoldo, A., ... & Toffolo, G. M. (2012). Time-frequency analysis of short-lasting modulation of EEG induced by intracortical and transcallosal paired TMS over motor areas. Journal of neurophysiology, 107(9), 2475-2484.

26. Mathewson, K. E., Gratton, G., Fabiani, M., Beck, D. M., & Ro, T. (2009). To see or not to see: prestimulus α phase predicts visual awareness. Journal of Neuroscience, 29(9), 2725-2732.

27. McDonnell, M.N.; Stinear, C.M. TMS measures of motor cortex function after stroke: A meta-analysis. *Brain Stimul.* **2017**, *10*, 721–734.

28. Meyer, B. U., Röricht, S., Von Einsiedel, H. G., Kruggel, F., & Weindl, A. (1995). Inhibitory and excitatory interhemispheric transfers between motor cortical areas in normal humans and patients with abnormalities of the corpus callosum. *Brain*, *118*(2), 429-440.

29. Momi, D., Ozdemir, R. A., Tadayon, E., Boucher, P., Di Domenico, A., Fasolo, M., ... & Santarnecchi, E. (2022). Phase-dependent local brain states determine the impact of image-guided transcranial magnetic stimulation on motor network electroencephalographic synchronization. The Journal of Physiology, 600(6), 1455-1471.

30. Murase, N., Duque, J., Mazzocchio, R., & Cohen, L. G. (2004). Influence of interhemispheric interactions on motor function in chronic stroke. Annals of Neurology: Official Journal of the American Neurological Association and the Child Neurology Society, 55(3), 400-409.

31. Mutanen, T. P., Kukkonen, M., Nieminen, J. O., Stenroos, M., Sarvas, J., & Ilmoniemi, R. J. (2016). Recovering TMS-evoked EEG responses masked by muscle artifacts. Neuroimage, 139, 157-166.

32. Mutanen, T. P., Metsomaa, J., Liljander, S., & Ilmoniemi, R. J. (2018). Automatic and robust noise suppression in EEG and MEG: The SOUND algorithm. Neuroimage, 166, 135-151.

33. Oostenveld, R., Fries, P., Maris, E., & Schoffelen, J. M. (2011). FieldTrip: open source software for advanced analysis of MEG, EEG, and invasive electrophysiological data. Computational intelligence and neuroscience, 2011.

34. Papenberg, G., Hämmerer, D., Müller, V., Lindenberger, U., & Li, S. C. (2013). Lower theta inter-trial phase coherence during performance monitoring is related to higher reaction time variability: a lifespan study. NeuroImage, 83, 912-920.

35. Pellicciari, M. C., Bonnì, S., Ponzo, V., Cinnera, A. M., Mancini, M., Casula, E. P., ... & Koch, G. (2018). Dynamic reorganization of TMS-evoked activity in subcortical stroke patients. Neuroimage, 175, 365-378.

36. Potter-Baker, K. A., Lin, Y. L., Machado, A. G., Conforto, A. B., Cunningham, D. A., Sankarasubramanian, V., ... & Plow, E. B. (2018). Variability of motor evoked potentials in stroke explained by corticospinal pathway integrity. Brain Stimulation: Basic, Translational, and Clinical Research in Neuromodulation, 11(4), 929-931.

37. Premoli, I., Castellanos, N., Rivolta, D., Belardinelli, P., Bajo, R., Zipser, C., ... & Ziemann, U. (2014). TMS-EEG signatures of GABAergic neurotransmission in the human cortex. *Journal of Neuroscience*, *34*(16), 5603-5612.

38. Rogasch, N. C., Sullivan, C., Thomson, R. H., Rose, N. S., Bailey, N. W., Fitzgerald, P. B., ... & Hernandez-Pavon, J. C. (2017). Analysing concurrent transcranial magnetic stimulation and electroencephalographic data: A review and introduction to the open-source TESA software. Neuroimage, 147, 934-951.

39. Sarasso, S., D'Ambrosio, S., Fecchio, M., Casarotto, S., Viganò, A., Landi, C., ... & Massimini, M. (2020). Local sleep-like cortical reactivity in the awake brain after focal injury. Brain, 143(12), 3672-3684.

40. Sebastianelli, L., Versace, V., Martignago, S., Brigo, F., Trinka, E., Saltuari, L., & Nardone, R. (2017). Low-frequency rTMS of the *unaffected hemisphere* in stroke patients: A systematic review. Acta Neurologica Scandinavica, 136(6), 585-605.

41. Stefanou, M. I., Desideri, D., Belardinelli, P., Zrenner, C., & Ziemann, U. (2018). Phase synchronicity of μ-rhythm determines efficacy of interhemispheric communication between human motor cortices. Journal of Neuroscience, 38(49), 10525-10534.

42. Tscherpel, C., Dern, S., Hensel, L., Ziemann, U., Fink, G. R., & Grefkes, C. (2020). Brain responsivity provides an individual readout for motor recovery after stroke. Brain, 143(6), 1873-1888.

43. van Wijk, B. C., Neumann, W. J., Kroneberg, D., Horn, A., Irmen, F., Sander, T. H., ... & Kühn, A. A. (2022). Functional connectivity maps of theta/alpha and beta coherence within the subthalamic nucleus region. NeuroImage, 119320.

44. Veniero, D., Brignani, D., Thut, G., & Miniussi, C. (2011). Alpha-generation as basic response-signature to transcranial magnetic stimulation (TMS) targeting the human resting motor cortex: A TMS/EEG co-registration study. Psychophysiology, 48(10), 1381-1389.

45. Vinck, M.; Oostenveld, R.; van Wingerden, M.; Battaglia, F.; Pennartz, C.M.A. An improved index of phase-synchronization for electrophysiological data in the presence of volume-conduction, noise and sample-size bias. Neuroimage 2011, 55, 1548–1565.
46. Zrenner, C., Desideri, D., Belardinelli, P., & Ziemann, U. (2018). Real-time EEG-defined excitability states determine efficacy of TMS-induced plasticity in human motor cortex. Brain stimulation, 11(2), 374-389.

Appendix

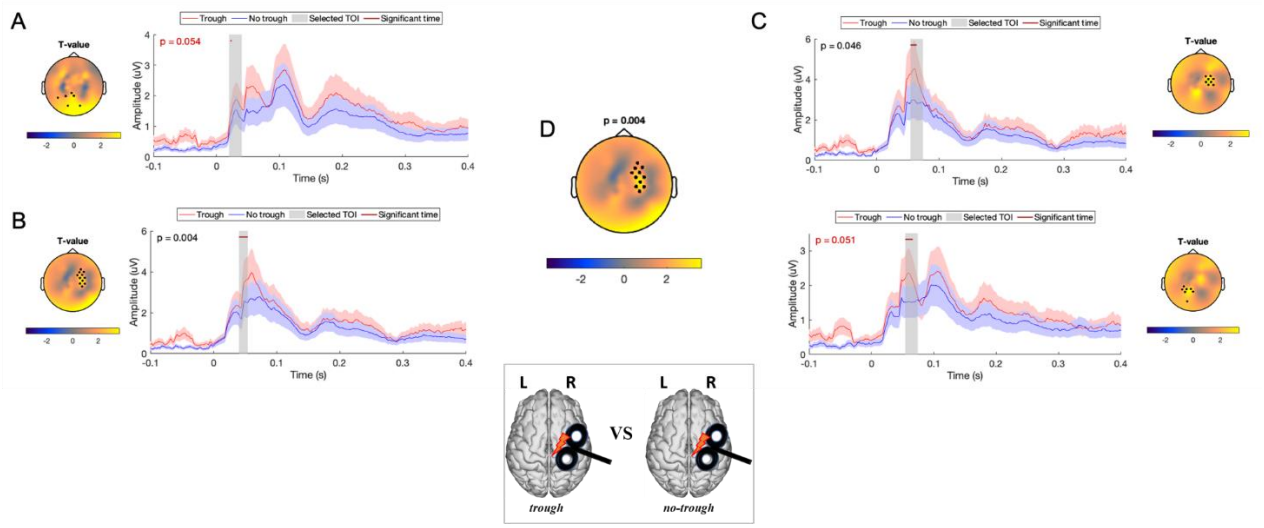

Suppl. Figure 2.1: rectified TEP activity for significant clusters comparing trough vs no trough for right hemisphere stimulation. Black/white dots in the topoplots refer to positive/negative clusters, respectively. Time window of interest: A) 20 -40 ms; B) 40 -55; C) 55 -75 ms. D) T value and cluster of significant electrodes in the comparison of ITPC between trough and no trough for right hemisphere stimulation in the beta band.

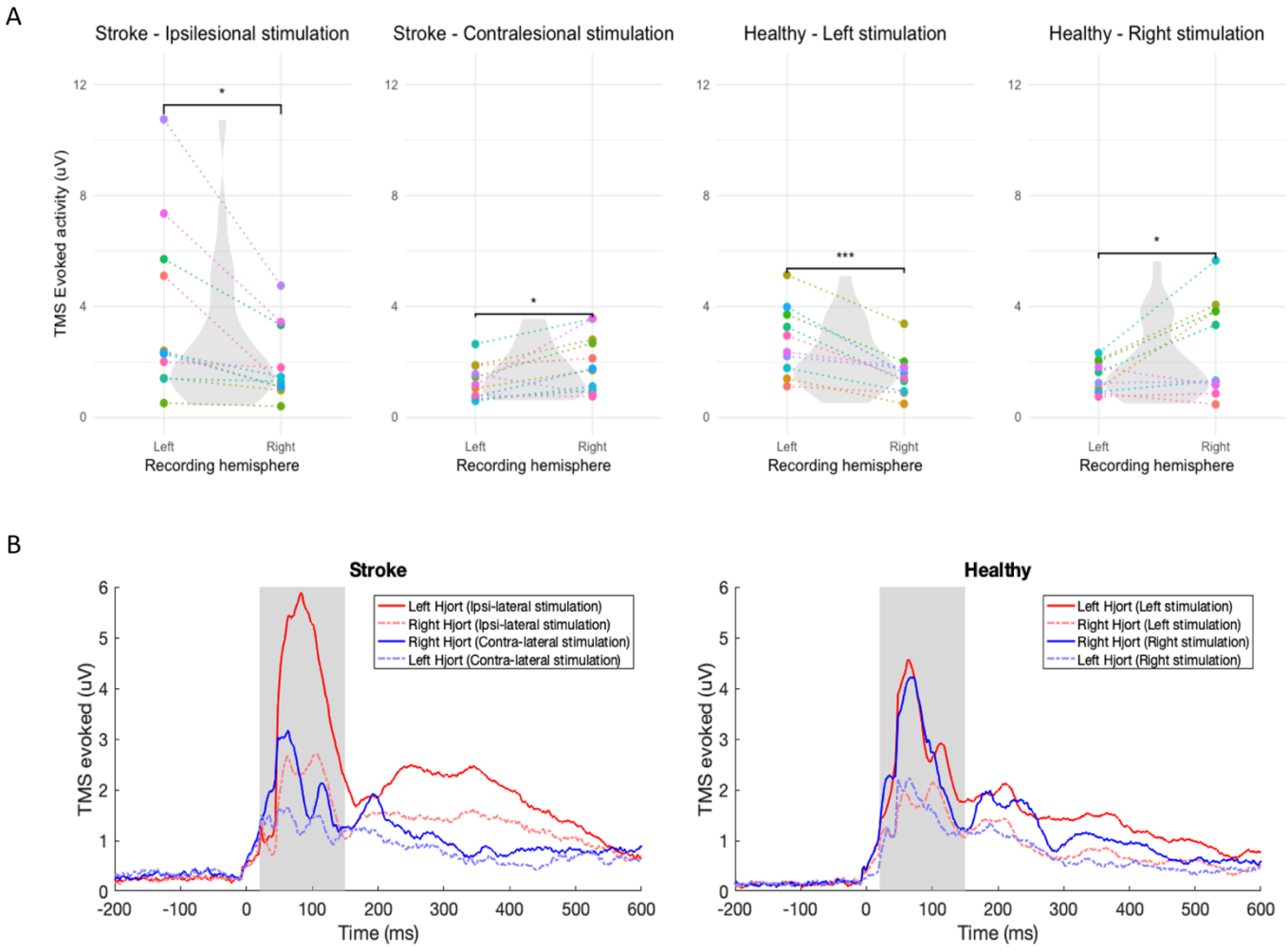

Suppl. Figure 2.2: A) Average rectified TEPs for all conditions and groups on Hjorts; B) TEP activity over Hjorts for all conditions in the stroke and control groups.

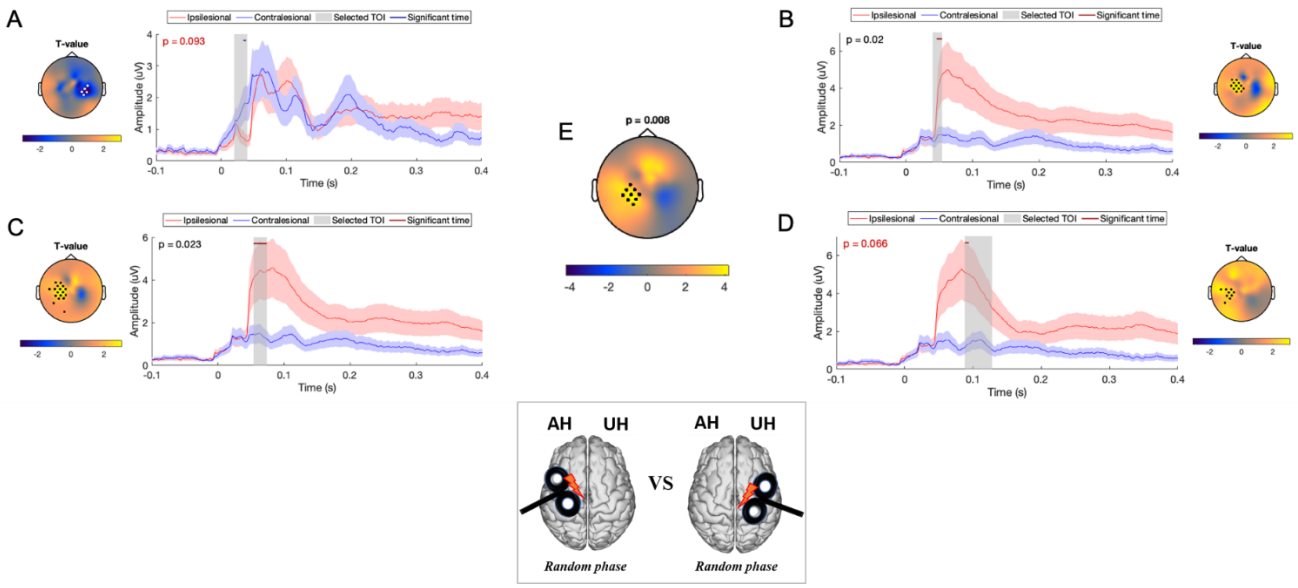

Suppl. Figure 2.3: Non phase dependent rectified TEP activity for significant clusters comparing ipsilesional vs contralesional stimulation. Black/white dots in the topoplots refer to positive/negative clusters, respectively. Time window of interest: A) 20-40 ms; B) 40-55; C) 55 -75; D) 89 – 129 ms. C) Non phase dependent T-value and cluster of significant electrodes in the comparison of ITPC between ipsilesional and contralesional stimulation in the theta band.

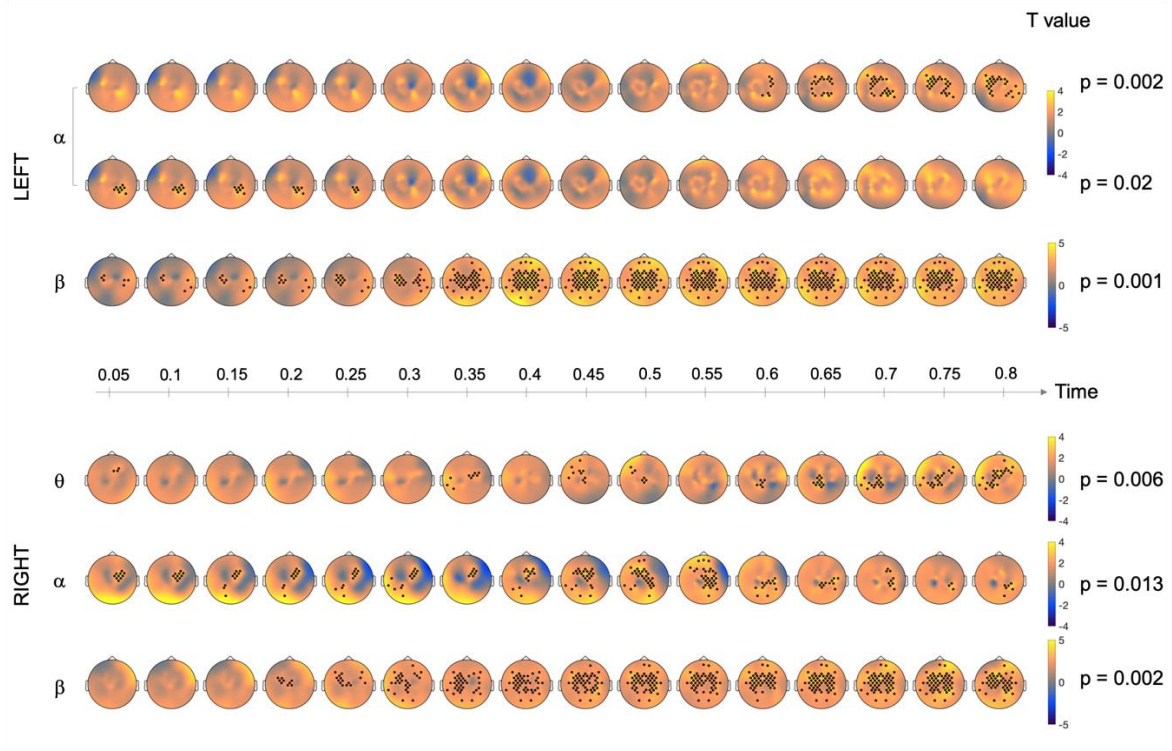

Suppl. Figure 2.4: Cluster statistics on TF between stimulation at trough vs no trough in right and left hemisphere separately, in the theta, alpha and beta band. Black dots in the topoplots refer to positive clusters.

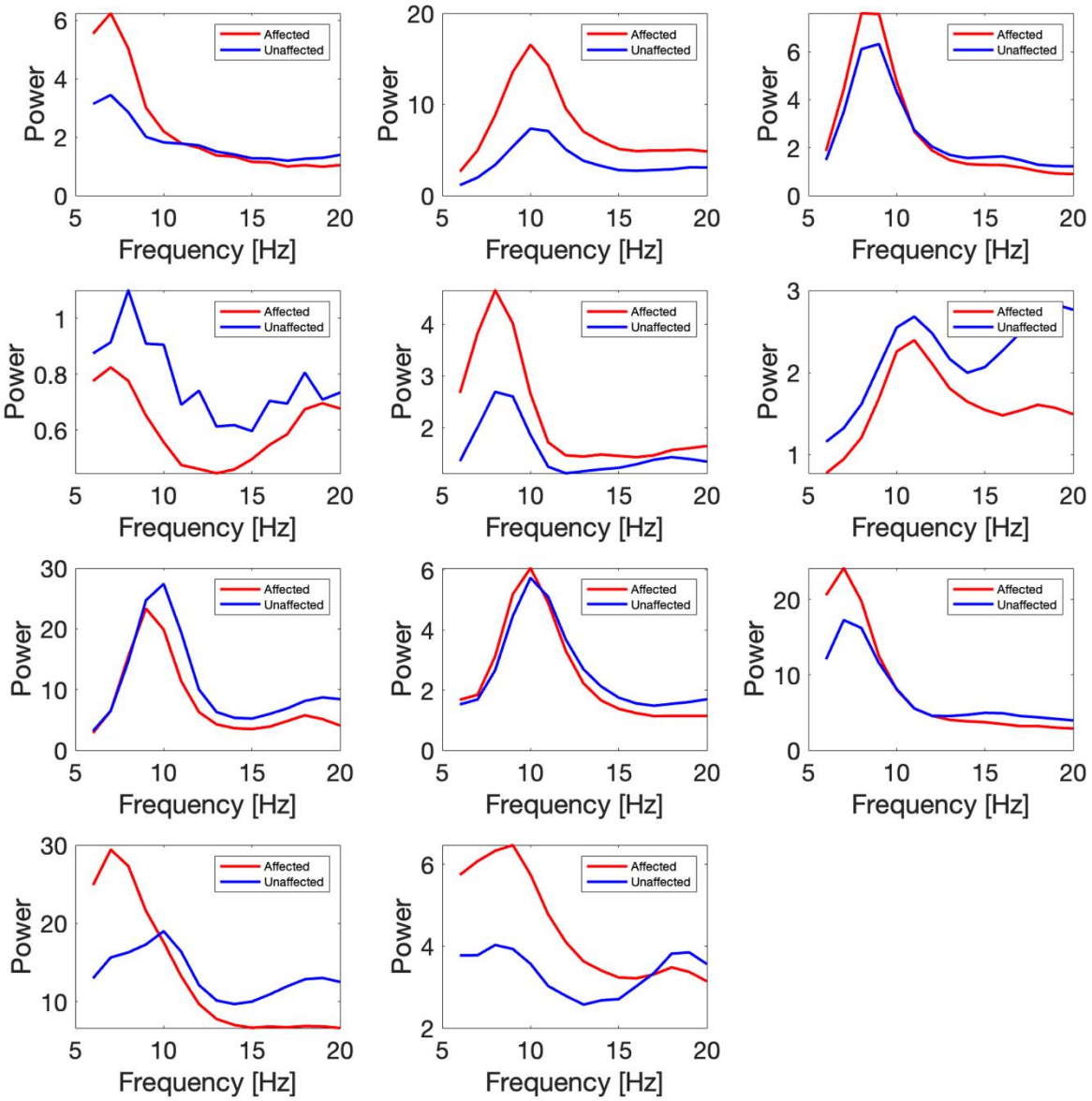

Suppl. Fig. 2.5: Power spectra for affected and unaffected Hjorths for each stroke patient. The power spectra were estimated on a baseline 500 ms time window, with a dpss taper. Each spectra is multiplied by the frequency in order to correct for 1/f.

Patient	Total Trials		*Trough* Trials		No *trough* Trials	
	UH stim	**AH stim**	**UH stim**	**AH stim**	**UH stim**	**AH stim**
1	215	441	58	202	157	239
2	174	348	35	61	139	287
3	187	355	66	123	121	232
4	159	348	35	75	124	273
5	307	332	65	46	242	286
6	194	354	31	57	163	297
7	148	260	32	85	116	175
8	130	231	49	34	81	197
9	169	301	34	38	135	263
10	185	298	50	128	135	170
11	161	447	50	151	111	296
12	193	330	91	12	102	318
13	116	261	35	15	81	246
14	330	211	39	26	291	185
15	193	382	13	39	180	343
16	82	252	4	50	78	202
17	98	353	14	43	84	310

Suppl. Table 2.1: Number of trials for each stimulation condition (UH/AH) and divided per phase condition. Only patients with >30 trials for trough stimulation were included in the final dataset (grey patients number were discarded).

Time window	TEPs CONTRASTS							
	AH Trough vs No-trough		UH Trough vs No-trough		AH vs UH Trough		AH vs UH No-trough	
	AH	UH	AH	UH	AH	UH	AH	UH
20 – 40 ms	+ (p = 0.031)					- (p = 0.035)		
40 – 55 ms	+ (p = 0.049) (p = 0.014)	+ (p = 0.005)	+ (p = 0.03)	+ (p = 0.004)	+ (p = 0.033)	- (p = 0.069)	+ (p = 0.031)	
55 – 75 ms		+ (p = 0.011)	+ (p = 0.019)	+ (p = 0.008)	+ (p = 0.049)		+ (p = 0.019)	
89 – 129 ms			+ (p = 0.009)	+ (p = 0.037)				

Suppl. Table 2.2: Summary of TEPs contrasts reported for each time window. For each contrast, the presence of a positive (+) or negative (-) cluster is reported for each hemisphere (AH and UH) separately with its respective p-values. When more than one cluster is found in one of the two hemispheres, p-values of both clusters are reported.

Frequency bands	ITPC CONTRASTS							
	AH Trough vs No-trough		UH Trough vs No-trough		AH vs UH Trough		AH vs UH No-trough	
	AH	UH	AH	UH	AH	UH	AH	UH
Theta			+ (p = 0.002)	+ (p = 0.002)	+ (p = 0.028)		+ (p = 0.008)	
Beta	+ (p = 0.001)	+ (p = 0.001)	+ (p = 0.004)	+ (p = 0.013)				

Suppl. Table 2.3: Summary of ITPC contrasts reported separately for the theta and beta frequency bands. For each contrast, the presence of a positive (+) or negative (-) cluster is reported for each hemisphere (AH and UH) separately with its respective p-values.

Frequency bands	TF CONTRASTS			
	AH Trough vs No-trough		UH Trough vs No-trough	
	AH	UH	AH	UH
Theta	+ (p = 0.01) **from 0.75 ms**		+ (p = 0.001) **from 0.35 ms**	+ (p = 0.001) **from 0.35 ms**
Alpha	+ (p = 0.001) **from 0.4 ms**	+ (p = 0.001) **from 0.25 ms**	+ (p = 0.001) **from 0.05 ms**	+ (p = 0.001) **from 0.05 ms**
Beta	+ (p = 0.001) **from 0.05 ms**	+ (p = 0.001) **from 0.2 ms**	+ (p = 0.001) **from 0.05 ms**	+ (p = 0.001) **from 0.25 ms**

Suppl. Table 2.4: Summary of TF contrasts reported separately for the theta, alpha and beta frequency bands. For each contrast, the presence of a positive (+) or negative (-) cluster is reported for each hemisphere (AH and UH) separately with its respective p-values. In bold, the time points from which the cluster is significant.

Chapter 3

Functional Connectivity States of Alpha Rhythm Sources in the Human Cortex at Rest: Implications for Real-Time Brain State Dependent EEG-TMS

This Chapter is aimed at investigating the functional coupling patterns between the three sectors of the brain previously studied with a phase-dependent approach (frontal, parietal and occipital cortices). Specifically, 203 healthy participants with resting state MEG data acquired in the Cam-CAN project were analysed. Connectivity patterns at source level at the Individual Alpha Frequency (IAF) were investigated. The choice of focusing on the connectivity in alpha depends on the fact that alpha represents the main rhythm of the human electroencephalogram and the oscillatory rhythm responsible for the opening and closing of windows with different excitability properties. Furthermore, alpha connectivity patterns correlate with task performance (both for cognitive and motor tasks) in stroke patients. In order to appreciate in the most sensitive way the connectivity patterns between the three sectors, two different but complementary phase-coherence metrics were used, namely the Weighted Pairwise Phase Consistency (WPPC) and Weighted Phase Lag Index (WPLI). It is here proposed that a compound approach consisting in the usage of complementary connectivity metrics can be the most sensitive approach in order to reliably assess inter-regional coupling patterns. This approach might be useful to assess changes in connectivity patterns before and after rehabilitation protocols in stroke patients.

3.1 Introduction

The origin of alpha waves and the function they subserve constitute long-lasting scientific issues in neuroscience. Already by 1929, Berger had managed to isolate alpha waves by means of a pioneering EEG set-up using scalp electrodes and described this rhythm as the most prominent in the human electroencephalogram (Berger, 1929). Recent advances due to brain source reconstruction and invasive electrophysiological recordings have provided evidence that alpha waves originate from several cortical and subcortical sites, with direct evidence suggesting both thalamus and diverse cortical areas as possible origins of such rhythm (Da Silva et al., 1980; Vijayan et al., 2012; Stolk et al., 2019).

The functional role of alpha oscillations also is still far from being completely understood. The "pulsed inhibition hypothesis", for instance, proposes that alpha oscillations actively inhibit neuronal firing in a phasic manner, opening and closing interleaved periods of "high" and "low" excitability of the cortex by cyclically producing bouts of inhibition (Klimesch et al., 2007; Jensen et al., 2010). This hypothesis is in line with the idea behind brain-state dependent stimulation, that the outcome of an electro/magnetic perturbation depends on the instantaneous phase state of a specific brain rhythm in a given area. In fact, studies investigating alpha in the occipital cortex demonstrate that the alpha phase at the instant of a visual stimulus predicts high or low probability of detection (Mathewson et al., 2009).

However, it is still not clear which is the exact role of alpha oscillations in opening states of cortical excitability. For example, the aforementioned "pulsed inhibition hypothesis" does not seem to apply to findings of brain-state dependent stimulation in the parietal cortex, where the same directionality of inhibition vs. excitation as in the visual cortex does not emerge (Zrenner et al., 2018; Bergmann et al., 2019; Desideri et al., 2019). In this regard, studies investigating μ-alpha in the parietal cortex show that a principle of pulsed facilitation rather than inhibition would better explain the role of alpha in the hand-knob of the sensorimotor cortex. In fact, it has been shown by means of

real-time EEG phase-dependent transcranial magnetic stimulation (TMS) that stimulation at μ-alpha troughs results in facilitated motor evoked responses (MEPs, Zrenner et al., 2018), while at peaks of the same oscillation, inhibition does not seem to occur in a significant proportion of instances (Bergmann et al., 2019).

Even if there is no consensus as to whether alpha shapes neuronal recruitment by determining windows of lower and higher excitability, or rather only by opening windows of greater excitability, alpha oscillations appear to have a role in shaping neural recruitment.

Most of the protocols conceived to modulate cortical excitability by means of TMS use a predefined stimulus sequence irrespective of the instantaneous brain-state, as opposed to a real-time brain-state dependent stimulation, which delivers the stimulus in determined phases of the alpha cycle (Zrenner et al., 2018). If the phase of alpha reflects a phasic increase and decrease of cortical excitability (as reported in the occipital cortex by (Mazaheri et al., 2010), we should find different outcomes depending on the local alpha phase at the instant of stimulation. First attempts in this direction have tried to post-hoc determine the phase of alpha waves at the moment of the stimulus. This has been mainly tested in the occipital cortex, where the conscious visual percept has been linked post-hoc to the alpha phase at the instant of stimulus presentation (Mathewson et al., 2009; Duguè et al., 2011). However, the effects were generally assessed by statistically estimating the probability that the stimulus could be delivered at a given phase. Differently, phase-state dependent stimulation leverages instantaneous EEG phase-states to trigger the TMS pulse exactly at the phase of interest, without post-hoc tracing of it back to the moment of analysis. Therefore, studies using this novel approach have led to more consistent and reproducible results. For example, EEG-TMS has been used to investigate motor excitability depending on mu-alpha in the parietal cortex. This line of research is relatively recent, but several consistent pieces of evidence show that participants with a detectable mu-alpha rhythm show larger motor evoked potentials (MEPs) when TMS stimulation at the motor spot is delivered at mu troughs or at the early rising phase, compared to the conditions where positive peaks or random phases are targeted (Zrenner et al., 2018; Stefanou et al., 2018; Schaworonkow et

al., 2018). These results are in line with the hypothesis of the alpha rhythm as a mechanism modulating cortical excitability. Attempts to link specific alpha phases to enhanced cortical excitability have also been made in studies targeting the dorsolateral frontal cortex (DLPFC), where alpha-synchronized rTMS at troughs appears to provide for a local alpha power decrease in patients with drug resistant depression disorder. The same result is not obtained by intermittent theta burst or random phase stimulation (Zrenner et al., 2020).

To sum up, the role of alpha phase has been investigated in at least three different cortical areas and a relationship between alpha phase and cortical excitability has been found in frontal, parietal and occipital regions (Zrenner et al., 2018; Mazaheri et al., 2010; Gordon et al., 2021). However, there is still no clear and organic consensus on a generalized functional role of the alpha phase. For example, the alpha phase in the occipital cortex seems to elicit opposite effects with respect to the other cortical areas: trough targeting has been proposed to decrease the possibility of perceiving the stimulus (Mathewson et al., 2009). Moreover, it has been shown that the conscious perception of a visual stimulus not only depends on alpha phase in the occipital cortex but also on that in fronto-central regions at the moment of stimulation (Mathewson et al., 2009; Duguè et al., 2011) this would be in line with the idea of the frontal control network allowing access to a conscious perception.

This evidence, together with the assumption that coherence between brain regions underlies integration of information (Fries et al., 2015), suggests that knowing the functional coupling between stimulated (or post-hoc investigated) regions and other areas potentially connected with the stimulation site is crucial in designing experiments aiming at a trial-based selective perturbation of a given “brain state”. In this light, considering the functional coupling patterns of the stimulated site is important in explaining EEG-TMS results and is even more crucial when EEG-TMS protocols are intended, not only in terms of a single stimulation site, but also as a technique for pathway-specific modulation targeting multiple functional hubs: the next horizon of brain-state dependent stimulation. In this regard, this technique has been shown to have the potential to modulate specific pathways (Nieminen et al., 2022), for example, by coupling the stimulation to an activity state of that pathway

(e.g., Stefanou et al., 2018). Therefore, reliable metrics are required that can extract extended network states through long-range connectivity. Such solid brain state landmarks would be certainly useful (before and after a neuro-modulatory intervention) to assess whether the brain-stimulation has exerted the desired network state modulation. Most importantly, they would be crucial when time-resolved connectivity state estimates, describing the connectivity pattern of the network, are used as real-time trigger condition. Nevertheless, gold-standard metrics for connectivity generally consist of pseudo-statistics regarding different phase consistency over several tens of trials and a consensus for a conceptual definition of single-trial instantaneous connectivity is still missing. For this reason, we here try to open the way to addressing the need for brain-state dependent protocols to take into account not only the local state which usually triggers the stimulus, but also a general sensitivity state of the system being modulated in its excitability.

Therefore, this study aims to identify suitable functional pathways between well-known cortical alpha generators, whose connectivity state can be assessed with MEG/EEG at rest. Here, we present a pipeline that effectively determines potential connections from resting MEG/EEG data using Weighted Pairwise Phase Consistency (WPPC; Vinck et al., 2010) and Weighted Phase Lag Index (WPLI; Vinck et al., 2011). It is worth noticing that the choice of a connectivity metric has to take into account its advantages and disadvantages in the context of application (Bastos et al, 2016; Gross et al, 2021). Here we used WPPC and WPLI, exploiting their partial complementarity, for the data under investigation. Both metrics depend on the consistency between the phases of the signal of interest, and are not biased by sample size. WPPC is based on the pairwise phase difference, thus it is still affected by zero-lag correlations introduced by the spatial spread of the inverse solution. As a matter of fact, WPPC also provides positive and statistically significant values when the phase difference is exactly zero. This is a result that does not reflect real synchronization, because the finite (but not null) propagation time of the nervous signal on the pathway connecting the two areas is not taken into account. In contrast, WPLI does not have this problem because it is computed from the sign of the imaginary part of the coherence, which vanishes for zero-lag correlations. However, the

WPLI signal to noise ratio is optimal for a phase delay of π/2, which corresponds at a typical frequency of 10 Hz to an absolute time delay of 25 ms. Since we are investigating the temporally resolved cortico-cortical connectivity, this is a large delay if compared to the typical brain conduction delays within the same hemisphere. Thus WPLI, despite being a less sensitive measure of phase consistency between the brain regions under investigation, is useful to confirm that the connectivity already detected by the more sensitive WPPC is real and not due to the spatial spread of the inverse solution. In this sense, the two metrices are partially complementary. With this methodological set-up, we investigated 203 healthy subjects with several minutes of resting MEG data and found alpha connectivity stronger for parietal-prefrontal areas rather than for occipito-parietal areas. The results of this study will be relevant to design real-time brain state-dependent EEG-TMS experiments: connectivity priors (Pezzulo et al., 2021) will be highly relevant as off-line acquired a priori information for the development of real-time connectivity state estimation algorithms.

3.2 Methods

3.2.1 Dataset and Acquisition

We analysed magnetoencephalographic (MEG) resting state recordings of 203 healthy participants (age range 18–57 years; see Figure 3.1a for age distribution) from the Cambridge Centre for Aging and Neuroscience (CamCAN) public dataset. Prior to inclusion in the dataset for neuroimaging measurements, all participants were tested for cognitive decline (MMSE > 24; Folstein et al., 1975), for matching vision, hearing and English language inclusion criteria and for absence of serious neurological and psychiatric conditions (see Taylor et al., 2017 for details about the dataset and acquisition parameters). For each participant, resting state activity (eyes closed; 8 min and 40 s) and empty-room noise background (3 min) were recorded using a 306-channel VectorView MEG system (102 magnetometers; 204 first order planar gradiometers; sampling rate = 1000 Hz; high pass

filter 0.03 Hz; low pass filter 330 Hz). Anatomical landmarks (nasion, left and right pre-auricular points) were registered, as well as at least 75 additional (isotrak) points, to model the head surface. For human resting state data, continuous monitoring of the head position (cHPI), electro-ocular (EOHG, EOVG) and electro-cardiac (ECG) recordings were available. Additionally, T1 weighted anatomical data were collected using a 3T Siemens TIM Trio scanner (MPRAGE, TR = 2250 ms, TE = 2.99 s; FOV = 256 × 256 × 192; voxel size 1 × 1 × 1 mm). All the subsequent analysis was performed only on planar gradiometers using Fieldtrip (Oostenveld et al., 2011), SPM (Friston et al., 2007), CAT12 (Gaser et al., 2022) and custom MATLAB code.

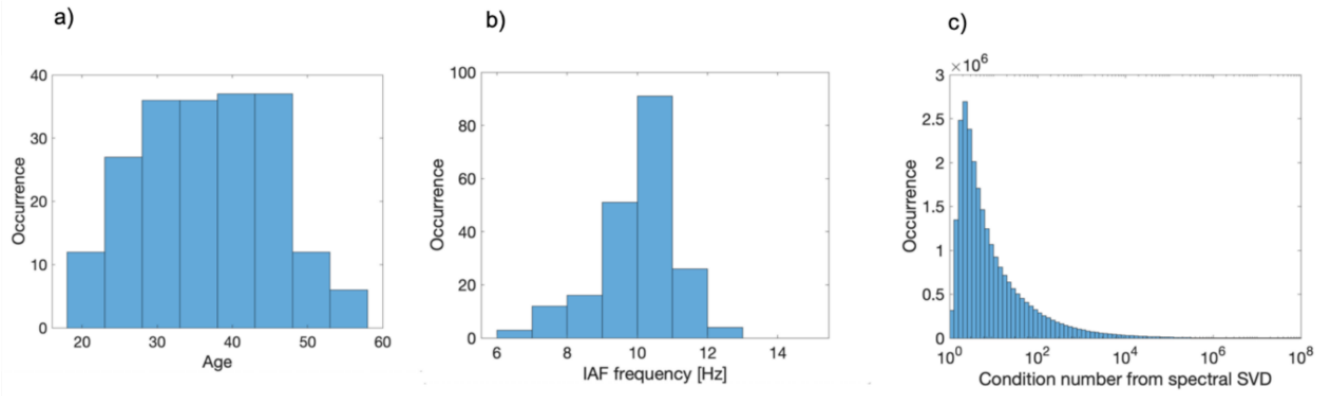

Figure 3.1. a) Distribution of sample age. **b**) Distribution of detected IAF on the whole sample. c) Distribution of all condition numbers from SVD, aiming to define optimal dipole direction for spectral data.

3.2.2 MEG Data Preprocessing

Collected MEG datasets (resting state and empty-room) were inspected and bad channels showing high noise levels and/or SQUID jumps were marked and removed from the data. External magnetic source nuisance was removed by means of temporal Signal Space Separation (tSSS, Taulu and Simola, 2006; Taulu et al., 2005) with a correlation threshold of 0.98 and a sliding time window of 10 s. Line noise contribution was removed by applying a 5th-order Butterworth two-pass filter centered at the line frequency and its first 3 harmonics, and spanning an interval of 2 Hz. Head

position of the resting state data was corrected every 200 ms using cHPI data and re-referenced to a common head position. Human MEG data were cleaned from physiological artifacts using an automated procedure. Muscular activity was detected by filtering data between 100 and 140 Hz, transforming each channel data into a z-score relative to the whole channel time series and rejecting segments where the z-score averaged across channels was greater than 5 for at least 200 ms. Then we ran an extended Infomax Independent Component Analysis (ICA; Lee et al., 1999; Hyvärinen et al., 2001) on data filtered between 0.5 and 125 Hz (Butterworth 4th order, two-pass) and resampled to 250 Hz. Data resampling and digital filtering commute with the ICA unmixing matrix estimation, provided the artifactual activity of interest lies in the spared frequency band (Hyvärinen et al., 2001). For this reason, and for computational efficiency, we computed ICA on resampled data and applied unmixing matrices to unfiltered data at the original sampling rate of 1000 Hz. Correlation coefficients of each extracted component with electro-physiological channels (EHOG, EVOG and ECG) were computed and rejected using a recursive z-score based procedure that robustly discarded all components with correlation more than 2 standard deviations from the coefficient distribution mean of all components. Data cleaned from artifacts were then filtered and segmented. Empty-room data, later used for noise covariance matrix estimation, were filtered broadly between 0.5 and 140 Hz (4th-order Butterworth two-pass filter) and segmented in 1 s epochs. Human resting state recordings were instead filtered around the alpha frequency band (4th-order Butterworth two-pass filter between 5 and 16 Hz) and split into 2 s segments. Finally, all empty-room and resting state segments exceeding a threshold of 10 standard deviations with respect to the channel average, were further discarded in order to deal with potential residual SQUID jumps and/or filter border effects.

3.2.3 Anatomical Data Processing

Structural T1w MRI scans were processed with the aim of extracting cortical surfaces for forward and inverse model calculation and for common space mapping. We processed T1w images

using the CAT 12 toolbox pipeline (Gaser et al., 2022). After bias normalization, denoising and skull stripping, volumetric data were automatically co-registered to a template space (IXII 555 MNI space; Gaser et al., 2022). Different tissue was then segmented in native space in order to extract surface models of the head, the brain enclosing surface and the cortical mantle. We modeled the cortical mantle with a tessellation (20,484 vertices) of the mid thickness surface, i.e., the surface in between the pial and the white/gray matter interface. The surface enclosing the brain and a surface model of the head were also modeled as 20,000 vertices meshes. In addition to the extracted surfaces in native subject space, co-registered spheres for projection on the FreeSurfer Average (5th order icosahedron "fsaverage5"; Fischl et al., 1999) superficial template space were computed, as well as the corresponding interpolation matrices between template and native coordinate spaces. Interpolation coefficients for each point were defined as inversely weighted average of first neighbourhood. The mapping of the native space cortical surface onto the FreeSurfer average allowed us to identify, in template space, vertices belonging to 360 regions of interests of the 'state of the art' multimodal parcellation from the Human Connectome Project (Glasser et al., 2016). This atlas was generated by combining structural, diffusion and resting state fMRI data from 210 healthy young adults. Being interested in phase consistency between frontal, parietal and occipital areas, we defined three corresponding brain sectors, for each hemisphere, by pooling together correspondent ROIs from the atlas. We selected the ROIs in order to achieve a sufficiently large coverage of the three sectors of interest, while avoiding excessive proximity that might lead to spurious connectivity due to potential spread of the inverse solution. Finally, this led to 16, 7 and 18 regions of interest for the occipital, parietal and frontal sectors, respectively. For the sake of computational efficiency, we refined the sectors by trimming the borders in order to have the same number of dipoles per sector (D = 930). A list of corresponding regions of interest, with MNI coordinates, can be found in Table 1. All the subsequent analyses were performed only on these ROIs.

ROI	Sector	MNI Coordinates of Centroid (mm)		
		x	y	z
V1	Occipital	−13.1	−82.0	1.5
V2	Occipital	−12.4	−81.5	3.6
ProS	Occipital	−18.5	−52.2	0.1
V3	Occipital	−18.3	−86.2	5.4
V4	Occipital	−29.7	−82.5	−3.9
V6	Occipital	−13.9	−78.0	27.2
V6A	Occipital	−18.6	−84.3	38.1
V7	Occipital	−23.8	−81.9	26.6
IPS1	Occipital	−22.6	−71.7	33.0
V3A	Occipital	−17.2	−88.4	23.0
V3B	Occipital	−28.2	−78.9	16.3
V3CD	Occipital	−35.3	−85.7	12.3
IP0	Occipital	−30.4	−73.5	25.5
PGp	Occipital	−39.8	−80.1	22.1
LO1	Occipital	−37.8	−82.9	4.2
LO2	Occipital	−42.7	−83.3	−4.9
1	Parietal	−47.1	−24.5	52.3
2	Parietal	−35.4	−34.4	49.7
3a	Parietal	−34.3	−21.8	41.8
3b	Parietal	−36.8	−24.1	51.6
4	Parietal	−26.7	−19.7	53.8
6mp	Parietal	−14.1	−13.2	65.7
6d	Parietal	−34.9	−12.7	61.9
8BL	Frontal	−11.6	35.1	50.8
9p	Frontal	−18.9	44.0	36.4
9m	Frontal	−7.7	51.0	21.8
9a	Frontal	−19.7	53.2	23.8
8Ad	Frontal	−23.3	24.7	41.2
9–46d	Frontal	−28.7	42.1	21.4
8BM	Frontal	−6.3	29.5	43.1
8Av	Frontal	−37.1	18.0	47.4
46	Frontal	−36.6	35.6	28.3
8C	Frontal	−40.3	16.1	35.0
p9–46v	Frontal	−43.3	29.2	26.3
a32pr	Frontal	−10.2	28.1	28.6
d32	Frontal	−10.0	38.5	21.1
a9–46v	Frontal	−37.1	47.7	8.8

ROI	Sector	MNI Coordinates of Centroid (mm)		
		x	y	z
10d	Frontal	−12.1	62.9	8.4
p10p	Frontal	−23.6	55.0	5.2
p47r	Frontal	−41.2	40.3	1.5
IFSa	Frontal	−42.0	31.2	13.2

Table 3.1. List of Region of Interest (ROI) defining the three sectors. A brief description (from van Essen) and the coordinate of the centroid in mm with respect to the template MNI space is reported.

3.2.4 MEG Source Reconstruction Based on Individual Anatomies

We used Minimum Norm Estimation (Ilmoniemi et al., 2019) to solve the inverse problem and compute the projection matrix from sensors to source space. Native space surfaces were co-registered to MEG coordinates in a first step, using correspondence between anatomical landmarks as recorded during the MEG session and in the MRI anatomical image. Second, co-registration was refined by aligning additional head surface points registered during MEG acquisition to the tessellation representing the head surface. In this procedure, MEG isotrak points anterior to the nasion were discarded since the anatomical MRI images were defaced prior to being publicly available. We then computed a forward model solution for planar gradiometers using the singleshell method and the brain enclosing surface as computed before, and depth normalizing lead fields with a factor of 0.5. The source model for MNE was defined as a free orientation set of dipoles uniformly distributed on the cortical surface (mean spacing 3.1 mm) and the inverse solution was computed, with a 1% noise covariance regularization. This procedure leads to a set of three time-series of estimated cortical activations for each resting state epoch and for each vertex of the source model mesh, in the three cartesian coordinate system. MEG is blind to the radial component of magnetic field generated by a current dipole in the source model (Illmoniemi et al., 2019; Hämäläinen et al., 1993). Thus, even for realistic forward solutions, the estimated current in the most radial direction, with respect to the head surface, is almost zero. Therefore, we performed a Singular Value Decomposition (SVD) of the three

source time series at each vertex and for each epoch, retaining only the components associated with the first two singular values, while the third was always almost zero. In this way we reduced the current estimate to its projection on the plane orthogonal to the radial direction, resulting in two source activity time series for each vertex and for each dipole represented hereafter by the two-dimensional vectors ***x(t)***.

3.2.5 Spectral Analysis

For each epoch and vertex of the cortical mesh, we computed Fourier coefficients ***X(f)*** from the time dependent activity vectors ***x(t)*** in a frequency interval f = [8:14] Hz using a Hanning window taper. Having thus two Fourier coefficients at each frequency, dipole and epoch, we decided to reduce spectral data defining an optimal dipole orientation as follows: we computed the cross spectral density matrix between the two Fourier components, performed an SVD and keeping only the direction relative to the first singular value. This resulted in an optimal dipole orientation uˆ that depends on the dipole position, the epoch and the frequency of interest, thus optimizing the detection of the brain signal at the frequency of interest. We reduced accordingly the Fourier coefficient vector to a scalar one defined as $X(f) = \boldsymbol{X}(f) \cdot \hat{u}$. As a measure of the quality of the procedure, we pooled together all condition numbers resulting from SVDs on all subjects: the average condition number was 1.5×10^3. This means that, on average, the dipole orientations were, in time, almost fixed (see also Gross et al, 2001) and thus our optimization procedure captures most of the spectral content of the data. The distribution of the logarithm of all condition numbers can be inspected in Figure 3.1c, showing the reliability of the assumption. Fourier coefficients in the optimized direction ***X(f)*** were then used to compute power spectral density at each vertex and for each epoch. Pooling together all spectral densities and detecting the peak in the frequency band of interest, we defined, for each subject, an Individual Alpha Frequency (IAF); a distribution of all the 203 IAFs is reported in Figure 3.1b. All the subsequent connectivity analysis was then performed at the individual alpha frequency. For this

reason, the frequency dependence of Fourier coefficients *X(f)* will be dropped hereafter in the notation.

3.2.6 Connectivity Analysis and Group Statistical Validation

We are interested in connectivity and phase relationships between region of interest belonging to the frontal, parietal and occipital areas within each hemisphere. For this reason, we computed two different spectral based connectivity metrics between all the combinations of areas belonging to the three different sectors. In particular, given the symmetricity of the connectivity metrics we use, we crossed occipital areas with parietal and frontal, and parietal region of interests with frontal ones. For each resulting combination, we computed the Weighted Pairwise Phase Consistency (WPPC; Vinck et al., 2011) and the Weighted Phase Lag Index (WPLI; Vinck et al., 2010). The WPPC is based on the distribution of the phase differences between all the pairs of observations (resting state 2 s epochs in our case). WPPC is a robust non-biased measure of phase consistency of brain signals, but it is still affected by zero-lag artificial correlations induced by the imperfection of the inverse model solution (Bastos 2016; Gross 2021). Complementary to WPPC, we estimated WPLI as a connectivity measure not affected by the artificial zero-lag correlations. Being based on the imaginary part of the coherence, WPLI is immune to zero-lag connectivity but it has another disadvantage: it achieves maximal Signal to Noise Ratio (SNR) when the two brain signals are in a $\pi/2$ relationship. For the frequency band of interest (around 10 Hz) this means a time delay of ~25 ms, a long time when compared to typical brain signal propagation time. However, both metrics strongly depend on a consistent phase relationship between signal of interest, and then they can complementarily provide information about the phase consistency of alpha rhythmicity between the sectors we are investigating.

Given the combination of two brain sectors (A and B) from the ones defined above (O = occipital; P = parietal; F = frontal) we computed whole sector connectivity matrices, using both WPLI and WPPC, as follows. Named for brevity as $X = X_A(d_a)$ and $Y = Y_B(d_b)$, the Fourier coefficients at each vertex d_a and d_b of the sectors A and B, respectively, we computed a regional dipole-wise

connectivity matrix $C_{AB}^{M}(d_a, d_b) \in \mathcal{M}(D \times D)$, where M represents the metrics (M = WPPC or WPLI). Henceforth, for the sake of clarity, subscripts and superscripts will be omitted when not necessary. In addition, we computed, for each metrics, correspondent null connectivity matrices $\tilde{C}_A(d_a, d_r)$ and $\tilde{C}_B(d_b, d_r)$ from sector of interest to a set of D dipoles $\{d_r\}$ randomly chosen within each subject space among the set of dipoles not belonging to any sector of interest. These null connectivity matrices were then used for group statistical validation, under the null hypothesis that connectivity to random dipoles, differently chosen for each subject, will be distributed according only to the metrics' bias and sensitivity. To this aim we performed a bootstrap procedure at the group level by comparing actual and random connectivity matrices: for each combination (A,B) and for each subject, the actual connectivity matrix C_{AB} and the random ones $\tilde{C}_A$ and $\tilde{C}_B$ were permuted 10,000 times in order to estimate the empirical distribution of the Fisher regularized difference of connectivity $dC \equiv \tan^{-1}(C_{AB}) - \tan^{-1}(\tilde{C}_{A/B})$. The comparison between the real dC with its null empirical distribution provided, for each dipole, a bootstrap p-value. (only positive tailed comparisons were considered). Resulting D^2 p-values were then FDR corrected (q = 0.05) and only significant elements of C_{AB} were considered in the subsequent analysis. Furthermore, we reduced the information in each connectivity matrix by summarizing connectivity between the two sets of ROIs $\{r_a\}$ and $\{r_b\}$ from the van Essen et al. atlas belonging to sectors A and B, respectively. To this aim we defined, for all connectivity metrics, the following two quantities:

$$\Delta(r_a, r_b) \equiv \frac{\#[C_{AB}(d_a \in r_a, d_b \in r_B)]}{D}$$

$$\Gamma(r_a, r_b) \equiv P_{95}\{f^{sg}[C_{AB}(d_a \in r_a, d_b \in r_B)]\}$$

where #[·] and f^{sg} [·] represents the count and the distribution of significant connectivity values, respectively, while P_{95} [·] represents the 95% percentile. The quantities Γ and Δ were computed between regions for each combination $\{r_a, r_b\}$ and from a single region of interest to all the target sector $\{r_a, \mathrm{B}\}$. Finally, bi-hemispheric results were collapsed by averaging the contribution of both

hemispheres. We defined the quantities Δ and Γ to summarize the connectivity between ROIs and/or sectors, given that inspecting he whole dipole by dipole connectivity matrices would have been confusing and not clear to the reader. The two quantities are conceptually derived from standard graph theory analysis. The connectivity degree $\Delta(r_a, r_b)$ simply counts, from the connectivity matrix, the number of statistically significant connections between dipoles of the two ROIs, disregarding the strength of the connectivity and normalizing the count to the total number of dipoles in the sector. This is conceptually analogous to the node degree in the context of network analysis. The mean significant connectivity $\Gamma(r_a, r_b)$ provides a refinement of the connectivity degree, including the information about the connectivity (or phase consistency) strength. This is achieved by selecting from the connectivity matrix only the statistically significant connections between the dipoles of the two ROIs, extracting the 95% percentile of the resulting distribution instead of just counting them. It is worth noticing that choosing the 95% percentile is a conservative choice, given that usually connectivity values bounded between 0 and 1, even when Fisher regularized, can give rise to non-symmetrical distributions.

3.3 Results

Degree and mean connectivity between each ROI combination ($\Delta(r_a,r_b)$ and $\Gamma(r_a,r_b)$) and from each ROI to the other sectors as a whole ($\Delta(r_a,B)$ and $\Gamma(r_a,B)$) for WPPC and WPLI are shown in Figure 3.2 and Figure 3.3 as color coded source maps and connecto-grams. All extracted values are listed in Table 3.2 and Table 3.3. In general, we can notice that the connectivity estimated from both metrics, each one differently depending on a consistent phase relationship, is predominant in the parietal–frontal connection. While the connection between occipital and frontal sectors appears to be still relevant, the weakest phase consistency has been found between the occipital and the parietal areas. The predominance of phase consistency in parieto–frontal connections is also confirmed by the value of Γ(P,F)=0.06, to be compared with Γ(O,P)=0.03 and Γ(O,F)=0.03 obtained by WPPC

considering the whole area as a single ROI in the analysis. When considering the same values but extracted from WPLI, the pattern is less evident ($\Gamma(O,P)=0.012$; $\Gamma(O,F)=0.015$ and $\Gamma(P,F)=0.013$), since the mean connectivity between sectors as detected by the imaginary part of the coherence is almost the same. However, this has to be interpreted in the light of the different sensitivity of the two metrics with respect to the absolute value of phase shift at IAF between the source activity in the two areas, which is ultimately related to the propagation time of the nervous signal on the pathway connecting the ROIs under consideration. As a matter of fact, comparing values of connectivity parameters as extracted from WPPC and WPLI, we can see that the former are in general larger than the first ones. The pattern of a predominant fronto-parietal connectivity with a less consistent pareto-occipital connectivity is also less marked in the WPLI case. We interpret this, methodologically, by considering the different sensitivity of WPPC and WPLI with respect to phase delay absolute values. Being based on the imaginary part of the coherence, WPLI is more sensitive to phase consistent signals whose time delay corresponds to values close to $\phi=\pi/2$, which translate in the alpha band into a propagation time delay of signals of ~25 ms. This time is relatively large if compared to typical brain conduction delays, therefore we expect the phase delay value giving rise to significant connectivity measures to be more toward a phase difference of $\phi=0$, thus expecting WPPC to be more sensitive. However, because of the finite conduction delays in the white matter, and in general in the brain, we expect more distant areas having larger propagation time. Thus, we expect phase consistency between distant areas to be more evident in the WPLI.

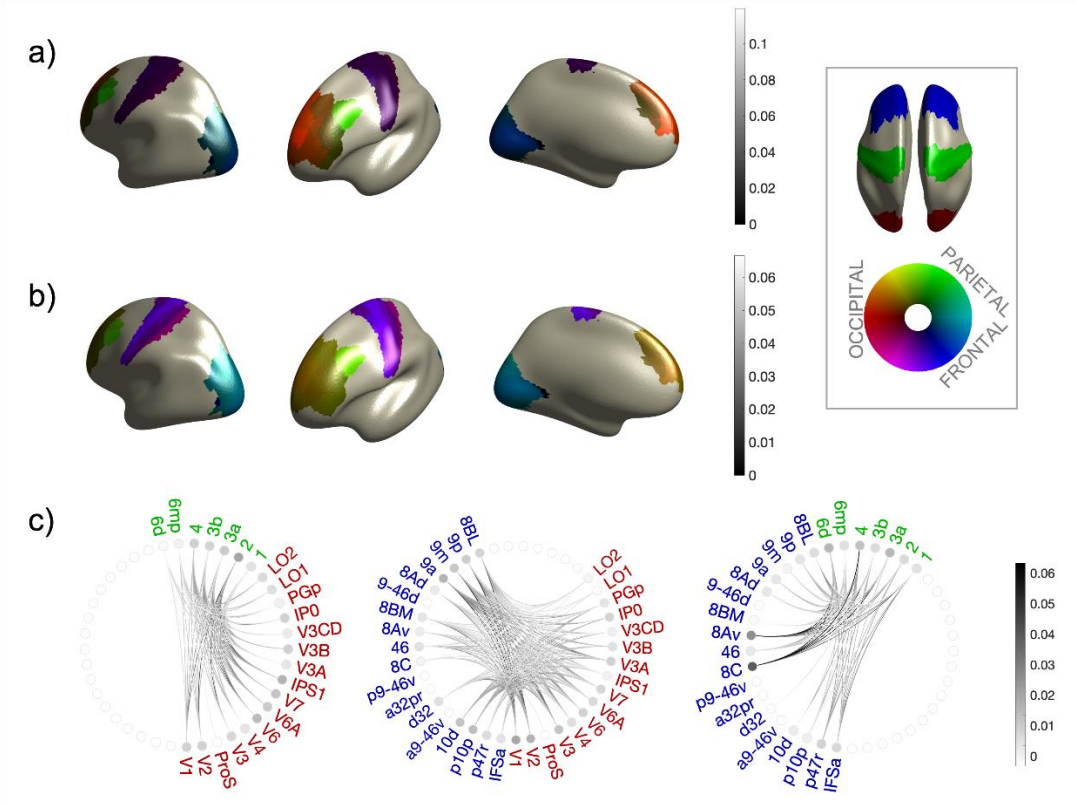

Figure 3.2. Results for WPPC connectivity. (**a**) Values of $\Delta(r_a,B)$, for all sector combinations in color code. (**b**) Values of $\Gamma(r_a,B)$, for all sector combinations in color code. (**c**) Connectome plots for the three relevant sector combinations computed from G. Red/green/blue ROI names belongs to occipital/parietal/frontal sectors respectively. The gray level of lines encodes the magnitude of $\Gamma(r_a,r_b)$ while the gray level of the dot encodes $\Gamma(r_a,B)$. In the inset the color code is explained: assigning red/green/blue colors to occipital/parietal/frontal sectors, respectively, the intensity of each area represents the overall magnitude of the parameter of interest, while the color encodes the proportion of the magnitude due to connectivity to the other sectors. So, for example, a parietal area more towards blue has more consistent phase relationship to the frontal sectors, while, if more towards red, the most relevant connection is to the occipital sector.

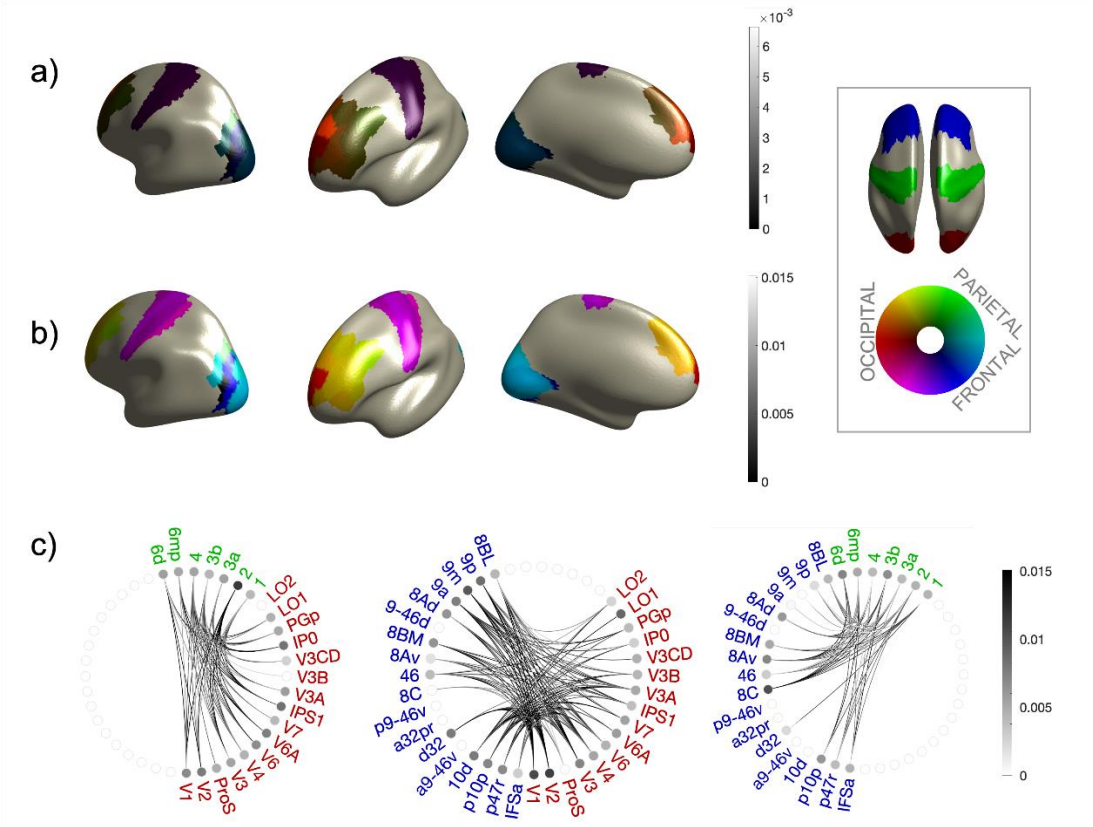

Figure 3.3. Results for WPLI connectivity. (**a**) Values of $\Delta(r_a,B)$, for all sector combinations in color code. (**b**) Values of $\Gamma(r_a,B)$, for all sector combinations in color code. (**c**) Connectome plots for the three relevant sector combinations computed from G. Red/green/blue ROI names belong to occipital/parietal/frontal sectors, respectively. The gray level of lines encodes the magnitude of $\Gamma(r_a,r_b)$ while the gray level of the dot encodes $\Gamma(r_a,B)$. In the inset the color code is explained: assigning red/green/blue colors to occipital/parietal/frontal sectors, respectively, the intensity of each area represents the overall magnitude of the parameter of interest, while the color encodes the proportion of the magnitude due to connectivity to the other sectors. So, for example, a parietal area more towards blue has more consistent phase relationship to the frontal sectors, while, if more towards red, the most relevant connection is to the occipital sector.

	Occipital		Parietal		Frontal	
V1			0.00005	0.01813	0.04801	0.03330
V2			0.00026	0.02336	0.03238	0.03052
ProS						
V3			0.00054	0.02260	0.01536	0.02715
V4			0.00007	0.01750	0.00167	0.01769
V6			0.01140	0.03235	0.01202	0.02595
V6A			0.00591	0.02071	0.01167	0.01895
V7			0.00787	0.02024	0.01866	0.02350
IPS1			0.01689	0.03146	0.00290	0.01733
V3A			0.00240	0.02260	0.01683	0.02353
V3B			0.00526	0.02268	0.00203	0.01546
V3CD			0.00017	0.01639	0.00426	0.01660
IP0			0.00256	0.02089	0.00459	0.01869
PGp			0.00036	0.01662	0.00583	0.01964
LO1					0.00054	0.01236
LO2			0.00007	0.01632	0.00008	0.01108
1	0.00147	0.01513			0.01000	0.02590
2	0.01323	0.03352			0.00150	0.02274
3a	0.00182	0.02163			0.01169	0.06285
3b	0.00166	0.01980			0.00928	0.04439
4	0.00153	0.01990			0.01354	0.06664
6mp	0.00026	0.01459			0.00653	0.03106
6d	0.00037	0.01261			0.02895	0.05629
8BL	0.09001	0.02671	0.00231	0.01952		
9p	0.08669	0.02861	0.00182	0.01623		
9m	0.10542	0.03381	0.00006	0.01323		
9a	0.11954	0.02970	0.00015	0.01537		
8Ad	0.03460	0.01914	0.00374	0.01783		
9–46d	0.05946	0.02154	0.00038	0.01336		
8BM	0.04143	0.02319	0.00015	0.01470		
8Av	0.00697	0.01461	0.06058	0.04594		
46	0.01625	0.01679	0.00248	0.01423		
8C	0.00071	0.01432	0.10138	0.05798		
p9–46v	0.00158	0.01213	0.01557	0.01848		
a32pr	0.00488	0.01591	0.00003	0.00649		
d32	0.02711	0.02249	0.00003	0.00840		
a9–46v	0.04548	0.01925	0.00283	0.01968		
10d	0.07100	0.02592	0.00028	0.01980		

	Occipital		Parietal		Frontal	
p10p	0.05559	0.02151	0.00038	0.01635		
p47r	0.01739	0.01740	0.01290	0.02046		
IFSa	0.00425	0.01535	0.00776	0.01874		

Table 3.2. Connectivity values for all ROIS towards each of the three sectors. Values of Γ(r,b) and Δ(r,B) computed from WPPC are shown.

	Occipital		Parietal		Frontal	
V1			0.00004	0.01007	0.00103	0.01402
V2			0.00002	0.01189	0.00103	0.01511
ProS					0.00008	0.00814
V3			0.00004	0.01173	0.00041	0.01337
V4					0.00012	0.01177
V6			0.00007	0.01102	0.00013	0.01063
V6A			0.00014	0.00900	0.00013	0.01001
V7					0.00019	0.01040
IPS1			0.00023	0.01053		
V3A			0.00005	0.01201	0.00014	0.01081
V3B					0.00016	0.01120
V3CD						
IP0			0.00016	0.01141	0.00003	0.00919
PGp			0.00009	0.01005	0.00009	0.01133
LO1						
LO2					0.00017	0.00917
1	0.00010	0.00946			0.00006	0.01010
2	0.00022	0.01309			0.00006	0.01011
3a	0.00008	0.01093			0.00022	0.01174
3b	0.00013	0.01032			0.00011	0.01131
4	0.00015	0.01078			0.00017	0.01302
6mp	0.00007	0.00970			0.00009	0.00931
6d	0.00018	0.01071			0.00027	0.01096
8BL	0.00266	0.01300	0.00008	0.01005		
9p	0.00664	0.01340	0.00006	0.00831		
9m	0.00505	0.01418	0.00003	0.00788		
9a	0.00261	0.01296				
8Ad	0.00063	0.01018	0.00010	0.00953		
9–46d	0.00206	0.01211	0.00002	0.00974		

	Occipital		Parietal		Frontal
8BM	0.00133	0.01180	0.00002	0.00744	
8Av	0.00011	0.00886	0.00074	0.01142	
46	0.00043	0.01072	0.00010	0.00949	
8C	0.00003	0.00789	0.00090	0.01296	
p9–46v	0.00017	0.00939	0.00025	0.01076	
a32pr	0.00051	0.01047	0.00002	0.00623	
d32	0.00134	0.01224	0.00003	0.00763	
a9–46v	0.00119	0.01163	0.00005	0.00786	
10d	0.00269	0.01193			
p10p	0.00150	0.01111	0.00012	0.00804	
p47r	0.00051	0.01068	0.00007	0.00797	
IFSa	0.00029	0.00949	0.00011	0.00918	

Table 3.3. Connectivity values for all ROIS towards each of the three sectors. Values of $\Gamma(r,b)$ and $\Delta(r,B)$ computed from WPLI are shown.

Inspecting more in detail $\Delta(r_a,B)$ and $\Gamma(r_a,B)$, as we can see from Figure 3.2a,b, the overall higher values for both the quantities extracted from WPPC correspond to the pareto–frontal connections, giving frontal area 8C the overall highest values ($\Delta(8C,P)=0.1$ and $\Gamma(8C,P)=0.06$)). This predominance can be also appreciated in the connecto-grams (Figure 3.2c), where connections between frontal areas 8C and 8av appear to be the highest in this sector's combination and with respect to the other sector combinations. This result is further confirmed by values obtained from WPLI, as shown in Figure 3.3. In this case also, referring to the parietal-frontal connection, area 8C is the most connected, with $\Delta(8C,P)=0.0009$ and $\Gamma(8C,P)=0.013$. We can thus conclude that this pattern is not due to the proximity of area 8C with respect to the frontal sector, WPLI being insensitive to zero-lag connections by design. However, in this case, the degree and the mean connectivity of areas 8c and 8av are not the highest with respect to other sector combinations, as can be appreciated in the connecto-grams of Figure 3.3c and in the color-coded source maps of mean connectivity in Figure 3.3b.

As regards the occipito–frontal connections, the highest WPPC connectivity and degree values has been found from frontal area 9a to the occipital sector, being $\Delta(9a,O)=0.12$ and $\Gamma(9a,O)=0.03$. The corresponding values for WPLI are $\Delta(9a,O)=0.003$ and $\Gamma(9a,O)=0.013$ while, in this case, areas 9m and 9p have also been found among the most connected to the occipital sector ($\Delta(9m,O)=0.007$ and $\Gamma(9m,O)=0.015$; $\Delta(9p,O)=0.007$ and $\Gamma(9p,O)=0.013$). This pattern is confirmed also by inspecting the connecto-grams in Figure 3.2c for WPPC and Figure 3.3c for WPLI, where, in the latter case, connectivity from frontal areas to occipital is more evident than in the WPPC case. As we pointed out before, we interpret this as a byproduct of the different sensitivity of WPPC and WPLI to coherent signals whose phase delay is more towards $\phi=0$ or $\phi=\pi/2$.

Finally, also in the single ROI connectivity values inspection, the occipito–parietal connectivity seems to be less relevant. This can be appreciated in the connecto-grams for WPPC in Figure 3.2c, where the highest values, in this case, can be found in frontal area 2 ($\Gamma(2,O)=0.034$ and in occipital area V6 ($\Gamma(V6,F)=0.033$) for the WPPC. This is confirmed also from WPLI results ($\Gamma(2,O)=0.013$ and ($\Gamma(V6,F)=0.012$). However, in this case the predominance of these two areas in the occipito-parietal connectivity is less marked as can be noticed from the connecto-grams in Figure 3.3c.

3.4 Discussion

Our aim was to provide the brain-state dependent EEG-TMS community with a work describing functional phase-dependent relationships between frontal, parietal and occipital areas. In these regions, alpha phase-dependent cortical excitability has been studied both in healthy controls and patients via brain-state dependent stimulation (Zrenner et al., 2018; Stefanou et al., 2018; Schaworonkow et al., 2018; Zrenner et al., 2020). Since the attempts at manipulating the effects of stimulation triggered by the phase detected on a region different from the target have no clear effectiveness (Zrenner et al., 2018), we believe that taking into account off-line phase-dependent connectivity patterns between the areas of interest would be of substantial help in predicting results from these studies.

Furthermore, consideration of the general phase-dependent connectivity state of the target region, (either trigger-region or not), could be essential for explaining changes in connectivity patterns for the time after application of plasticity protocols up to the moment where the behavioural measure has returned to baseline. Considering not only the TMS trigger-state (phase of the frequency of interest) but also the general connectivity state of the brain between the regions of interest would in fact be useful both for predicting plasticity protocols' efficacy and for interpreting results. For these reasons, we investigated spectral-resolved connectivity metrics that depend on a consistent phase relationship at IAF between frontal, parietal and occipital regions at rest. Results showed greater functional coupling between frontal and parietal areas, compared to very low functional coupling values between frontal and occipital and parietal and occipital pairs (Figure 3.2). These results are consistent with previous evidence of a fronto-parietal network at rest (e.g., Markett et al., 2014). We used MEG data and three different phase-coherence measures to show that a clear coupling emerges at IAF between frontal and parietal parcels at rest.

The ability to assess the strength of frontoparietal coupling from resting state data before and after an intervention makes this a suitable pathway for the investigation of pathway-specific plasticity. The alpha frequency band is relevant because this is the frequency band where phase-specific modulation of cortical excitability was previously demonstrated both in the motor system (Zrenner et al., 2018; Stefanou et al., 2018; Schaworonkow et al., 2018) and in the prefrontal cortex (Zrenner et al., 2020). Therefore, in frontal and sensorimotor regions, state-dependent stimulation based on the phase of alpha frequency appears effective in modulating cortical excitability at rest. However, when TMS is applied to the motor cortex in response to the phase of alpha recorded from the occipital cortex at rest, no modulation of corticospinal excitability was found (Zrenner et al., 2018).

For future development of real-time estimators of instantaneous connectivity states, we propose that connectivity metrics which depend on phase relationship between areas, and therefore describe whether two regions share trial-averaged functional coupling, can provide off-line connectivity priors in order to enable more accurate time-resolved connectivity estimates. This broad state of functional

coupling will, in fact, constitute a novel level of a priori information to assess whether real-time EEG-TMS paradigms will be effective in modulating cortical excitability in one area when the trigger is recorded from another area. In this light, for example, our finding of the limited functional coupling at rest between occipital and parietal areas can help elaborate on the reason why no effect was found when the hand knob of the motor cortex was stimulated on the basis of the occipital alpha phase (Zrenner et al., 2018).

Therefore, we propose that, in order to improve the efficacy of brain-state dependent stimulation protocols, the definition of "brain state" should not only refer to the instantaneous phase of the considered frequency which is triggering the stimulus, but also to the predisposition of the network to be globally perturbed by a stimulus triggered by a given phase of a determined frequency. In this regard, measures of functional coupling of regions at rest or during tasks that involve different functional coupling patterns would allow the obtaining of "off-line" connectivity priors.

In essence, beside the targeting of a local oscillation phase, brain-state dependent stimulation might leverage the off-line acquired, a priori knowledge regarding functional patterns in order to causally test the functional coupling between the brain regions involved. As an example of potential relevance of this approach, it has been shown that a network of prefrontal and occipito–parietal areas is involved in visual target detection and that alpha phase in this network is essential for a correct visuospatial processing (Capotosto et al., 2009; Hamm et al., 2012). Standard brain-state dependent stimulation could be used in order to further test the relationship between these cortical areas. In fact, brain-state dependent stimulation could potentially modulate cortical excitability of one area given the phase of alpha from another region. However, according to our approach, this brain-state dependent stimulation could lead to more effective results only when the two regions are embedded in a functional pattern that describes a state of sensitivity to be modulated (Stefanou et al., 2018; Bastos et al., 2016). A relevant part of cortical excitability could derive therefore from functional coupling of the target areas at rest (or during a task) at a given frequency.

This new perspective would also be useful for developing new and more effective individualized approaches for rehabilitation via brain-state dependent stimulation. In this regard, stimulation rehabilitative protocols have been proposed in stroke patients for whom specific adaptive connectivity patterns between specific cortical regions should be reinforced in order to achieve recovery (Brancaccio et al., 2022). In this light, our approach combining brain-state dependent stimulation with phase-dependent connectivity measures would nicely suit this purpose.

Finally, it must be noticed that our work is the first attempt at measuring coherence at IAF during rest between these three regions of the cerebral cortex. Most of the resting state literature consists of fMRI studies, which lack the temporal resolution that MEG measures provide (Fox et al., 2006; Mantini et al., 2007; Smitha et al., 2017). It is also worth noticing that, depending on the connectivity metric employed, we obtain slightly different results in the coupling between frontal and occipital areas, with the WPLI showing some functional coupling between the two regions compared to other measures. The WPLI is a measure based on the imaginary part of coherence. This metric is not sensitive to zero-lag spurious correlations. However, its maximum SNR spuriously coincides with $\pi/2$. Since we are investigating IAF which, on average, refers to around 10 Hz, the maximum SNR of WPLI measures has a phase-lag of about 25 ms. For these reasons, the functional relationship between distant areas like the frontal and occipital cortices might be captured thanks to this longer phase-lag that allows to pick-up the coupling between signals with longer propagation time.

To summarize, our findings suggest that brain-state dependent stimulation could benefit from taking into account a broader concept of "state" of the system. Depending on whether brain-state dependent stimulation is practiced at rest or during a task, one should consider the functional coupling patterns between the areas of interest in the frequency band whose phase is used as a trigger. Furthermore, we suggest that the physical distance between the regions could also be taken into account when choosing the coherence metric to assess functional coupling based on a consistent phase relationship in the frequency band of interest.

3.5 Conclusions

Brain-state dependent brain-stimulation has the potential to reliably modulate specific neural pathways using a “Closed-Loop” approach (Zrenner et al., 2016). How to achieve a time-resolved real-time estimation of EEG-derived brain connectivity states remains a key challenge. In this study, we addressed the off-line estimation of phase-based connectivity patterns between different regions of interest, presenting a pipeline to determine candidate pathways for real-time paradigms, for instance where the trigger-signal is extracted from one cortical site, and the stimulation targets a different site, or considering the target region and downstream effects to distal cortical regions.

In summary, offline connectivity measures have a twofold purpose: first, the estimate of connectivity patterns before and after can represent a biomarker of cortico-cortical changes after single and repetitive state-dependent TMS. In fact, for mu-alpha, stimulation at troughs was found to enhance Transcranial evoked potentials (TEPs) in both ipsi and contralateral hemisphere at 100 ms after stimulus even when the stimulus was provided at 90% of motor threshold (Desideri et al., 2019). Moreover, the same kind of stimulation has been found to be responsible for an enhancement of connectivity between the two sensorimotor cortices (Momi et al., 2021). Connectivity joined with TEP analysis could be even more relevant when analyzing non-motor areas such as the dorsolateral prefrontal cortex, where one cannot rely on as reliable and consistent an outcome as that of the MEPs.

Second, an off-line connectivity analysis can be used as prior information for future online estimates, to determine a correlation between areas oscillating at the same frequency or in an anticorrelation, a phase state which was previously suggested as a possible marker of functional segregation (Maris et al., 2016), or no correlation at all. The offline measures can serve as a benchmark for determining the optimal trade-off between the temporal resolution (window-length) and the estimator error variance for a given experimental condition, noting that the window-length must be short enough to capture physiological transitions (Ermolova et al., 2021).

Bibliography

1. Bastos, A.M.; Schoffelen, J.M. A tutorial review of functional connectivity analysis methods and their interpretational pitfalls. *Front. Syst. Neurosci.* **2016**, *9*, 175.

2. Berger, H. Über das elektroenkephalogramm des menschen. *Arch. Psychiatr. Nervenkrankh.* **1929**, *87*, 527–570.

3. Bergmann, T.O.; Lieb, A.; Zrenner, C.; Ziemann, U. Pulsed facilitation of corticospinal excitability by the sensorimotor μ-alpha rhythm. *J. Neurosci.* **2019**, *39*, 10034–10043.

4. Brancaccio, A.; Tabarelli, D.; Belardinelli, P. A new framework to interpret individual interhemispheric compensatory communication after stroke. *J. Pers. Med.* **2022**, *12*, 59.

5. Capotosto, P.; Babiloni, C.; Romani, G.L.; Corbetta, M. Frontoparietal cortex controls spatial attention through modulation of anticipatory alpha rhythms. *J. Neurosci.* **2009**, *29*, 5863–5872.

6. Da Silva, F.L.; Vos, J.E.; Mooibroek, J.; Van Rotterdam, A. Relative contributions of intracortical and thalamo-cortical processes in the generation of alpha rhythms, revealed by partial coherence analysis. *Electroencephalogr. Clin. Neurophysiol.* **1980**, *50*, 449–456.

7. Desideri, D.; Zrenner, C.; Ziemman, U.; Belardinelli, P. Phase of sensorimotor μ-oscillation modulates cortical responses to transcranial magnetic stimulation of the human motor cortex. *J. Physiol.* **2019**, *597*, 5671–5686.

8. Dugué, L.; Marque, P.; VanRullen, R. The phase of ongoing oscillations mediates the causal relation between brain excitation and visual perception. *J. Neurosci.* **2011**, *31*, 11889–11893.

9. Ermolova, M.; Metsomaa, J.; Zrenner, C.; Kozák, G.; Marzetti, L.; Ziemann, U. Spontaneous phase-coupling within cortico-cortical networks: How time counts for brain-state-dependent stimulation. *Brain Stimul.* **2021**, *14*, 404–406.

10. Fischl, B.; Sereno, M.I.; Tootell, R.B.H.; Dale, A.M. High-resolution intersubject averaging and a coordinate system for the cortical surface. *Hum. Brain Mapp.* **1999**, *8*, 272–284.

11. Folstein, M.F.; Folstein, S.E.; McHugh, P.R. 'Mini-mental state' a practicalmethod for grading the cognitive state of patients for the clinician. *J. Psychiatr. Res.* **1975**, *12*, 189–198.

12. Fox, M.D.; Corbetta, M.; Snyder, A.Z.; Vincent, J.L.; Raichle, M.E. Spontaneous neuronal activity distinguishes human dorsal and ventral attention systems. *Proc. Natl. Acad. Sci. USA* **2006**, *103*, 10046–10051.

13. Fries, P. Rhythms for cognition: Communication through coherence. *Neuron* **2015**, *88*, 220–235.

14. Friston, K.J. *Statistical Parametric Mapping: The Analysis of Funtional Brain Images*, 1st ed.; Elsevier: Amsterdam, The Netherlands; Academic Press: Boston, MA, USA, 2007.

15. Gaser, C., Dahnke, R., Thompson, P. M., Kurth, F., & Luders, E. (2022). CAT-a computational anatomy toolbox for the analysis of structural MRI data. BioRxiv.

16. Glasser, M.F.; Coalson, T.S.; Robinson, E.C.; Hacker, C.D.; Harwell, J.; Yacoub, E.; Ugurbil, K.; Andersson, J.; Beckmann, C.F.; Jenkinson, M.; et al. A multi-modal parcellation of human cerebral cortex. *Nature* **2016**, *536*, 171–178.

17. Gordon, P.C.; Dörre, S.; Belardinelli, P.; Stenroos, M.; Zrenner, B.; Ziemann, U.; Zrenner, C. Prefrontal theta-phase synchronized brain stimulation with real-time EEG-Triggered TMS. *Front. Hum. Neurosci.* **2021**, 335.

18. Gross, J.; Kluger, D.S.; Abbasi, O.; Chalas, N.; Steingräber, N.; Daube, C.; Schoffelen, J.-M. Comparison of undirected frequency-domain connectivity measures for cerebro-peripheral analysis. *Neuroimage* **2021**, *245*, 118660.

19. Gross, J.; Kujala, J.; Hamalainen, M.; Timmermann, L.; Schnitzler, A.; Salmelin, R. Dynamic imaging of coherent sources: Studying neural interactions in the human brain. *Proc. Natl. Acad. Sci. USA* **2001**, *98*, 694–699.

20. Hämäläinen, M.; Hari, R.; Ilmoniemi, R.J.; Knuutila, J.; Lounasmaa, O.V. Magnetoencephalography—Theory, instrumentation, and applications to noninvasive studies of the working human brain. *Rev. Mod. Phys.* **1993**, *65*, 413–497.

21. Hamm, J.P.; Dyckman, K.A.; McDowell, J.E.; Clementz, B.A. Pre-cue fronto-occipital alpha phase and distributed cortical oscillations predict failures of cognitive control. *J. Neurosci.* **2012**, *32*, 7034–7041.

22. Hyvärinen, A.; Karhunen, J.; Oja, E. *Independent Component Analysis*; Wiley: Hoboken, NJ, USA, 2001.

23. Ilmoniemi, R.; Sarvas, J. *Brain Signals: Physics and Mathematics of MEG and EEG*; MIT Press: Cambridge, MA, USA, 2019.

24. Jensen, O.; Mazaheri, A. Shaping functional architecture by oscillatory alpha activity: Gating by inhibition. *Front. Hum. Neurosci.* **2010**, *4*, 186.

25. Klimesch, W.; Sauseng, P.; Hanslmayr, S. EEG alpha oscillations: The inhibition–timing hypothesis. *Brain Res. Rev.* **2007**, *53*, 63–88.

26. Lee, T.-W.; Girolami, M.; Sejnowski, T.J. Independent component analysis using an extended infomax algorithm for mixed subgaussian and supergaussian sources. *Neural Comput.* **1999**, *11*, 417–441.

27. Mantini, D.; Perrucci, M.G.; Del Gratta, C.; Romani, G.L.; Corbetta, M. Electrophysiological signatures of resting state networks in the human brain. *Proc. Natl. Acad. Sci. USA* **2007**, *104*, 13170–13175

28. Maris, E.; Fries, P.; van Ede, F. Diverse phase relations among neuronal rhythms and their potential function. *Trends Neurosci.* **2016**, *39*, 86–99.

29. Markett, S.; Reuter, M.; Montag, C.; Voigt, G.; Lachmann, B.; Rudorf, S.; Elger, C.E.; Weber, B. Assessing the function of the fronto-parietal attention network: Insights from resting-state fMRI and the attentional network test. *Hum. Brain Mapp.* **2014**, *35*, 1700–1709.

30. Mathewson, K.E.; Gratton, G.; Fabiani, M.; Beck, D.M.; Ro, T. To see or not to see: Prestimulus α phase predicts visual awareness. *J. Neurosci.* **2009**, *29*, 2725–2732.

31. Mazaheri, A.; Jensen, O. Rhythmic pulsing: Linking ongoing brain activity with evoked responses. *Front. Hum. Neurosci.* **2010**, *4*, 177.

32. Momi, D.; Ozdemir, R.A.; Tadayon, E.; Boucher, P.; Shafi, M.M.; Pascual-Leone, A.; Santarnecchi, E. Network-level macroscale structural connectivity predicts propagation of transcranial magnetic stimulation. *Neuroimage* **2021**, *229*, 117698.

33. Nieminen, J.O.; Sinisalo, H.; Souza, V.H.; Malmi, M.; Yuryev, M.; Tervo, A.E.; Stenroos, M.; Milardovich, D.; Korhonen, J.T.; Koponen, L.M.; et al. Multi-locus transcranial magnetic stimulation system for electronically targeted brain stimulation. *Brain Stimul.* **2022**, *15*, 116–124.

34. Oostenveld, R.; Fries, P.; Maris, E.; Schoffelen, J.-M. FieldTrip: Open source software for advanced analysis of MEG, EEG, and invasive electrophysiological data. *Comput. Intell. Neurosci.* **2011**, *2011*, 868305.

35. Pezzulo, G.; Zorzi, M.; Corbetta, M. The secret life of predictive brains: What's spontaneous activity for? *Trends Cogn. Sci.* **2021**, *25*, 730–743.

36. Schaworonkow, N.; Gordon, P.C.; Belardinelli, P.; Ziemann, U.; Bergmann, T.O.; Zrenner, C. μ-rhythm extracted with personalized EEG filters correlates with corticospinal excitability in real-time phase-triggered EEG-TMS. *Front. Neurosci.* **2018**, *12*, 954.

37. Smitha, K.A.; Akhil Raja, K.; Arun, K.M.; Rajesh, P.G.; Thomas, B.; Kapilamoorthy, T.R.; Kesavadas, C. Resting state fMRI: A review on methods in resting state connectivity analysis and resting state networks. *Neuroradiol. J.* **2017**, *30*, 305–317.

38. Stefanou, M.I.; Desideri, D.; Belardinelli, P.; Zrenner, C.; Ziemann, U. Phase synchronicity of μ-rhythm determines efficacy of interhemispheric communication between human motor cortices. *J. Neurosci.* **2018**, *38*, 10525–10534.

39. Stolk, A.; Brinkman, L.; Vansteensel, M.J.; Aarnoutse, E.; Leijten, F.S.; Dijkerman, C.H.; Knight, R.T.; de Lange, F.P.; Toni, I. Electrocorticographic dissociation of alpha and beta rhythmic activity in the human sensorimotor system. *eLife* **2019**, *8*, e48065.

40. Taulu, S.; Simola, J. Spatiotemporal signal space separation method for rejecting nearby interference in MEG measurements. *Phys. Med. Biol.* **2006**, *51*, 1759–1768.

41. Taulu, S.; Simola, J.; Kajola, M. Applications of the signal space separation method. *IEEE Trans. Signal Process.* **2005**, *53*, 3359–3372.

42. Taylor, J.R.; Williams, N.; Cusack, R.; Auer, T.; Shafto, M.A.; Dixon, M.; Tyler, L.K.; Henson, R.N. The Cambridge Centre for ageing and neuroscience (Cam-CAN) data repository: Structural and functional MRI, MEG, and cognitive data from a cross-sectional adult lifespan sample. *Neuroimage* **2017**, *144*, 262–269.

43. Vijayan, S.; Kopell, N.J. Thalamic model of awake alpha oscillations and implications for stimulus processing. *Proc. Natl. Acad. Sci. USA* **2012**, *109*, 18553–18558.

44. Vinck, M.; Oostenveld, R.; van Wingerden, M.; Battaglia, F.; Pennartz, C.M.A. An improved index of phase-synchronization for electrophysiological data in the presence of volume-conduction, noise and sample-size bias. *Neuroimage* **2011**, *55*, 1548–1565.

45. Vinck, M.; van Wingerden, M.; Womelsdorf, T.; Fries, P.; Pennartz, C.M.A. The pairwise phase consistency: A bias-free measure of rhythmic neuronal synchronization. *Neuroimage* **2010**, *51*, 112–122.

46. Zrenner, B.; Zrenner, C.; Gordon, P.C.; Belardinelli, P.; McDermott, E.J.; Soekadar, S.R.; Fallgatter, A.J.; Ziemann, U.; Müller-Dahlhaus, F. Brain oscillation-synchronized stimulation of the left dorsolateral prefrontal cortex in depression using real-time EEG-triggered TMS. *Brain Stimul.* **2020**, *13*, 197–205.

47. Zrenner, C.; Belardinelli, P.; Müller-Dahlhaus, F.; Ziemann, U. Closed-loop neuroscience and non-invasive brain stimulation: A tale of two loops. *Front. Cell. Neurosci.* **2016**, *10*, 92.

48. Zrenner, C.; Desideri, D.; Belardinelli, P.; Ziemann, U. Real-time EEG-defined excitability states determine efficacy of TMS-induced plasticity in human motor cortex. *Brain Stimul.* **2018**, *11*, 374–389.

Chapter 4

The region-specific impact of aging on cortical myelin content and thickness

This Chapter is aimed at investigating the effects of aging on cortical thickness and cortical myelin content. Specifically, 610 healthy participants aged between 18 and 89 years old underwent T1-weighted, T2-weighted and MTI sequences in the context of the Cam-CAN project. Participants were divided in three age groups representative of young, middle and late adulthood respectively and changes in cortical thickness and cortical myelin content were assessed for each group. In particular, cortical myelin content was investigated employing both the T1/T2 ratio and MTR in order to evaluate which is the most stable proxy for cortical myelin content. We show a dissociation in the aging patterns of somatosensory and motor regions, neighbouring areas that have been historically assimilated. Moreover, we show that the MTR is the most reliable metric to assess cortical myelin content. The results on the age-related brain structural changes are here discussed with respect to their implication on the choice of healthy controls in clinical population studies.

4.1 Introduction

Age-related changes in brain structure have been well documented both in post-mortem studies and using non-invasive methods of brain structure investigation. These studies have converged on evidences of a general age-related degeneration both in terms of global brain volume reduction and grey and white matter thinning (Salat et al., 2004; Raz, 2000; Gunning-Dixon et al., 2008; Davis et al., 2009). However, most of these works have focused on the grey matter, therefore exploring the progressive age-related so-called cortical thinning. In this regard, there are two relevant points that

need to be stressed. First, studies on cortical thickness changes associated with healthy aging did not use large samples and, most importantly, samples representative of the full life span. Secondly, it is clear that cortical thinning is not the only type of age-related structural brain change. Among all the other factors of brain structural aging we think, as suggested by the title of this chapter, that the cortical loss of myelin content should be taken into account when evaluating brain changes due to aging, especially in conjunction with the evaluation of cortical grey matter loss.

As for the first point, most of the previous studies have investigated the cortical thickness changes due to aging including small sample sizes in their analyses. In fact, even when the sample size of a work seems to be sufficiently large with respect to a typical non age-related structural study, it can still be limited in order to be sensitive to small age-related cortical degenerations effects, especially in non-longitudinal settings (Fjell et al., 2009). Moreover, several studies suffer from a non-uniform or limited age distribution in the sample. One of the first attempts at investigating cortical changes due to aging processes lies in the work by Salat and colleagues (2004), in which the authors used a sample of 106 participants aged between 18 to 93 years. They showed that, (1) by middle-age (from 41 to 57 years in their work), the cortical thinning was observable over the whole cortex, (2) the fastest thinning rate was present in the primary motor cortex, and (3) the greatest magnitude of thinning was found in prefrontal, precentral regions, with the temporal regions being the most spared by age-related degeneration. Another work by Thambisetty et al. (2010) has longitudinally studied age-related changes of the cortical thickness in a cohort of 66 subjects followed up for 8 years and aged between 60 and 84 years. They found that cortical thinning interests the whole cortex, with frontal and parietal areas showing the highest thinning rate compared to occipital and temporal areas. Moreover, Hutton et al. (2009) used both voxel-based cortical thickness and voxel-based morphometry to assess grey matter changes in 48 participants aged between 22 and 60 years. They found that the most prominent age-related changes in the cortex were visible at the level of the prefrontal, orbitofrontal and temporal regions, jointly with the insula, cingulate, and precentral gyri.

Taken together, these evidences show both consistency and discrepancy in the findings on cortical degeneration due to aging, with the most consistent result being represented by the degeneration of the frontal and, in some cases, parietal cortex. These discrepancies have been discussed in a review by Raz and Rodrigue (2006) and attributed to the variability due to heterogeneity in the samples, small sample sizes and different analysis pipelines employed in the previous studies (e.g. volumetric approaches vs voxel-based morphometry). Recent studies have made attempts to overcome these issues. For example, Fjell et al. (2009) have used the same surface-based segmentation procedure to assess cortical thickness in 6 separated and independent samples including 883 participants in total. Importantly, even if the total number of participants included across all samples was 883, the average number per sample consisted in 147 participants. Also, the investigated life span is claimed to range from 18 to 93 years, even though 3 out of 6 samples were mainly representative of middle age (see Table 1 from Fjell et al., 2009). With these premises in mind, Fjell and colleagues (2009) found that, across all samples studied, superior, middle and inferior frontal cortices were in general the most affected by aging, confirming the results on the vulnerability of these regions to aging processes. Moreover, they found that the temporal cortices (both superior and middle gyri) were also affected in the 6 samples used, together with the temporopatietal junction. Differently, the occipital cortex showed vulnerability to aging only in 4 out of 6 samples, while the temporal lobe and the anterior cingulate cortex were found to be well preserved despite aging. Importantly, Fjell and colleagues (2009) also reported that the age-effects differed over the frontal, temporal and occipital cortices across the investigated samples. This result confirms the variability introduced by the heterogeneity of the participants in the different samples and the consequent necessity to assess brain changes due to healthy aging in larger and more homogeneously age -distributed cohorts, in order to reduce the effects of participants' heterogeneity. It is also important to stress that all the afore-mentioned studies have focused on restricted age ranges. In fact, almost all the studies discussed so far are largely representative of the middle-age (< 60 years old), while only a few works have tried to investigate age-related changes in broader age-spans. In this context, only three studies managed to investigate

brain age-related changes in samples covering almost the full life span. McGinnis et al. (2011) investigated cortical thinning in 316 participants aged between 18 to 96 years old, while Lemaitre et al. (2012) investigated changes in grey matter volume, cortical thickness and surface area in a cohort of 216 participants aged between 18 to 87 years old. Finally, Frangou et al. (2020) investigated cortical thickness changes using cross-sectional data from 17075 participants aged between 3 to 90 years old. While all the three studies found a general and widespread degeneration of the brain due to aging, they still all highlight that the frontal cortex is not the only area vulnerable to degeneration. In fact, both Lemaitre et al. (2012) and McGinnis et al. (2011) criticized the so-called *last in first out hypothesis* (Raz, 2000), according to which regions that develop late also degenerate early in life (e.g. the frontal cortex). For example, Lemaitre and colleagues (2012) found that early developing regions like the precentral gyrus show early cortical thinning due to aging processes, reporting evidence clearly in contrast with the *last in first out hypothesis* as this framework predicts early developing regions to be the least affected by aging.

The effects seen in Lamaitre et al. (2012) and McGinnis et al. (2011) were only partially confirmed by Frangou et al. (2020), as they found that late life stages are associated mainly with entorhinal and temporopolar degeneration. Also, Frangou and colleagues (2020) report high inter-individual variability to be especially present at the level of the frontal regions, anterior cingulate and temporal cortex. However, if inter-individual variability necessarily needs to be overcome by employing larger samples, like in Frangou et al. (2020), it should be noticed that data of that study were acquired with different scanners, potentially adding multi-site related variability to the results.

Therefore, attempts at describing age-related brain changes in participants covering broad age-ranges should employ big and single-site datasets in order to optimally extract small age-related structural effects from the sample variance, inevitably contaminated by heterogeneity and inter-individual variability.

It is necessary at this point to consider how cortical thickness and grey matter alterations in general do not represent the only degeneration that can be related to brain aging processes. Another relevant biomarker affected by aging is cortical myelin content. However, also in this case, evidences are based on relatively small samples and different metrics. For example, Deoni and colleagues (2015) used both quantitative T1-weighted and myelin water fraction (MWF) imaging to assess cortical myelin maturation in 215 children aged between 1 to 6 years. Sensory areas (somatosensory, motor, auditory and visual cortices) were found to develop earlier in terms of cortical myelin content compared to temporal, prefrontal and associative cortices. This led the authors to conclude that sensory areas are the first to develop while the frontal cortices develop last, in accordance with the *last in first out hypothesis* (Deoni et al., 2015). However, further reports on cortical myelin content changes over broader age ranges found different results. For example, Kwon and colleagues (2020), using the ratio between T1-weighted and T2-weighted images (T1w/T2w ratio) of 686 adolescents and young adults (< 35 years old), found the regional growth in myelin content to be more homogeneous in young adults than adolescents, while the primary motor cortex showed the highest increase in myelination during adolescence. This result appears in contrast with the last in first out hypothesis, since the motor cortex is considered to develop early in this framework. Therefore, if both myelin content and grey matter are taken into account, the motor cortex seems to develop relevantly later compared to other regions, suggesting a need for revision of the last if first out framework. Kwon and colleagues' (2020) results are in accordance with previous studies, showing the highest myelination in sensory cortices by means of T1w/T2w in adolescents and young adults. In fact, Shafee and colleagues (2015) also employing T1w/T2w images from 1555 scans of young adults aged between 18 and 35 years, found somatosensory, motor and visual regions to show the highest increase in myelin with age, while the frontal and temporal cortices showed the lowest levels of myelination. This latter result had been already reported by Glasser and Van Essen (2011), who first used the T1w/T2w ratio as a proxy metric sensitive to cortical myelin content. However, Baum and colleagues (2022) found rapid increases in myelin content in sensorimotor areas of adolescents, as well as later

gradual age-related gains in myelin content of associative areas, in contrast with (Kwon et al 2020) and (Shafee et al., 2015). Therefore, mixed results also emerge in studies investigating age-related myelin changes. Again, this lack of accordance can be in part ascribed to the non-overlapping age-ranges investigated. In this regard, Grydeland and colleagues (2013) used both T1w/T2w ratio and mean diffusivity (MD) to assess myelin changes in a group of participants with a large age range between 19 to 83 years. Participants were divided in three groups of young (<20 years), middle-age (20 – 57 years), and old participants (>57) (with roughly 85 participants per group). They proposed that myelin cortical development might follow an inverted U-shaped trajectory, with increases in myelin content up to the 30s, followed by a plateau, and a later decrease from the 50s on. This pattern was strongest in frontal, parietal and temporal associative areas. In the paracentral lobule, the U-shaped trajectory was not detected. This region showed a more prolonged gain in myelin content and a less steep decline around the 50s. Wu and colleagues (2016) used the so called magnetization transfer ratio (MTR) rather than the T1w/T2w ratio as a proxy to assess cortical myelin concentration in a group of 66 participants aged between 30 and 85 years. They also found an inverted U-shaped trajectory in myelin changes in the frontal, temporal and temporopatietal regions (therefore suggesting maturation up to the 50s and demyelination from the 60s and beyond). However, they found no significant changes in the MTR of primary motor, somatosensory and auditory regions with age, which led the authors to suggest that these areas are not subject to degeneration during aging. Finally, Karolis et al. (2019) employed the MTR proxy to assess cortical myelin changes associated with age in a cohort of 97 participants aged between 20 and 74 years. In contrast to Wu et al. (2016) they found important age-related changes in sensory and motor cortices.

These differences from studies investigating comparable and broad age span might be again ascribed to the different metrics and sample sizes. In fact, Wu and colleagues (2016) and Karolis et al. (2019) are, to our knowledge, the only ones employing the MTR to assess age-related changes in cortical myelin content, while all other studies mentioned so far have employed the T1w/T2w ratio. In this

regard, it is fundamental to describe the key differences between these two metrics. Glasser and Van Essen (2011) conceived T1w/T2w ratio as an MRI-proxy sensitive to myelin content: it returns a unitless quantity correlating with myelin tissue concentration (Shafee et al, 2015). However, not only myelin but also iron molecules contribute to the ratio of the T1w/T2w contrast (Shafee et al., 2015; Fukunaga et al., 2010). Since iron is also accumulated over the life-span (Dröge et al., 2007), this represents a confound in the results obtained with T1w/T2w ratio especially when this metric is employed to investigate age-related myelin changes. Another limitation of this metric consists in the intensity histogram of the images used to compute the ratio varying across participants: a normalization procedure is necessary before T1w/T2w computation, a step that potentially increases inter-subject variability and in turn the overall variance in group analyses. This is a methodological drawback that has been partially tackled by Ganzetti et al. (2014) exploiting the tissue intensity outside of the brain in order to normalize intensities range before T1w/T2w ratio computation. However, none of the previously mentioned works used this calibration algorithm on the T1w/T2w ratio. Moreover, the unitless quantity resulting from the T1w/T2w ratio after histogram normalization, is still subject-dependent and therefore typically normalized using a z-value approach before group level analysis, thus assuming a Gaussian distributed T1w/T2w contrast distribution over the subject's brain. Furthermore, results on cortical myelin content might be affected not only by the effect of age related iron accumulation, but also by non-optimal MRI images' intensity normalization across participants and potential age related errors in whole brain z-value based normalization. Regarding the MTR, this is also an MRI-proxy of the concentration of myelin in brain tissues. However, differently from the T1w/T2w ratio, it is specifically designed to assess myelin content. Directly probing myelin concentration with MR techniques would require to measure relaxation times (T1 or T2) of protons bound in macromolecules. Unfortunately, these protons loose magnetization on a time scale of approximatively 10 μs, a relaxation time too short to be probed with an MR sequence (Sled, 2018). For this reason, the measure of myelin concentration with non-invasive MR based methods is optimized but indirect. Magnetization Transfer Imaging is based on the phenomenon of magnetization

transfer between populations of protons in brain tissues. Shortly, a saturation pulse is delivered in order to induce a magnetization in the pool of protons bound in macromolecules. Right after the saturation pulse, a standard sequence is used to probe relaxation times of free protons. This leads to a "saturated image". The same procedure is repeated without the saturation pulse, leading to a "baseline image". When the saturation pulse is applied, protons bound in macromolecules lose their magnetization by means of different relaxation processes. Among those, they partially transfer their magnetization to the free protons population. This leads to a reduced intensity of T1w or T2w contrasts in the image acquired right after the saturation pulse. The MTR is then defined as the ratio between the intensity reduction and the baseline image. This unitless proxy, ranging by construction between 0 and 1, is then proportional to the concentration of protons bound in myelin macromolecules in the voxel of interest. Differently from the T1w/T2w ratio, the MTR approach compares images acquired within the same scan and, in terms of free protons probing, with the same parameters. For this reason, no preliminary intensity normalization is required on the baseline and saturated images. In addition, being the MTR proxy a unitless ratio bound by construction between 0 and 1, it does not require whole brain normalization before group analysis. MTR is the most optimized non-invasive MR based measure of myelin content in the brain. However, it requires a specific acquisition that cannot be later used for other purposes, like in the case of T1w/T2w ratio. The MTR has also been shown to correlate better than the T1/T2 ratio with histologic studies (van der Weijden et al., 2021; Hagiwara et al., 2018).

In this light, the presence of both accordance and discrepancies in previous works' results can be ascribed to the differences between the metrics employed, in the samples' dimension and in the age-range of the investigated subsamples. For this reason, a systematic investigation of the results obtained with T1w/T2w and MTR on the same samples needs to be accomplished to understand which metric is more stable and reliable in assessing myelin content and its changes over the life-

span. This, in fact, would be not only useful to understand brain changes in healthy aging, but also essential to better understand the brain changes that interest clinical populations suffering from conditions often emerging in the elderly. In particular, evaluating the reliability of cortical myelin proxies would be especially useful in the assessment of stroke patients. In fact, stroke patients are usually in their elderly and suffer not only from the stroke lesion but also from the common age-related structural changes of the brain, with cortical myelin content being of particular interest. In fact, it has been shown that cortical myelin content correlates with corticospinal excitability, which is a measure that is commonly used as a predictor of recovery in stroke patients. For example, Kwon and colleagues (2020) have found a correlation between cortical myelin content in sensorimotor areas and the participants' performance in an eye-hand coordination task. Furthermore, Dubbioso and colleagues (2021) have shown that a higher degree of myelin content at the level of the precentral gyrus enables a more precise synchronization of motor commands with the visual cue in a finger tapping experiment. Also, it has been found that the more rostral the motor hotspot is in a participant, the lower the myelination level in the motor hotspot and the longer the MEPs latencies (Betti et al., 2022; Dubbioso et al., 2021). Furthermore, Lazari et al. (2022) have recently shown a relationship between the levels of myelination of the tracts connecting the left PMv and right M1 and the action reprogramming behavior that these regions support, therefore further supporting the notion of an impact of myelination levels on behavioral performance. In stroke patients, this link had been already suggested by Lakhani et al. (2017), who showed a positive correlation between the two hemispheres' asymmetry in terms of cortical myelin content and the motor impairment in the affected limb. This finding led Lakhani and colleagues (2017) to propose that myelination levels should be used as a marker of post-stroke neurobiological changes. However, cortical myelin content has never been systematically included in the assessment of stroke patients or in the assessment of corticospinal excitability differences between stroke patients and age-matched controls.

The aforementioned pieces of evidence are useful to explain the aim of the study reported here. In this work, we investigate on a big cohort of participants (N= 610; age: 18 – 89; Cam-CAN Dataset (Shafto et al., 2014; Taylor et al., 2017)) age-related changes both in gray matter and cortical myelin content. With respect to the latter, we chose to investigate cortical myelin content using both the T1w/T2w ratio and the MTR, with the aim to assess the most stable and reliable metric of cortical myelination. Aging has an impact not only on gray matter degeneration but also on myelin content and different cortical regions are differentially affected. In particular, it will be shown that MTR is the most stable metric of cortical myelin content as expected, and sensory and motor sectors show different patterns of development from young adulthood to old age. Furthermore, it will be shown that the relationship between the T1w/T2w ratio and the MTR is variable over the cortex, clearly suggesting that the relationship between the two metrics and the quantities they really measure is still far from being understood. Given the pieces of evidence previously reported on the relationship between myelination levels and behavioral motor performance, it is here proposed that stroke patients should be evaluated also in terms of cortical myelin content, using MTR as a reliable metric. We consider that myelination assessment could be used in order to compare the individual stroke patient cortical myelin content with standard values in peers of the same age, in a normative approach logic. Assessing the cortical myelin content in the individual patient with respect to the expected normal myelination levels at their age might in fact help predict the potential individual recovery margin. Last but not least, individual cortical myelin content should be also taken into account when evaluating stroke patients with respect to controls in corticospinal excitability studies. In this regard, many of the studies investigating differences between stroke and controls in terms of corticospinal excitability include healthy control participants who are not age-matched to the stroke patients, as they are generally younger than patients on average (e.g. Kang et al., 2011; Kang et al., 2012; Kim et al., 2014; Julkunen et al., 2016; Garcia et al., 2016; Birchenall et al., 2019; Kemlin et al., 2019). In this regard, given the aforementioned evidence on the relationship between corticospinal excitability

levels and cortical myelin, it comes to reason that stroke patients should be only compared with controls in the same age range and, if possible, with controls showing similar levels of myelination.

In summary, this is a work where both cortical thickness and cortical myelin content changes are investigated in relation to age, with cortical myelin content being assessed with two different and debated metrics. The MTR is shown to be the most stable and reliable one in assessing cortical myelin content, leading to similar or different results compared to the T1w/T2w ratio, depending on the examined brain region. It is here proposed that these structural age-related changes should not be overlooked when evaluating the potential recovery of the individual patient and differences between patients and controls in corticospinal excitability experiments.

4.2 Methods

4.2.1 Dataset and Acquisition

MRI data from 610 healthy participants out of all the approximatively 700 participants recruited at the Cambridge Centre for Ageing and Neuroscience (Cam-CAN; Shafto et al., 2014; Taylor et al., 2017) were included in this study. The Cam-CAN dataset is a big repository including both raw and preprocessed structural (T1w, T2w, DWI, MTR) and functional (sensorimotor task, movie-watching and resting state) MRI and MEG (sensorimotor task and resting state) data on healthy participants covering the whole adult life-span. Subjects that underwent all the MRI scans described in the following Recording Section (T1, T2 and MTI) were included in this study. This lead to a final dataset of 610 healthy subjects (310 females) with age ranging between 18 and 89 years.

4.2.2 MRI Recordings

All MRI datasets were collected in a single site (Cambridge Centre for Ageing and Neuroscience) using the same 3 T Siemens TIM Trio scanner with a 32-channel head coil. Each participant underwent: a T1-weighted Magnetization Prepared Rapid Gradient Echo (MPRAGE) sequence with repetition time (TR) = 2250 ms; echo time (TE) = 2.99 ms; inversion time (TI) = 900 ms; flip angle = 9°; field of view (FOV) = 256 × 240 × 192 mm; resolution = 1 mm isotropic;); a T2-weighted single slab three-dimensional turbo spin echo SPACE sequence (Mugler and Brookeman, 2004) with TR = 2800 ms; TE = 4.08 ms; flip angle α = 9°; field of view (FOV) = 256 × 240 × 192 mm; resolution = 1 mm isotropic. To the purpose of myelin evaluation, each participant underwent a Magnetization Transfer Imaging session (MTI) consisting of two MT-prepared Spoiled Gradient (SPGR) sequences, with and without the application of a Gaussian shaped RF pulse (offset frequency 1950 Hz, bandwidth 375 Hz, duration 9984 μs) for myelin protons saturation. The SPGR sequence parameters were TE = 5 ms; flip angle α = 12°; field of view (FOV) = 192 × 192 mm; resolution = 1.5 x 1.5 mm; the repetition time were set to 50 or 30 ms, depending on the estimated SAR for the subject exceeding or not the limits, respectively. For more detailed information on the MRI recordings parameters collected during Stage 2 of the Cam-CAN project, the reader is invited to read Table 1 from Taylor et al. (2017).

4.2.3 Data Preprocessing

T1-weighted images were first processed to define anatomy and extract cortical thickness values over the cortex. Each volume was denoised and debiased for the correction of field inhomogeneities using SPM software (Friston, 2003). Then, the Computational Anatomy Toolbox 12 (CAT12) (Gaser et al., 2022) was used for the segmentation of Gray Matter (GM), White Matter (WM) and Cerebro Spinal Fluid (CSF). Also, the total intracranial volume (TIV) was computed and the brain extraction

implemented. Moreover, each volume was non-linearly registered on a template in MNI space (IXI database of 555 subjects; http://www.brain-development.org). The method implemented in CAT12 was then used to extract the cortical thickness values while concurrently defining the mid-thickness central surface as a mesh of approximatively 327000 vertices. The mid-thickness surface is anatomically defined as the surface in between the pial and the white/gray matter interface. A final spherical mapping-based projection onto the FreeSurfer average template (with a Gaussian smoothing kernel of FWHM = 15 mm) was performed in order to allow for group analyses (Fischl et al., 2012). Also T2-weighted images were denoised and debiased for the correction of field inhomogeneities using SPM. Then they were co-registered (rigid body co-registration) on the individual T1-weighted image. After these steps, both the T1- and T2-weighted images were calibrated using a non-linear approach (Ganzetti et al., 2014) based on the intensity extracted from internal brain tissues (GM, WM, CSF) (Glasser and Van Essen., 2011). At this point, the ratio between the T1 and T2-weighted images was computed. The final volumetric values of T1w/T2w ratio were then extracted on the mid-thickness mesh, resulting in a surface-based map of myelin content as estimated by T1w/T2w ratio. A final spherical mapping projection on to the FreeSurfer average template (with a Gaussian smoothing kernel of FWHM = 5 mm) was performed in order to perform group analyses. Also the MTI images (with and without saturation pulse, denoted as M0 and MS respectively) were co-registered to the T1-weighted (rigid body co-registration) and the brain extracted using the brain mask previously computed in the T1w analysis. Successively, the MT ratio was computed as (M0−MS)/M0 (Wolff and Balaban, 1989; Mehta et al., 1996). Finally, the volumetric MTR values were extracted on the mid-thickness mesh, resulting in a surface-based map of myelin content as estimated by MTR. Finally, a spherical mapping projection on to the FreeSurfer average template (Gaussian smoothing kernel of FWHM = 5 mm) was performed in order to allow group analyses on MTR as well. At the end, we obtained mid-thickness surface maps of thickness, T1w/T2w ratio and MTR projected on the FreeSurfer average group template.

4.2.4 Data Analysis and Statistics

Before computing the group analyses, other steps have been performed. First, the mid-thickness maps of thickness, T1w/T2w ratio and MTR were reduced from the original 327000 vertices to 7117 regions (henceforth named *isorois*) that were defined by pooling together 4th order neighbors on the mesh. Furthermore, the MTR maps were corrected for the two different TR used for the acquisition. In fact, MTR sequences had been recorded with two different repetition times (TR) depending on participants' SAR estimation (TR = 50 or 30 ms). TR influences the temporal distance between the saturation pulse and the following standard Spoiled Gradient (SPGR) sequence. Smaller TR (SPGR sequence closer to saturation pulse) results in overall greater ratio for myelin content. Therefore, prior to pooling all MTR results together for group analysis, the following correction was applied: the mean of the distributions of all MTR surface values (all subjects with TR = 50 ms or TR = 30 ms) was computed; being the two distributions well gaussian shaped (see Suppl. Fig. 4.6), all TR = 50 ms MTR data were corrected by subtracting the mean difference with respect to the TR = 30 ms dataset. Finally, the T1w/T2w ratio maps were z-values corrected for each subject, considering the distribution of all T1w/T2w ratio values on the whole subject mid-thickness surface as a single Gaussian distribution. At this point, data were ready for group analyses. In order to implement them, demographic information was collected and subjects were divided in three age groups (from 18 to 90 y.o in 24 y steps -> 18-42; 43-66; 67-90). All dipoles (from all subjects belonging to an age group) of each isoroi were pooled together (separately for each age group) and the average values of CT, T1w/T2w z-ratio corrected and MTR (TR corrected) were computed. For the sake of clarity, for each quantity (CT, T1/T2 and MTR) the TIV was regressed out and from now on, CT, T1/T2 and MTR will be always intended as TIV-corrected. Furthermore, for each quantity, the linear change with age was assessed by means of a linear fit for each isoroi. Also, in order to understand how the myelin content influences the thinning of the cortex we further regressed out from CT both our proxies for myelin content (T1w/T2w ratio and MTR, separately). This resulted in two additional thinning maps

(slopes of the linear fits on the cortex) representing how CT changes with age when either the T1w/T2w ratio or the MTR were regressed out as a confound. The same approach was used to conversely understand how myelin content is affected by cortical thinning, resulting in two more surface maps with the slopes of myelin data linear fits where, from the T1w/T2w and MTR, the CT was regressed out. Furthermore, in order to understand the direct relationship between CT and myelin content changes in the three different age groups, two additional linear fits between CT and T1w/T2w ratio and MTR were computed. The last comparison was purely methodological and was used in order to understand the consistency level of the two proxies used for myelin content estimation (T1w/T2w and MTR). All of the above results of linear fits were thresholded at $p < 0.05$ and corrected for FDR with $q = 0.05$, considering the total number of isorois (7117). Furthermore, a quantitative analysis was implemented for each of the metrics' averages and linear fits' slopes described to appreciate the aforementioned changes. Average values and significant slopes (linear fit $p < 0.05$ with respect of a null-hypothesis of a flat line) were extracted for all the isorois belonging to the frontal, sensory, motor, premotor and occipital sectors separately. We defined these sectors using ROIs from the HCP multimodal atlas (Glasser et al., 2016). For a list of ROIs included in the different sectors see Table 1. These values, pooled by sector, were then statistically compared across the three age groups with a two-tailed non-paired t-test, in order to exploit significant differences at a whole sector level.

Sector	Hemisphere	ROI name	MNI coordinates (mm)		
			x	y	z
Motor	Left	4	-27	-20	54
	Right	4	26	-18	55
Somatosensory	Left	3b	-37	-24	52
		1	-47	-25	53
		2	-35	-35	50
		3a	-35	-22	42
	Right	3b	35	-24	52
		1	47	-23	53
		2	36	-33	50
		3a	34	-20	42
Premotor	Left	6d	-35	-13	62
		6mp	-15	-13	66
		6a	-24	-2	52
	Right	6d	35	-12	61
		6mp	16	-11	65
		6a	26	0	50
Frontal	Left	9a	-20	53	24
		9p	-19	44	36
		a10p	-27	54	-3
		a47r	-40	46	-9
		p47r	-41	40	2
		a10p	-27	54	-3
	Right	9a	18	58	21
		9p	20	46	33
		a10p	25	57	-7
		a47r	38	49	-6
		p47r	43	42	-2
		a10p	25	57	-7
Occipital	Left	V1	-13	-82	1
		V2	-13	-82	3
		V3	-19	-87	5
	Right	V1	14	-80	3
		V2	13	-80	5
		V3	20	-88	9

Table 4.1: List of ROIs from the HCP multimodal atlas that are included in each sector of interest. For each ROI, the MNI coordinates are reported.

4.3 Results

First, the results for the CT changes with age and its relationship with cortical myelin content are reported. As it can be appreciated from Figure 4.1A, the average values for the CT change depend on the age group. In fact, in the early adulthood group (18 – 42 y.o.), the lowest values of CT are registered at the level of the sensory and occipital cortex (~ 2 mm), with frontal and premotor parietal areas showing in average greater CT values (~ 3 mm). Differently, in the mid-adulthood group (42 – 66 y.o.) and late adulthood group (66 – 89 y.o.), the CT is generally reduced (~ 2 mm), with more anterior regions (frontal, premotor and motor) showing larger thickness than posterior ones. The changes in the sectors of interest can be better appreciated in Figure 4.1B, where the results from t-tests between age groups on the average CT are shown, together with violin plots describing the shape of CT values' distribution in each brain area of interest and for each age group, separately. As it can be appreciated from these quantitative analyses, all sectors show a decrease in CT average values with age, with all contrasts being significant ($p < 0.0001$). Confirming the results in Figure 4.1A, also in Figure 4.1B it can be appreciated that the motor, sensory and occipital cortices show the lowest CT average values compared to frontal and premotor cortices and that, despite CT loss with age, these regions keep showing the greater CT also in the third group.

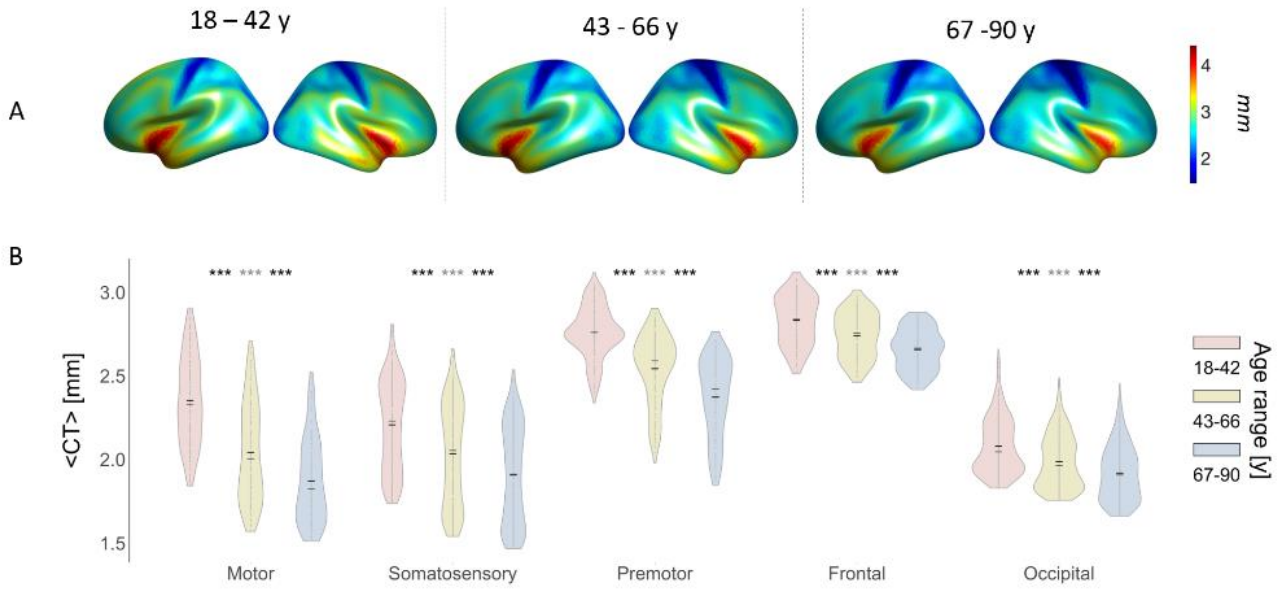

Figure 4.1: Results for average Cortical thickness in the three age groups; A) CT average maps for the 7117 isorois for the three age groups separately; B) CT values distribution for each group in each brain sector of interest (mean in black, median in grey); significance asterisks summarize the results of a t-test between the three age groups for each brain sector separately (*** for p< 0.0001; ** for p < 0.001; * for p< 0.05). Grey asterisks refer to the comparison between the first and the third group.

In Figure 4.2A.1, the CT slope is reported separately for the three age groups. From the linear fits between CT and age, the general trend is a loss between 0.01 and 0.02 mm per year in the young adulthood group, with the motor and premotor cortex showing in this group the largest thinning. Differently, in the second mid-adulthood group, the CT slope tends to stabilize especially in the premotor and motor cortex. In the third late adulthood group, the linear fit between CT and age shows a greater thinning compared to the second age group in frontal and occipital areas. In general, the somatosensory cortex shows to be the most stable over the age groups compared to the rest of the cortex. Figure 4.2B.1 shows the distribution of the CT slope for each group and the results from the t-tests across the age groups, separately for the different brain regions of interest. The decreased slope in sensory cortex thinning is confirmed by these quantitative analyses since the sensory cortex shows a significant thinning rate in the middle-age group compared to the young age group and a significant difference in CT slope between the first group and the third one ($p < 0.0001$), but a non-significant

difference in CT slope values between second and third group. Differently, in the motor and premotor cortex the thinning rate is fast in the first group already and then gets significantly slower with age (for all the contrasts $p < 0.0001$, except for the premotor cortex contrast between the first and second group which shows no differences in CT slope). Therefore, sensory cortices show a more stable thinning over the life span, while premotor and motor cortices suffer from a fast thinning in the first age group which slows down with aging. Differently from both the sensory and the premotor and motor districts, the frontal and occipital cortices show similar behaviors, with the thinning rate getting significantly faster as age increases (for all contrasts $p < 0.0001$).

As for the relationship between CT slope and myelin, in Figure 4.2A.2 we report the results for the linear fits between CT (with MTR regressed out) and age, in order to investigate what changes in the relationship between CT and age when the effects of the myelin content (as assessed with MTR) are not taken into account. In order to better appreciate the differences between Figure 4.2A.1 (CT vs age) and 4.2A.2 (CT with MTR regressed out vs age), we computed the contrast reported in figure 4.2A.3, representing the difference between figure 4.2A.1 and 4.2A.2 (the difference is shown only for values which are significant in both original surface maps). In Figure 4.2A.3, a visible difference due to MTR effects in the linear fit between CT and age is shown. In this regard, Figure 4.2A.3 shows the main effect of MTR on the relationship between CT and age visible over the parietal district in all age groups (particularly in the second and third age groups). A slight increase in the age-related thinning rate (faster CT slope) of ~ 0.005 mm per year over the parietal cortex is detectable when the MTR is regressed out from CT. In figure 4.2B.2 (distribution of the CT slope values when the MTR is regressed out) the sensory cortex appears the most affected by the MTR regression. In fact, the CT slope in the sensory cortex becomes non-significantly different across age groups when the MTR is regressed out from the CT slope. Frontal, premotor, motor and occipital regions do not suffer from MTR regression in terms of CT slope, as their result remains the same as in figure 4.2B.1 when the MTR effect on CT is not regressed out from the CT before computing the linear fit with age.

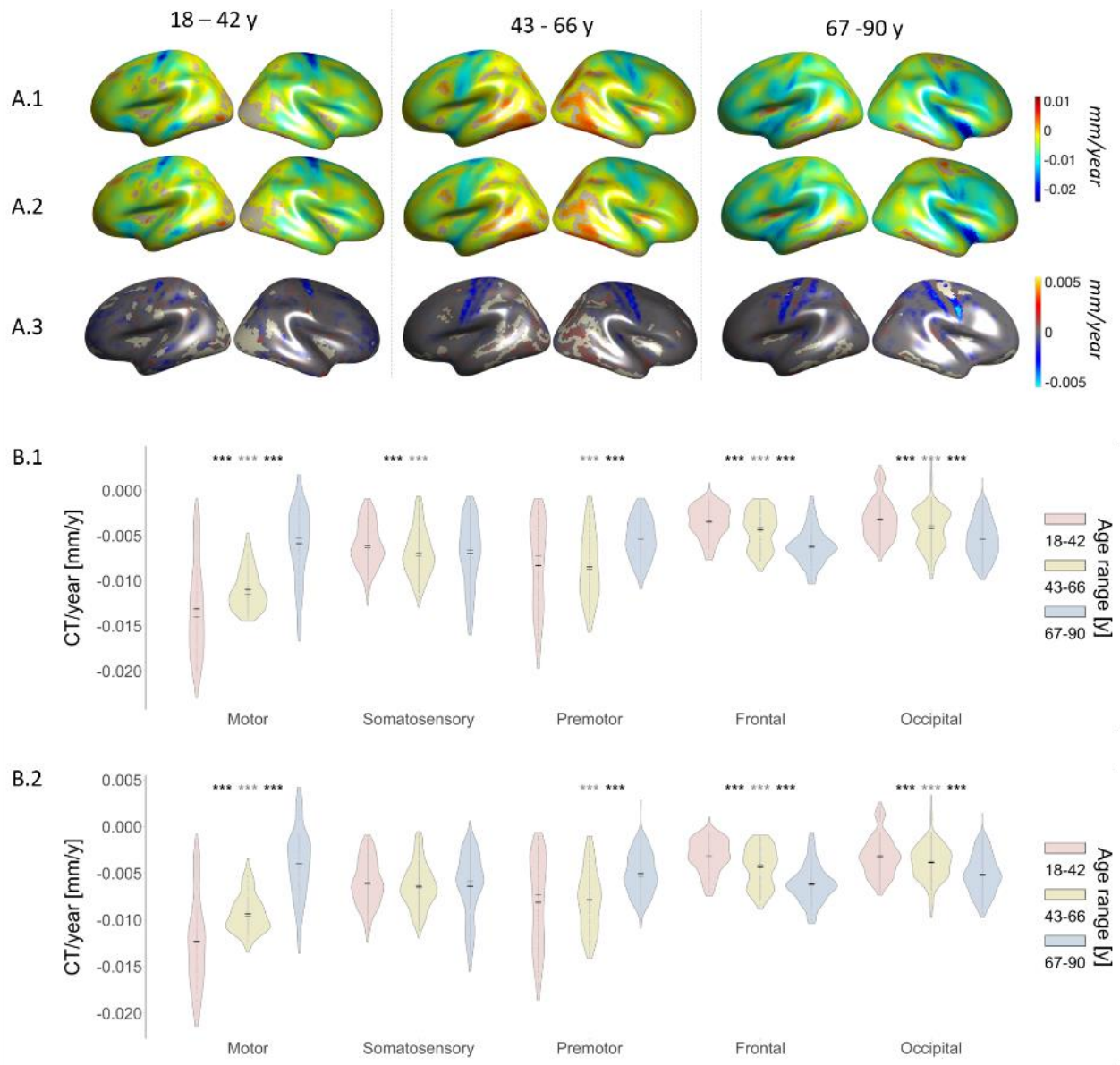

Figure 4.2: Results for the linear fit between Cortical Thickness and Age (Cortical thinning/CT Slope) in the three age groups (with and without MTR regressed out from CT before computing the linear fit between CT and Age); A.1) Source map of the slope values from the linear fit between CT and Age; A.2) Source maps of the slope values from the linear fit between CT and Age, with MTR regressed out as a confound.; A.3) Source map of the difference between A.1 and A.2: the difference is computed only between the values that are significant in both original contrasts; B.1) CT slope values distribution for each group in each brain sector of interest (mean in black, median in grey); B.2) CT slope values distribution with MTR regressed out as a confound for each group in each brain sector of interest (mean in black, median in grey); significance asterisks summarize the results of a t-test between the three age groups for each brain sector separately (*** for $p < 0.0001$; ** for $p < 0.001$; * for $p < 0.05$). Grey asterisks refer to the comparison between the first and the third group.

The same logic was applied in the investigation of the relationship between CT and age, depending on whether the contribution of the myelin content as assessed with the T1w/T2w ratio this time, is taken into account or not. In this regard, Suppl. Figure 4.1A.1 reports the results for the linear fit between CT and age, while Suppl. Figure 4.1A.2 reports the result for the contrast between the CT and age when T1w/T2w is regressed out from CT (CT slope when T1w/T2w is regressed out). Also here, the difference between Suppl. Figure 4.1A.1 and Suppl. Figure 4.1A.2 becomes remarkable computing the difference between the significant values obtained from the two linear fits between CT and age (when T1w/T2w is regressed out). This difference is reported in Suppl. Figure 4.1A.3, where myelin content estimation with T1w/T2w ratio does not provide for detectable group difference in the relationship between CT and age as in case of myelin content estimated with the MTR. In fact, by comparing Figure 4.2A.3 and Suppl. Figure 4.1A.3, the cortical myelin content appears to increase the thinning rate when this is estimated with MTR and regressed out from CT in its linear fit with age. On the contrary, the same does not seem to happen when the myelin content is estimated with T1w/T2w. In this regard, the reader is invited to compare the Suppl. Figure 4.1B.1 and Suppl. Figure 4.2B.2: from this comparison, it can be appreciated that the CT slope does not change in any region's contrast between groups when the T1w/T2w ratio effect is regressed out from the linear fit between CT and age.

Furthermore, the same analyses (average, linear fits and sector-specific t-tests between age groups) were run on the cortical myelin content proxies. As for the average MTR, in Figure 4.3A first age group, the frontal regions are the least myelinated and myelination levels in these areas tend to be larger in the second group compared to the first, but then to decrease again in the third group, suggesting a tendency towards an inverted U-shaped trajectory of MTR in frontal areas. On the other hand, the sensory, motor and occipital districts seem to be the mostly affected by age in terms of myelin content. In these regions, the average MTR decreases dramatically from the first group to the

third group. The premotor district seems to be more stable in terms of myelin content as changes in these regions become clear only in the third group. These results are further corroborated by the quantitative analyses, t-tests and MTR values distributions, presented in figure 4.3B, with the frontal regions showing the lowest myelination levels in the first group and a significant increase in myelin content between the first and second group ($p < 0.0001$). Differently, motor, sensory and occipital cortices show a similar degeneration in cortical myelin content, with significant decreases in MTR values as age increases (all contrasts show $p < 0.0001$). The premotor cortex confirms its different behavior, with rather stable MTR levels with age and no significant differences in MTR levels between the first and second group.

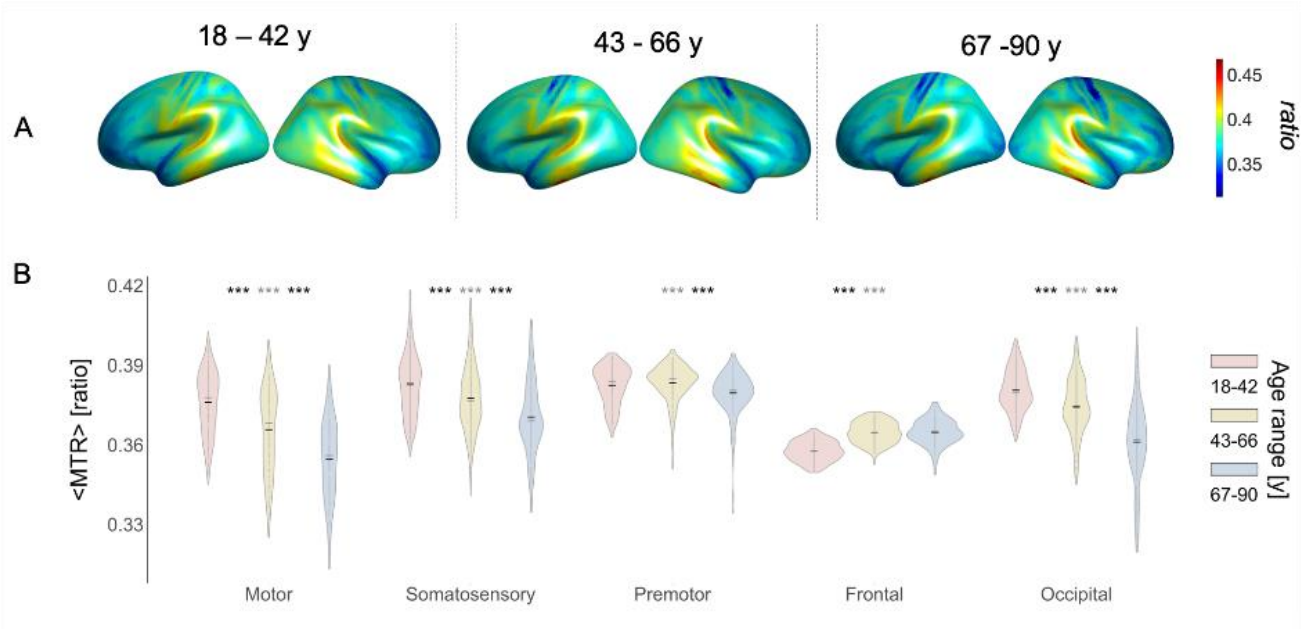

Figure 4.3: Results for average MTR values in the three age groups; A) MTR average maps for the 7117 isorois for the three age groups separately; B) MTR values distribution for each group in each brain sector of interest (mean in black, median in grey); significance asterisks summarize the results of a t-test between the three age groups for each brain sector separately (*** for $p< 0.0001$; ** for $p < 0.001$; * for $p< 0.05$). Grey asterisks refer to the comparison between the first and the third group.

To better appreciate this age-dependent change in MTR, in Figure 4.4A.1 the MTR slope is reported as the group-wise result of the linear fit between MTR and age. In the first group there is an increase in cortical myelin content of frontal associative areas, while in the second group a stability seems to be reached in frontal areas (more grey, non-significant regions), while the posterior occipital

regions show a decrease in myelin content. In the third group, the anterior areas show a steeper negative slope compared to the second group, while the somatosensory cortex shows some gain in cortical myelin content. The sensory regions deserve in fact a separate discussion as their behavior in terms of myelin content change with age is different compared to the rest of the cortex. These observations are confirmed by the quantitative analyses shown in Figure 4.4B.1: here sensory and occipital regions behave differently from the rest of the cortex with a U-shape trajectory in MTR slope. Especially in the somatosensory regions the myelin content (as assessed with MTR) is positive in the first group (MTR increases), it becomes negative in the second group (MTR decreases) and then it significantly slows down in the third age group (all p-values < 0.0001).

To disentangle the effects of CT on the MTR changes with age, the linear fit in figure 4.4A.2 was also computed. In this figure, the CT is regressed out from the MTR and then the MTR fit with age (MTR slope) is computed. The MTR slope changes with age shown in figure 4.4A.1 are not different from the ones shown in figure 4.4A.2, suggesting the effects observed in the MTR slope not to be due to confounding effects by CT, but rather predominantly determined by actual age-related effects on cortical myelin content. In fact, in figure 4.4A.3 the differences computed between the significant results in figure 4.4A.1 and 4.4A.2 are shown with their scale being extremely small compared to MTR changes in both figure 4.4A.1 and 4.4A.2. Thus, despite some effects of CT on the MTR visible over parietal areas in the second and third group, the influence of CT over MTR myelin estimate is small compared to the ones really due to age-related effects on the MTR proxy of cortical myelin. These results are confirmed by the quantitative analyses computed over the different sectors of interest, since the patterns observed in figure 4.4B.1 (t-tests and distributions for MTR slope) and 4.4B.2 (t-tests and distributions for MTR slope when CT is regressed out) are not different. The only two appreciable differences, by comparing figure 4.4B.1 with figure 4.4B.2, are 1) in motor cortex, the MTR slope becomes positive in the first group when the CT is regressed out, suggesting that the cortical myelin slope (MTR) is positive in the first group when the effect of CT is not taken into

account; 2) in frontal regions, there is a loss of significance in the difference between the second and third group, a comparison that was significant in the direct linear fit between MTR and age without CT regressions ($p < 0.05$). In all other age groups and in all sectors, the CT regression from the MTR in its fit with age does not change the MTR slope.

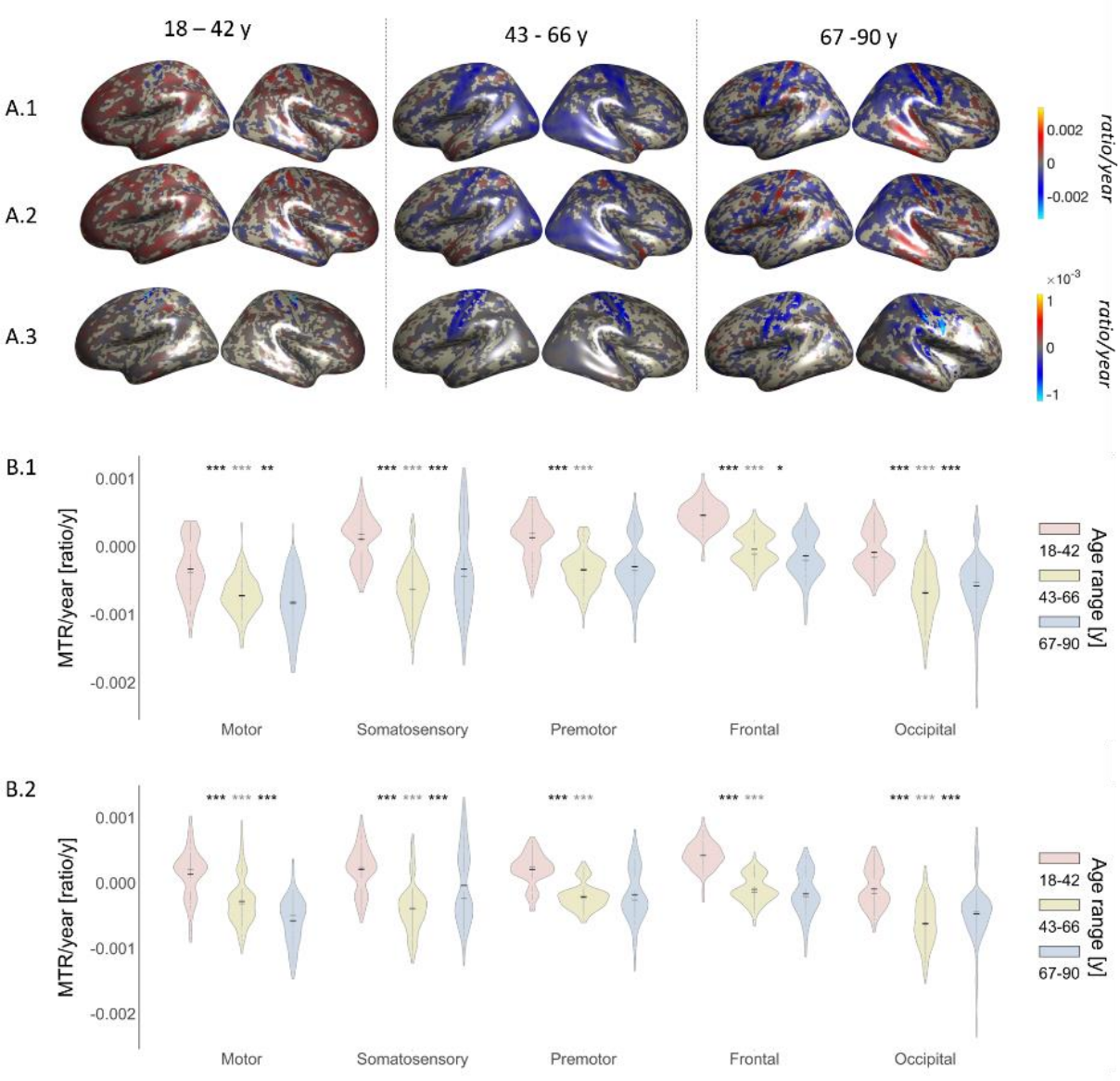

Figure 4.4: Results for the linear fit between MTR and Age (MTR Slope) in the three age groups (with and without CT ratio regressed out from MTR before computing the linear fit between MTR and Age); A.1) Source map of the slope values from the linear fit between MTR and Age; A.2) Source maps of the slope values from the linear fit between MTR and Age, with CT regressed out as a confound.; A.3) Source map of the difference between A.1 and A.2: the difference is computed only between the values that are significant in both original contrasts; B.1) MTR slope values distribution for each group in each brain sector of interest (mean in black, median in grey); B.2) MTR slope values distribution with CT regressed out as a confound for each group in each brain sector of interest (mean in black, median in grey); significance asterisks summarize the results of a t-test between the three age groups for each brain sector separately (*** for $p < 0.0001$; ** for $p < 0.001$; * for $p < 0.05$). Grey asterisks refer to the comparison between the first and the third group.

As for the results on the age-related changes over myelin content as assessed with the T1w/T2w ratio, in Suppl. Figure 4.2 and Suppl. Figure 4.3 the average and slope of T1w/T2w are reported separately for each age group. From a comparison between results in figure 4.3 and 4.4 (MTR) and Suppl. Figure 4.2 and 4.3 (T1w/T2w ratio), it is clear that myelin estimates computed with MTR and T1w/T2w ratio return very different results both in terms of cortical patterns of average myelin content and myelin slope with age. In fact, Suppl. Figure 4.2A and Suppl. Figure 4.2B show no dramatic changes between the different age groups in terms of average amount of cortical myelin content when this is assessed with the T1w/T2w ratio proxy. The sensory, premotor and motor regions appear to be the most myelinated in the first age group, which is not far from the results obtained on the MTR average values for the first group (see Figure 4.3A for a comparison). However, the T1w/T2w ratio does not show the age-related average loss of myelin content which is reported when this is MTR-assessed. In this regard, Suppl. Figure 4.2B, representing the t-test results between groups and distributions of T1w/T2w values, shows numerous non-significant results in the between groups t-test comparisons. Therefore, the T1w/T2w ratio is not particularly sensitive to age-related changes in cortical myelin content. For example, the T1w/T2w ratio averages (Suppl. Fig. 4.2) show no significant changes in myelin content across the three age groups in occipital and premotor areas. Also, in motor and sensory areas the only significant difference in T1w/T2w average values is between the first and third group ($p < 0.0001$ and $p < 0.001$, respectively). This latter result suggests that T1w/T2w ratio is more affected by variability compared to the MTR. Finally, a pattern similar to the average MTR-assessed myelin one is visible in frontal regions, since the T1w/T2w ratio average values in frontal regions appear to significantly increase with age ($p < 0.0001$).

The T1w/T2w slope results reported in Suppl. Figure 4.3A.1 show very unstable patterns, making it quite difficult to detect clear regional patterns of myelin slope with age. In this figure, the T1w/T2w slope shows a change in myelin content with age, but apart from a loss of myelin content in the motor areas of the second group, other regions are not well distinguishable in terms of peculiar age-related

myelin trajectories. The instability of the T1w/T2w ratio slope is also evident in Suppl. Figure 4.3A.2, where the CT is regressed out from the T1w/T2w ratio before computing the linear fit with age. These unclear age-related effects on the T1w/T2w are also visible in Suppl. Figure 4.3A.3, where the only slightly appreciable effect is a contribution of the CT over the T1w/T2w estimate of parietal areas in the second group. In fact, in Suppl. Figure 4.3B.1 the only result o on the T1w/T2w slope which could resemble the pattern observed in the MTR slope (Fig. 4.4), is in the occipital regions, with a steeper T1w/T2w slope as age increases ($p < 0.0001$ for all the three contrasts). Differently, the T1w/T2w slope over frontal cortices shows a statistical pattern completely different from the one observed with the MTR: an increase in myelin content with age significantly different between first and second age group ($p < 0.0001$) is detected. In the premotor, motor and sensory sectors, the T1w/T2w slope shows again less sensitivity compared to MTR at detecting age-related changes in cortical myelin content (less significant differences between age-groups). However, the pattern evidenced in these regions with MTR is reflected in the T1w/T2w slope results. Furthermore, in Suppl. Figure 4.3B.2 we report results for the between age-groups t-tests and distributions of estimated myelin in the linear fit with age when CT is regressed out from T1w/T2w ratio. From this analysis, it can be seen that T1w/T2w ratio fit with age suffers from the CT regression more compared to the MTR slope. In fact, in the motor cortex, the t-test between the first and second group on the T1w/T2w slope does not return significant differences when CT is regressed out from T1w/T2w in its fit with age, while in Suppl. Figure 4.3B.1 we found a significant result ($p < 0.05$). Also, in the premotor cortex the first and third group show a significant difference in Suppl. Figure 4.3B.2 (T1w/T2w slope when CT is regressed out from T1w/T2w ratio), while this was not the case in Suppl. Figure 4.3B1 (T1w/T2w slope when CT is not regressed out from T1w/T2w ratio). Finally, no significant difference is detected also in the occipital cortex in T1w/T2w slope between the second and third group when the CT is regressed out from T1w/T2w ratio, while this contrast was significant ($p<0.0001$) in Suppl. Figure 4.3B.1. Importantly, the peculiar tendency toward a U-shaped trajectory of sensory and occipital regions is detected also with the T1w/T2w ratio.

Due to different results obtained using the MTR and T1w/T2w proxy, we also computed the linear fits shown in figure 4.5, in Suppl. Figure 4.4 and Suppl. Figure 4.5. In Figure 4.5A, the linear fit between CT and MTR is reported, which shows a positive linear relationship between the MTR and CT over parietal areas but a negative linear relationship between the MTR and CT in the rest of the brain regions, especially in the first age group. These results are confirmed by the between age-groups t-tests in Figure 4.5B, where the parietal district shows a positive linear relationship between CT and MTR which tends to increase with age. The occipital and frontal regions show a negative relationship between CT and MTR in the first age group. However, the relationship between CT and MTR in these areas becomes significantly positive with age, with frontal areas showing a stronger positive relationship between the two metrics across all age groups, while the occipital regions show this difference only between the first and the second group ($p < 0.0001$).

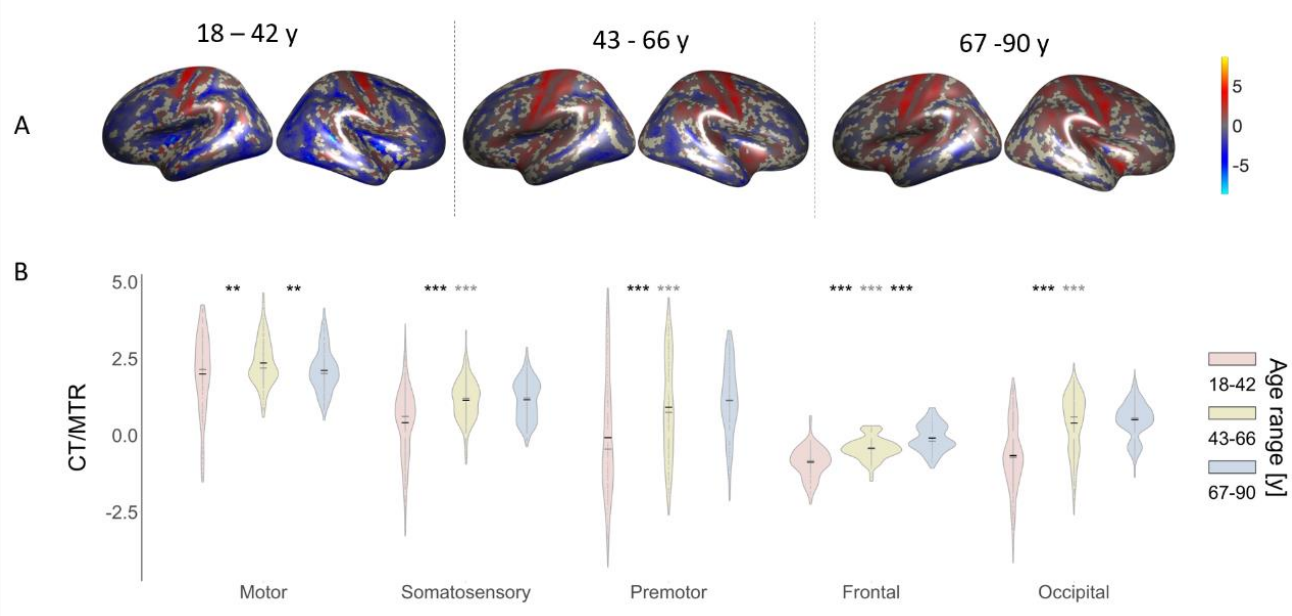

Figure 4.5: Results for the linear fit between CT and MTR in the three age groups; A) Source map of slope values from the linear fit between CT and MTR; B) Slope distribution from the linear fit between CT and MTR for each group in each brain sector of interest (mean in black, median in grey); significance asterisks summarize the results of a t-test between the three age groups for each brain sector separately (*** for $p < 0.0001$; ** for $p < 0.001$; * for $p < 0.05$). Grey asterisks refer to the comparison between the first and the third group.

In Suppl. Figure 4.4A, the same linear fit is computed between the CT and T1w/T2w proxy of cortical myelin. This fit shows a tendency toward similar results as in Figure 4.5A, especially in first and second age groups, but with unclear patterns in sensorimotor areas. By comparing the results in the third group in Figure 4.5A and Suppl. Figure 4.4A, it can be also noticed that while a decrease in CT in every brain region but in parietal ones determines an increase in the T1w/T2w estimate (negative relationship), this is not true for the CT vs MTR fit. These results are confirmed by the results reported in Suppl. Figure 4.4B where the between-groups t-tests and distributions are shown. In Suppl. Figure 4.4B, in fact, the relationship between CT and T1w/T2w is negative especially in frontal, premotor and occipital regions until the last age group but this is not true for the fit between CT and MTR which shows a progressive tendency with age towards a positive relationship between CT and myelin.

Given the differences evidenced so far between MTR and T1w/T2w, the last fit was computed as shown in Suppl. Figure 4.5A, representing the direct linear fit between the MTR and T1w/T2w ratio. Here the two cortical myelin proxy do not show an (almost) constant relationship with each other as expected. In fact, their relationship changes dramatically depending on the brain region taken into account. Suppl. Figure 4.5B, shows the results for the between-groups t-tests and distributions of the fit between T1w/T2w and MTR. The two proxies show a positive relationship that tends to increase with age ubiquitously on cortex with the exception of the sensory area.

4.4 Discussion

The aim of this chapter is to provide the reader with a work investigating age-related brain structural changes on a large and homogeneously distributed cohort of participants aged between 18 and 89 years. Importantly, the aim was to demonstrate that 1. Age-related changes are present not only at the level of cortical thickness, but also at the level of cortical myelin concentration; 2. T1/T2 ratio is a less reliable measure of cortical myelin content than the MTR proxy.

As for the first point, it has been shown here that aging processes not only affects the thickness of the grey matter, but also the myelination levels of brain regions. Importantly, this happens differently depending on the region of the cortex. As for the CT results, in all brain regions a general loss of cortical thickness can be appreciated with age, with frontal and premotor cortex showing the highest thickness values (Figure 4.1A and 4.1B). The distinct behaviours of the different brain district appear evident in the slope of CT with age, which describes the speed at which thinning occurs in the different brain regions. In fact, CT slope (thinning) shows that the premotor and motor cortex are very much different compared to the rest of the brain in terms of thinning rate in the different age-groups. In Figures 4.2A.1 and 4.2B.1, the premotor and motor cortices show in fact a faster thinning in the first group and then a slow-down in thinning rate with age. Differently, the sensory cortex shows a more "stable" thinning over the life span, with a thinning stabilization in the second group which does not differ from thinning rate in the third age group. The frontal and occipital cortices also show a different pattern, with thinning rate getting increasingly fast with age. Our results on the CT slope are partially in line with previous results (e.g. Salat et al., 2004; Thambisetty et al., 2010; Fjell et al., 2009). For instance, also Salat and colleagues (2004) found the fastest thinning rate by middle-age to occur in the motor cortex. However, it must be noticed that our age sample ranges from 18 to almost 90 years, with a big cohort of participants (N = 610) included in our sample. Instead, Thambisetty et al.' work (2010) only included participants aged from 60 years old and Salat et al. (2004) included only 106 participants for the same life span investigated in our work. Therefore, our finding of a fast thinning in motor areas already in the first group of age depends on the fact that, on the one hand, Thambisetty and colleagues did not investigate thinning before 60 years, while, on the other hand, Salat and colleagues included a sample size that was too small to appreciate gradual changes in CT. Differently, McGinnins and colleagues (2011) found that sensory and motor cortices show highest thinning predominantly in the last part of life, partially overlapping with our third age group. However, the number of participants included in McGinnis et al. (2011)' age groups was smaller than ours (mean N per age-group = 79; N in older age group = 38). Therefore, while their

analysis was sensitive to the general larger thinning in the motor cortex compared to the rest of the brain (an effect that we also found), their ANOVA tests in the between groups analyses might have suffered from the different sample sizes in the compared groups, leading to non-significant differences in the comparisons of CT slope in the motor cortex until the last group of age. Hence, while our evidence converges with some of the previous works, we were additionally able to extract finer differences between age groups, thanks to the large dataset employed in our analyses. In this regard and most importantly, none of the previous works has highlighted the difference in aging patterns of motor vs. sensory areas. In fact, the sensory regions show a slower thinning compared to premotor and motor cortices in the first age group, with a significant increase in the thinning rate between the first and second age groups and a final thinning stabilization between the second and third age group, therefore from middle-age. On the contrary, the premotor and motor regions first show a fast thinning rate that gradually slows down with age. It is worth to notice that these differences cannot be ascribed to field inhomogeneities in the MR head coil, since both motor and sensory areas lie almost in the same coil position during the MRI scan.

The similarity between premotor and motor cortices and their dissimilarity with the sensory cortex are also evident in the CT slope when the MTR is regressed out in figure 4.2A.2 and 4.2B.2. In fact, when CT (with MTR regressed out) is fitted against age, sensory cortices show a stable thinning over life (no differences between age groups), while premotor and motor regions still show a larger thinning compared to sensory cortices as well as a slowdown in thinning with age. This dissociation between sensory and premotor/motor cortices reminds the results of a recent work by Wagstyl and colleagues (2020) which shows by means of a quantitative 3D laminar atlas of the human cerebral cortex, layers III, V and VI of the cortex to exhibit opposite behaviours in the premotor and motor cortex compared to the sensory cortex. Although Wagstyl et al. (2020) did not investigate these different regional-dependent behaviours in individuals with different ages, their results support the

dissociation we found in the aging patterns, in terms of cortical thickness, of these different sectors of the human brain.

Regarding the results in age-related cortical myelin changes, these were assessed using two different proxies of myelin content, namely the MTR and T1w/T2w ratio. Both MTR and T1w/T2w show some accordance with previous works investigating cortical myelin content in humans. In fact, we found that premotor, motor and sensory regions are the most myelinated districts of the cortex (e.g., Patel et al., 2020; Shafee et al., 2015; Glasser and Van Essen., 2011), with these results being coherent in both MTR and T1w/T2w cortical myelin averages estimates (Figure 4.3 and Suppl. Figure 4.2). Moreover, MTR slope shows a loss of cortical myelin content with age in all brain regions (Figure 4.4). Also in these analyses, different patterns were found in the cortical myelin thinning rate depending on the examined areas. In fact, we found a progressive increase in the rate of myelin loss in more anterior regions (frontal, motor and premotor), while sensory and occipital regions showed a U-shaped trajectory with the myelin thinning being faster in the second age group compared to the first age group, to slow down again in the third age group (Figure 4.4B.1). It is worth to notice that these patterns on a progressive age-related increase in myelin loss in anterior regions and U-shaped trajectory in posterior ones are even more pronounced when the effect of CT is regressed out from the linear fit between MTR and age (Figure 4.4B.2). This suggests that these patterns are mainly due to myelin and not to the confounding effects of CT on cortical myelin content as assessed with MTR. Our results on the average amount of cortical myelin (as assessed with the MTR proxy: Figures 4.3A and 4.3B) show that these are in line with Patel et al. (2020) and Wu et al. (2016), who used the MTR to assess cortical myelin content. However, our results on the myelin thinning rate do not confirm Wu and colleagues' findings as they could not find any significant change in cortical myelin content with age in sensory and motor areas. Their nil finding is probably due to the small sample size employed, as they included only 66 participants to investigate MTR changes over a huge life span (30 to 85 years). Differently, Karolis et al. (2019) also employed the MTR to assess cortical myelin

loss with age and found age-related changes in myelin content in parietal regions, as we report in our results. Nevertheless, none of the previous works reported the dissociation we highlight between sensory and motor regions in CT changes with age, a dissociation that we also found in the age-related changes of the MTR estimates (with and without CT regression). In fact, common age-related changes in sensory and occipital cortices can be noticed in Figure 4.4B.1 and 4.4B.2 as opposed to the different age-related changes in more anterior regions (frontal, premotor and motor). These commonalities between somatosensory and occipital regions were also found in the investigation by Wagstyl and colleagues (2020) of the laminar features of the different brain regions. In fact, they found common structural properties between sensory and occipital regions as opposed to the ones typical of frontal, premotor and motor districts. Our results suggest that the different functional roles of sensory areas (compared to anterior areas) may be supported not only by differences in the cortical thickness properties of the cortex, but also in their myelin content. Interestingly, this difference between anterior regions compared to visual and sensory regions seem also in accordance with works showing that these districts are different in terms of neuronal density and distribution of neurotransmitter receptors, with sensory areas (visual and somatosensory) differing from motor and frontal cortices in terms of GABA, serotonin and dopamine receptors' concentration (Wagstyl et al., 2020). Nevertheless, previous works have often assimilated sensory and motor regions (Huntenburg et al., 2017; Thiebaut de Schotten et al., 2017; Margulies et al., 2016; see Wagstyl et al., 2020;), therefore more studies are needed in order to understand the structural dissociation between sensory and motor cortices both at the level of cortical thickness and myelin content, in order to relate these divergences to different functional roles proper of sensory and motor districts.

Furthermore, we found that the age-related changes in myelin content, as assessed with the T1w/T2w proxy, in part differ from the ones obtained using the MTR. First of all, in the T1w/T2w results on the myelin thinning with age, the frontal, premotor and motor cortices appear to have a

tendency towards an inverted U-shaped trajectory (Suppl. Figure 4.3B1). In fact, the frontal and premotor cortex show a faster thinning in the first group which slows down and stabilizes in the second and third age groups. The motor cortex shows a clear inverted U-shaped trajectory, with significant decrease in myelin thinning in the second compared to the first age group, and a later acceleration in the third age group. These results are in accordance with the work by Grydeland and colleagues (2013) who also employed T1w/T2w as a myelin proxy to investigate age-related myelin changes over the life span and found a tendency for an inverted U-shaped trajectory in anterior regions. However, our results differ from Grydeland and colleagues' as we find a dissociation between age-related changes in sensory regions vs anterior regions also when myelin was assessed with the T1w/T2w ratio. In fact, we found that the occipital and somatosensory cortices show a progressive increase in myelin thinning rate with age, with a tendency towards a stabilization in myelin thinning in the second age group. Importantly, we show that the CT regression (from the fit between the T1w/T2w and age) affects more the results in T1w/T2w estimates compared to the regression of CT from the fit between the MTR and age (which instead only led to an enhancement of the effects seen in the relationship between MTR and age). In fact, in the comparison between Suppl. Figure 4.3B.1 and Suppl. Figure 4.3B.2 in premotor, motor and occipital cortices, results change in the relationship between T1w/T2w and age when CT is regressed out from the T1w/T2w before computing the linear fit with age. In particular, CT regression from the T1w/T2w determines a more pronounced difference in premotor regions between the first and second group, therefore leading to a more significant deceleration in myelin thinning with age in this region. In the motor cortex, changes in T1w/T2w slope due to the CT regression are detected in the first and second group, which do not show differences in thinning rates like they did when CT regression was not implemented. Also, in the occipital cortex, the significant increased thinning in the third compared to the second group disappears, suggesting that in this region the CT regression from T1w/T2w leads to estimates that are similar to the ones obtained with the MTR proxy. Therefore, we show that the T1w/T2w ratio is much more susceptible to the CT regression compared to the MTR estimate. In

other words, T1w/T2w myelin estimates are more affected by the cortical thickness. In this regard, it has to be considered that the T1w/T2w ratio depends on the intensity of the T1-weighted and T2 weighted image as being obtained from the ratio between the two images. At the same time, the CT extraction depends on the intensity of the T1-weighted image as CT is ultimately computed from the contrast differences between grey matter and white matter of the T1-weighted image. Conversely, the MTR is obtained from the ratio between two images obtained with specifically designed sequences that are different from the T1-weighted image used both in T1w/T2w computation and CT extraction and the MTR only involves the original T1-weighted image for rigid-body co-registration. For these reasons, the greater co-dependency between the T1w/T2w ratio and CT can be explained with a shared dependency of the two metrics on the intensity of the common T1w image. Therefore, we consider the results obtained with the MTR, which is also less affected than the T1w/T2w contrast by iron molecules accumulation, as more stable and likely reflecting more reliably the changes in real cortical myelin content.

In this light, in Figure 4.5 and Suppl. Figure 4.4, the relationship between CT and MTR and CT and T1w/T2w were respectively computed. Because of the reasons reported above on the strongest impact of CT removal on T1w/T2w fit with age, the results in Figure 4.5A and 4.5B are considered as more reliable in describing the relationship between myelin concentration and CT compared to Suppl. Figure 4.4A and 4.4B. The direct fit between CT and MTR shows a positive relationship between cortical thickness and myelin content in motor and sensory cortices as assessed with the MTR proxy. In the motor cortex, this relationship increases with age, with the second age group showing a stronger positive relationship between the two metrics compared to the first age group. In the sensory cortex, the positive relationship between CT and MTR increases in the second age group compared to the first and then remains stable in the third age group. In the premotor cortex, in the first age group, the relationship between cortical thickness and MTR is weak with its linear fit values lying at zero. With age, we detect a significant positive relationship between the two metrics also in the premotor cortex.

Therefore, in premotor, motor and sensory cortices the relationship between cortical thickness and myelin content (as assessed with MTR) suggests that the greater the thickness, the greater the myelin. These results are also confirmed by the linear fit between CT and myelin content as assessed with the T1w/T2w ratio in Suppl. Figure 4.4A and 4.4B, with the exception being in the sensory cortex where the relationship between CT and T1w/T2w ratio is non-existent in all three age groups. These results are in line with previous works that correlated the T1w/T2w ratio maps with cortical thickness maps (Shafee et al., 2015; Glasser et al., 2011). However, to our knowledge, none of the previous works explored the changes in the relationship between CT and cortical myelin content with age, as we did in this work. Therefore, our results for the first time provide information on the relationship between CT and cortical myelin content with age. We show that during young adulthood, only in sensory and motor areas thickness is positively correlated with myelin, while this relationship becomes a feature of the whole cortex with aging.

Finally, from a methodological point of view, we were interested in the relationship between the T1w/T2w and MTR proxy of myelin. Despite the previous reported results on differences between the two proxies of cortical myelin content, we further assessed whether between the two metrics there was a constant relationship across the brain, as it would be theoretically expected. What we found is that the two metrics show an unstable and non-constant relationship across brain regions, as it can be appreciated in Suppl. Figure 4.5. This result is consistent with previous works showing that the MTR and T1w/T2w ratio show only moderate correlations, with the T1w/T2w ratio being more affected by iron molecules (e.g. Nakamura et al., 2017; Pareto et al., 2020). To our knowledge, this is the first work to provide a linear fit between the two proxies' cortical maps over the life span. Thanks to this analysis, we show that all over the brain, but in temporal cortices, the T1w/T2w and MTR share a positive relationship which tends to increase with age especially in frontal, motor and occipital regions, while in premotor and sensory cortices the relationship between the two proxies does not seem to change with age.

To summarize our results, we report that greater cortical thickness values are found in more anterior regions (frontal and premotor), followed by motor, sensory and occipital regions. Therefore, we found an anterior-posterior gradient of average cortical thickness values. We did not find the same gradient when cortical thinning is examined, despite previous works have supported this framework (Thambisetty et al., 2010). In fact, we show that cortical thinning regional patterns are more complex than merely bound to a law of spatial gradient degeneration. Specifically, we found frontal and occipital areas to increase in their thinning rate with age, while motor and premotor areas show a greater thinning rate in the first age group that later slows down with age. Sensory areas behave differently, with their thinning rate being more stable over life (see Figure 4.2). In this regard, the work by Thambisetty and colleagues (2010) investigated thinning in a group of 66 adults longitudinally followed up from their 60s up to their 80s. Therefore, they did not have a complete picture of age-related thinning and could only appreciate the increased thinning in frontal areas with age and the slowdown in thinning of more posterior areas. For this reason, they could not be aware that parietal cortices suffer from a faster thinning rate compared to more anterior regions in early adulthood, while frontal regions show much slower thinning. From this, their conclusions of an anterior-posterior gradient where frontal areas would be more affected by aging.

The results on the cortical myelin content show the parietal areas, and especially sensory areas, to be the most myelinated ones, while frontal regions show the least average amount in myelin content (Figure 4.3). These results are in line with previous findings (e.g. Shafee et al., 2015). However, to our knowledge we are the first to report a dissociation in the rate of age-related cortical myelin changes between anterior and posterior areas and especially between sensory and motor areas. In fact, we report that motor regions show an increase in myelin loss rate with age, while sensory areas show a U-shaped trajectory, similar to the one observed in occipital areas. This structural dissociation between somatosensory and motor areas, that we found both in cortical thinning and cortical myelin

age-related changes, was until present only reported in works investigating the structure of the brain at the laminar level (Wugstyl et al., 2020).

Therefore, it is here proposed that the anterior-posterior gradient hypothesis is too simplistic to account for the regional differences in brain degeneration. First, the anterior-posterior gradient hypothesis was formulated on the basis of results obtained on samples representative of short age span. Secondly, this account was formulated on the basis of results only obtained on grey matter degeneration, without taking into account cortical myelin concentration (Thambisetty et al., 2010; Resnick et al., 2003). The same critic can be applied to the last in first out account (Raz, 2000). Instead, a complete picture describing age-related changes in the brain should take into account both cortical thickness and cortical myelin and rely on results from studies including larger samples representative of longer age-spans than the samples in the aforementioned studies.

To conclude, age-related changes in brain structure affect both cortical thickness and cortical myelin concentration, with sensory and motor regions showing different aging behaviours in both quantities. This dissociation has been highlighted only in few other works focusing on the microscale features of the cortex (e.g. laminar organization; see Wugstyl et al., 2020). The fact that we were able to detect these differences between the two sectors in vivo is to be ascribed to the large sample employed in our study (N = 610) and the comparable sample sizes included in the three investigated age groups (N = 200 in each age group). Furthermore, we show that the MTR is a more reliable proxy for cortical myelin content as its results are less affected by CT regression compared to the T1w/T2w ratio's. Importantly, our results show that the "anterior-posterior" and "last in first out" frameworks need revision, as the age-related observed changes in brain structure need to be explained taking into account also the myeloarchitectonic properties of the brain. In general, we think that these differences need to be further investigated using both laminar (micro-level) and cortical thickness and myelin

concentration assessments (macro-level). Furthermore, more studies are needed where sensory and motor cortices are treated separately in order to bring new knowledge on the mechanisms and implications of their different degenerative patterns.

4.5 Conclusions

In the present work we used structural MRI recordings from a big cohort of participants (N = 610) recorded in the CAM-Can Project. To our knowledge, this is the first work where structural age-related brain changes are investigated 1) employing a large and uniformly age distributed data sample 2) with recordings form the same scanner 3) comparable sample sizes in the three age groups and 4) using two different proxies (T1w/T2w ratio and MTR) to assess cortical myelin concentration. In this work, it is shown that cortical thickness and myelin content both degenerate with aging, showing different regional aging patterns. In particular, we provide evidence for a dissociation between sensory and motor cortices that has been highlighted only in works investigating the brain structural properties at the laminar level. This dissociation is particularly evident when age-related brain changes are investigated using the MTR, while the T1w/T2w ratio is here shown to be more affected by cortical thickness and therefore to be a less reliable measure of cortical myelin content. Given the previous evidence assessing a relationship between cortical myelin content and cortical excitability, we propose that, in the future, the MTR should be used as a further parameter to assess the state and prognosis of clinical populations, in particular stroke patients. In this regard, stroke patients are often in their elderly and for this reason, a part from the lesion, they are also affected by normal age-related structural changes. Therefore, future research might benefit from extracting and norming, also with the aim of machine learning approaches, brain structural features that can be predictive of stroke recovery, including cortical myelin content as assessed with MTR. Finally, because of the reported structural changes due to aging in both cortical thickness and in myelin content, we propose that

future works investigating corticospinal excitability in stroke patients as compared with controls, should only include age-matched controls to control for age-dependent differences in cortical myelin content that in turn affect corticospinal excitability.

Bibliography

1. Baum, G. L., Flournoy, J. C., Glasser, M. F., Harms, M. P., Mair, P., Sanders, A. F., ... & Somerville, L. H. (2022). Graded Variation in T1w/T2w Ratio during Adolescence: Measurement, Caveats, and Implications for Development of Cortical Myelin. Journal of Neuroscience, 42(29), 5681-5694.

2. Betti, S., Fedele, M., Castiello, U., Sartori, L., & Budisavljević, S. (2022). Corticospinal excitability and conductivity are related to the anatomy of the corticospinal tract. Brain Structure and Function, 227(3), 1155-1164.

3. Birchenall, J., Térémetz, M., Roca, P., Lamy, J. C., Oppenheim, C., Maier, M. A., ... & Lindberg, P. G. (2019). Individual recovery profiles of manual dexterity, and relation to corticospinal lesion load and excitability after stroke–a longitudinal pilot study. Neurophysiologie Clinique, 49(2), 149-164.

4. Davis, S. W., Dennis, N. A., Buchler, N. G., White, L. E., Madden, D. J., & Cabeza, R. (2009). Assessing the effects of age on long white matter tracts using diffusion tensor tractography. Neuroimage, 46(2), 530-541.

5. Deoni, S. C., Dean III, D. C., Remer, J., Dirks, H., & O'Muircheartaigh, J. (2015). Cortical maturation and myelination in healthy toddlers and young children. Neuroimage, 115, 147-161.

6. Dröge, W., & Schipper, H. M. (2007). Oxidative stress and aberrant signaling in aging and cognitive decline. Aging cell, 6(3), 361-370.

7. Dubbioso, R., Madsen, K. H., Thielscher, A., & Siebner, H. R. (2021). The myelin content of the human precentral hand knob reflects interindividual differences in manual motor control at the physiological and behavioral level. Journal of Neuroscience, 41(14), 3163-3179.

8. Fischl, B. (2012). FreeSurfer. Neuroimage, 62(2), 774-781.

9. Fjell, A. M., Westlye, L. T., Amlien, I., Espeseth, T., Reinvang, I., Raz, N., ... & Walhovd, K. B. (2009). High consistency of regional cortical thinning in aging across multiple samples. Cerebral cortex, 19(9), 2001-2012.

10. Frangou, S., Modabbernia, A., Williams, S. C., Papachristou, E., Doucet, G. E., Agartz, I., ... & Salvador, R. (2022). Cortical thickness across the lifespan: Data from 17,075 healthy individuals aged 3–90 years. Human brain mapping, 43(1), 431-451.

11. Friston, K. J. (2003). Statistical parametric mapping. In Neuroscience databases (pp. 237-250). Springer, Boston, MA.

12. Fukunaga, M., Li, T. Q., van Gelderen, P., de Zwart, J. A., Shmueli, K., Yao, B., ... & Duyn, J. H. (2010). Layer-specific variation of iron content in cerebral cortex as a source of MRI contrast. Proceedings of the National Academy of Sciences, 107(8), 3834-3839.

13. Ganzetti, M., Wenderoth, N., & Mantini, D. (2014). Whole brain myelin mapping using T1-and T2-weighted MR imaging data. Frontiers in human neuroscience, 8, 671.

14. Garcia, M. A. C., Catunda, J. M. Y., Souza, M. N. D., Fontana, A. P., Sperandei, S., & Vargas, C. D. (2016). Is the frequency in somatosensory electrical stimulation the key parameter in modulating the corticospinal excitability of healthy volunteers and stroke patients with spasticity?. Neural plasticity, 2016.

15. Gaser, C., Dahnke, R., Thompson, P. M., Kurth, F., & Luders, E. (2022). CAT-a computational anatomy toolbox for the analysis of structural MRI data. BioRxiv.

16. Glasser, M. F., & Van Essen, D. C. (2011). Mapping human cortical areas in vivo based on myelin content as revealed by T1-and T2-weighted MRI. Journal of neuroscience, 31(32), 11597-11616.

17. Grydeland, H., Walhovd, K. B., Tamnes, C. K., Westlye, L. T., & Fjell, A. M. (2013). Intracortical myelin links with performance variability across the human lifespan: results from T1-and T2-weighted MRI myelin mapping and diffusion tensor imaging. Journal of Neuroscience, 33(47), 18618-18630.

18. Gunning-Dixon, F. M., Brickman, A. M., Cheng, J. C., & Alexopoulos, G. S. (2009). Aging of cerebral white matter: a review of MRI findings. International Journal of Geriatric Psychiatry: A journal of the psychiatry of late life and allied sciences, 24(2), 109-117.

19. Hagiwara, A., Hori, M., Kamagata, K., Warntjes, M., Matsuyoshi, D., Nakazawa, M., ... & Aoki, S. (2018). Myelin measurement: comparison between simultaneous tissue relaxometry, magnetization transfer saturation index, and T1w/T2w ratio methods. Scientific reports, 8(1), 1-12.

20. Huntenburg, J. M., Bazin, P. L., Goulas, A., Tardif, C. L., Villringer, A., & Margulies, D. S. (2017). A systematic relationship between functional connectivity and intracortical myelin in the human cerebral cortex. Cerebral Cortex, 27(2), 981-997.

21. Hutton, C., Draganski, B., Ashburner, J., & Weiskopf, N. (2009). A comparison between voxel-based cortical thickness and voxel-based morphometry in normal aging. Neuroimage, 48(2), 371-380.

22. Julkunen, P., Könönen, M., Määttä, S., Tarkka, I. M., Hiekkala, S. H., Säisänen, L., ... & Jäkälä, P. (2016). Longitudinal study on modulated corticospinal excitability throughout recovery in supratentorial stroke. Neuroscience letters, 617, 88-93.

23. Kang, Y. J., Ku, J., Kim, H. J., & Park, H. K. (2011). Facilitation of corticospinal excitability according to motor imagery and mirror therapy in healthy subjects and stroke patients. Annals of rehabilitation medicine, 35(6), 747-758.

24. Kang, Y. J., Park, H. K., Kim, H. J., Lim, T., Ku, J., Cho, S., ... & Park, E. S. (2012). Upper extremity rehabilitation of stroke: facilitation of corticospinal excitability using virtual mirror paradigm. Journal of neuroengineering and rehabilitation, 9(1), 1-8.

25. Karolis, V. R., Callaghan, M. F., Tseng, C. E. J., Hope, T., Weiskopf, N., Rees, G., & Cappelletti, M. (2019). Spatial gradients of healthy aging: a study of myelin-sensitive maps. Neurobiology of Aging, 79, 83-92.

26. Kemlin, C., Moulton, E., Leder, S., Houot, M., Meunier, S., Rosso, C., & Lamy, J. C. (2019). Redundancy among parameters describing the input-output relation of motor evoked potentials in healthy subjects and stroke patients. Frontiers in neurology, 10, 535.

27. Kim, Y. J., Ku, J., Cho, S., Kim, H. J., Cho, Y. K., Lim, T., & Kang, Y. J. (2014). Facilitation of corticospinal excitability by virtual reality exercise following anodal transcranial direct current stimulation in healthy volunteers and subacute stroke subjects. Journal of neuroengineering and rehabilitation, 11(1), 1-12.

28. Kwon, D., Pfefferbaum, A., Sullivan, E. V., & Pohl, K. M. (2020). Regional growth trajectories of cortical myelination in adolescents and young adults: longitudinal validation and functional correlates. Brain imaging and behavior, 14(1), 242-266.

29. Lakhani, B., Hayward, K. S., & Boyd, L. A. (2017). Hemispheric asymmetry in myelin after stroke is related to motor impairment and function. NeuroImage: Clinical, 14, 344-353.

30. Lazari, A., Salvan, P., Verhagen, L., Cottaar, M., Papp, D., van der Werf, O. J., ... & Johansen-Berg, H. (2022). A macroscopic link between interhemispheric tract myelination and cortico-cortical interactions during action reprogramming. Nature communications, 13(1), 1-12.

31. Lemaitre, H., Goldman, A. L., Sambataro, F., Verchinski, B. A., Meyer-Lindenberg, A., Weinberger, D. R., & Mattay, V. S. (2012). Normal age-related brain morphometric changes: nonuniformity across cortical

thickness, surface area and gray matter volume?. Neurobiology of aging, 33(3), 617-e1.

32. Margulies, D. S., Ghosh, S. S., Goulas, A., Falkiewicz, M., Huntenburg, J. M., Langs, G., ... & Smallwood, J. (2016). Situating the default-mode network along a principal gradient of macroscale cortical organization. Proceedings of the National Academy of Sciences, 113(44), 12574-12579.

33. Mugler, J. P. (2004). Efficient spatially-selective single-slab 3D turbo-spin-echo imaging. In Proc Intl Soc Mag Reson Med (Vol. 11, p. 695).

34. McGinnis, S. M., Brickhouse, M., Pascual, B., & Dickerson, B. C. (2011). Age-related changes in the thickness of cortical zones in humans. Brain topography, 24(3), 279-291.

35. Mehta, R. C., Pike, G. B., & Enzmann, D. R. (1996). Magnetization transfer magnetic resonance imaging: a clinical review. Topics in magnetic resonance imaging: TMRI, 8(4), 214-230.

36. Nakamura, K., Chen, J. T., Ontaneda, D., Fox, R. J., & Trapp, B. D. (2017). T1-/T2-weighted ratio differs in demyelinated cortex in multiple sclerosis. Annals of neurology, 82(4), 635-639.

37. Pareto, D., Garcia-Vidal, A., Alberich, M., Auger, C., Montalban, X., Tintoré, M., ... & Rovira, À. (2020). Ratio of T1-weighted to T2-weighted signal intensity as a measure of tissue integrity: comparison with magnetization transfer ratio in patients with multiple sclerosis. American Journal of Neuroradiology, 41(3), 461-463.

38. Patel, Y., Shin, J., Drakesmith, M., Evans, J., Pausova, Z., & Paus, T. (2020). Virtual histology of multi-modal magnetic resonance imaging of cerebral cortex in young men. NeuroImage, 218, 116968.

39. Raz, N. (2000). Aging of the brain and its impact on cognitive performance: Integration of structural and functional findings.

40. Raz, N., & Rodrigue, K. M. (2006). Differential aging of the brain: patterns, cognitive correlates and modifiers. Neuroscience & Biobehavioral Reviews, 30(6), 730-748.

41. Resnick, S. M., Pham, D. L., Kraut, M. A., Zonderman, A. B., & Davatzikos, C. (2003). Longitudinal magnetic resonance imaging studies of older adults: a shrinking brain. Journal of Neuroscience, 23(8), 3295-3301.

42. Rowley, C. D., Bazin, P. L., Tardif, C. L., Sehmbi, M., Hashim, E., Zaharieva, N., ... & Bock, N. A. (2015). Assessing intracortical myelin in the living human brain using myelinated cortical thickness. Frontiers in neuroscience, 396.

43. Salat, D. H., Buckner, R. L., Snyder, A. Z., Greve, D. N., Desikan, R. S., Busa, E., ... & Fischl, B. (2004). Thinning of the cerebral cortex in aging. Cerebral cortex, 14(7), 721-730.

44. Shafee, R., Buckner, R. L., & Fischl, B. (2015). Gray matter myelination of 1555 human brains using partial volume corrected MRI images. Neuroimage, 105, 473-485.

45. Shafto, M. A., Tyler, L. K., Dixon, M., Taylor, J. R., Rowe, J. B., Cusack, R., ... & Matthews, F. E. (2014). The Cambridge Centre for Ageing and Neuroscience (Cam-CAN) study protocol: a cross-sectional, lifespan, multidisciplinary examination of healthy cognitive ageing. BMC neurology, 14(1), 1-25.

46. Sled, J. G. (2018). Modelling and interpretation of magnetization transfer imaging in the brain. Neuroimage, 182, 128-135.

47. Stanisz, G. J., Kecojevic, A., Bronskill, M. J., & Henkelman, R. M. (1999). Characterizing white matter with magnetization transfer and T2. Magnetic Resonance in Medicine: An Official Journal of the International Society for Magnetic Resonance in Medicine, 42(6), 1128-1136.

48. Taylor, J. R., Williams, N., Cusack, R., Auer, T., Shafto, M. A., Dixon, M., ... & Henson, R. N. (2017). The Cambridge Centre for Ageing and Neuroscience (Cam-CAN) data repository: Structural and functional MRI, MEG, and cognitive data from a cross-sectional adult lifespan sample. neuroimage, 144, 262-269.

49. Thambisetty, M., Wan, J., Carass, A., An, Y., Prince, J. L., & Resnick, S. M. (2010). Longitudinal changes in cortical thickness associated with normal aging. Neuroimage, 52(4), 1215-1223.

50. Thiebaut de Schotten, M., Urbanski, M., Batrancourt, B., Levy, R., Dubois, B., Cerliani, L., & Volle, E. (2017). Rostro-caudal architecture of the frontal lobes in humans. Cerebral Cortex, 27(8), 4033-4047.

51. van der Weijden, C. W., García, D. V., Borra, R. J., Thurner, P., Meilof, J. F., van Laar, P. J., ... & de Vries, E. F. (2021). Myelin quantification with MRI: A systematic review of accuracy and reproducibility. Neuroimage, 226, 117561.

52. Van Essen, D. C., & Glasser, M. F. (2014). In vivo architectonics: a cortico-centric perspective. Neuroimage, 93, 157-164.

53. Wagstyl, K., Larocque, S., Cucurull, G., Lepage, C., Cohen, J. P., Bludau, S., ... & Evans, A. C. (2020). BigBrain 3D atlas of cortical layers: cortical and laminar thickness gradients diverge in sensory and motor cortices. PLoS biology, 18(4), e3000678.

54. Wolff, S. D., & Balaban, R. S. (1989). Magnetization transfer contrast (MTC) and tissue water proton relaxation in vivo. Magnetic resonance in medicine, 10(1), 135-144.

55. Wu, M., Kumar, A., & Yang, S. (2016). Development and aging of superficial white matter myelin from young adulthood to old age: Mapping by vertex-based surface statistics (VBSS). Human brain mapping, 37(5), 1759-1769.

56. Zrenner, C., Belardinelli, P., Ermolova, M., Gordon, P. C., Stenroos, M., Zrenner, B., & Ziemann, U. (2022). μ-rhythm phase from somatosensory but not motor cortex correlates with corticospinal excitability in EEG-triggered

Appendix

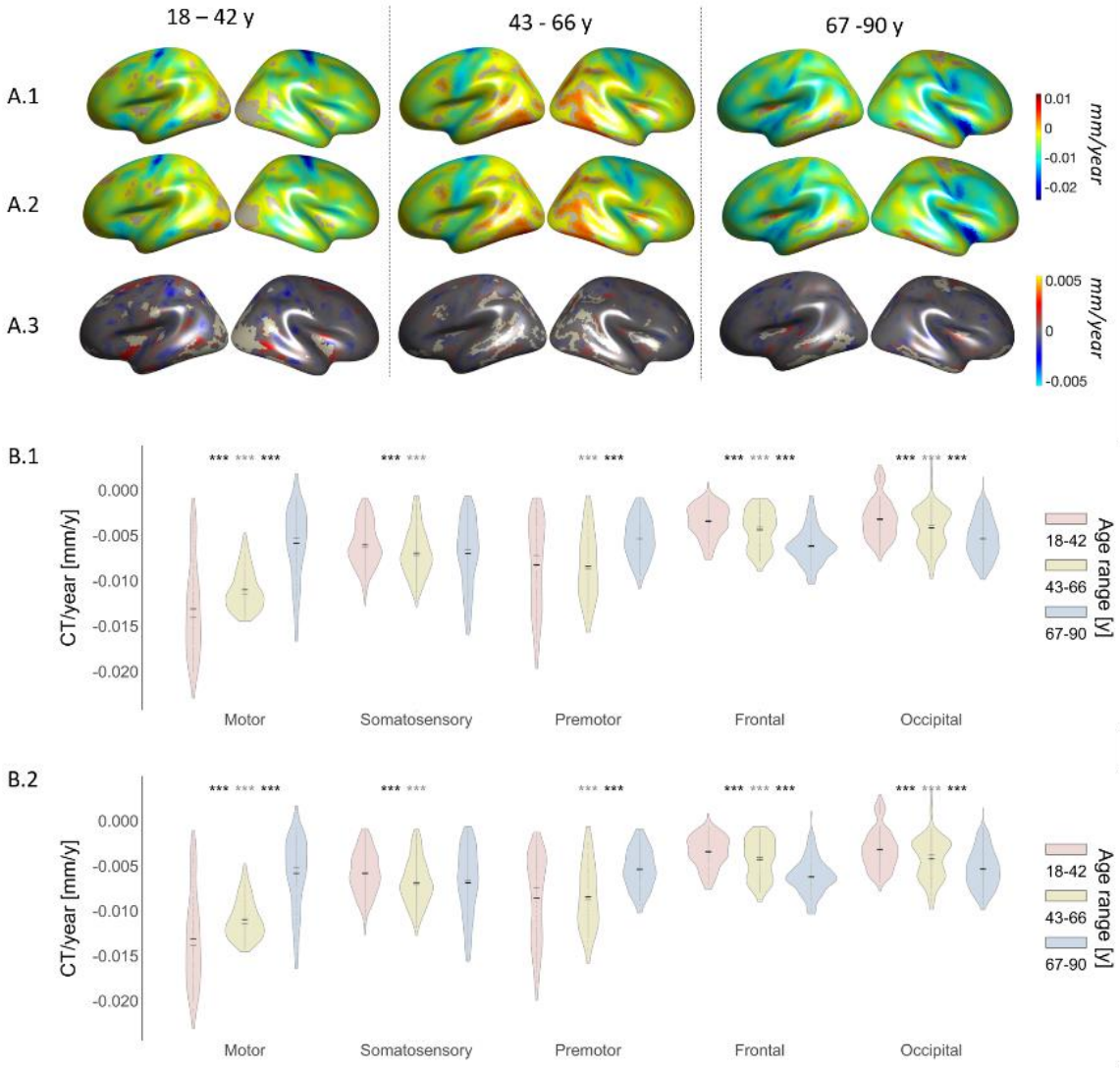

Suppl. Figure 4.1: Results for the linear fit between Cortical Thickness and Age (Cortical thinning/CT Slope) in the three age groups (with and without T1w/T2w ratio regressed out from CT before computing the linear fit between CT and Age); A.1) Source map of the slope values from the linear fit between CT and Age; A.2) Source maps of the slope values from the linear fit between CT and Age, with T1w/T2w ratio regressed out as a confound.; A.3) Source map of the difference between A.1 and A.2: the difference is computed only between the values that are significant in both original contrasts; B.1) CT slope values distribution for each group in each brain sector of interest (mean in black, median in grey); B.2) CT slope values distribution with T1w/T2w ratio regressed out as a confound for each group in each brain sector of interest (mean in black, median in grey); significance asterisks summarize the results of a t-test between the three age groups for each brain sector separately (*** for p< 0.0001; ** for p < 0.001; * for p< 0.05). Grey asterisks refer to the comparison between the first and the third group.

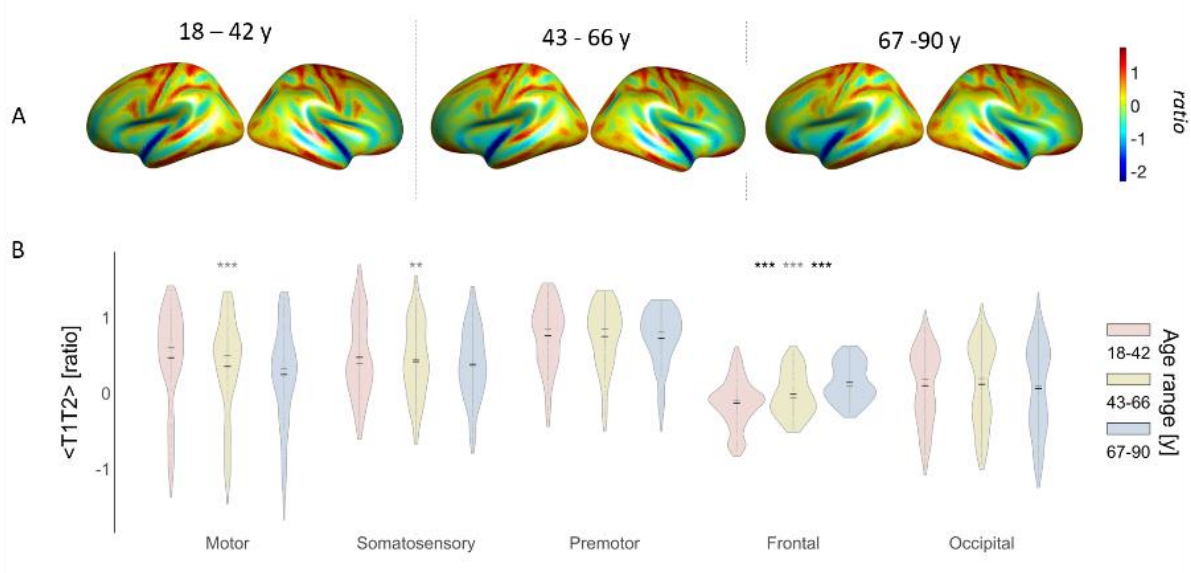

Suppl. Figure 4.2: Results for average T1w/T2w ratio values in the three age groups; A) T1w/T2w ratio average maps for the 7117 isorois for the three age groups separately; B) T1w/T2w ratio values distribution for each group in each brain sector of interest (mean in black, median in grey); significance asterisks summarize the results of a t-test between the three age groups for each brain sector separately (*** for p< 0.0001; ** for p < 0.001; * for p< 0.05). Grey asterisks refer to the comparison between the first and the third group.

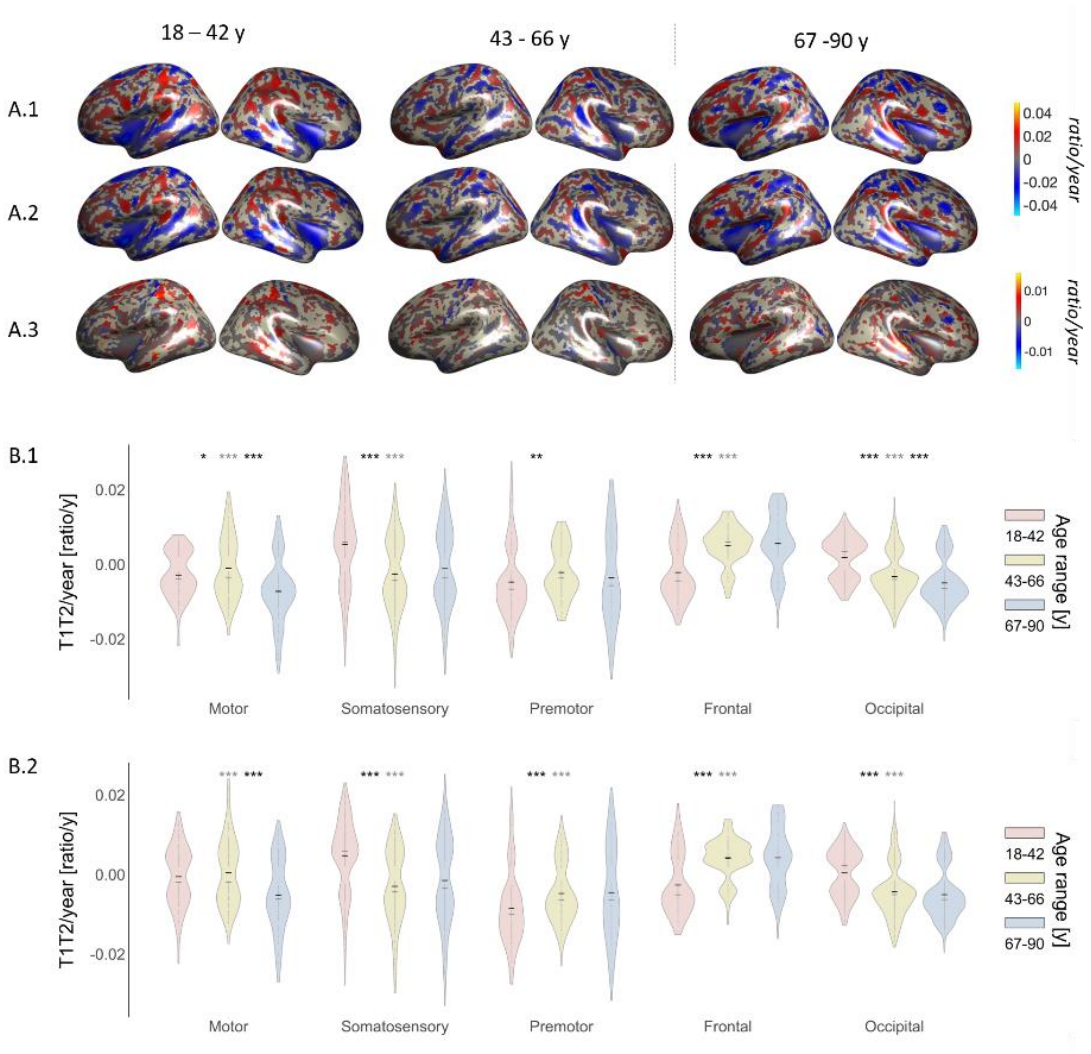

Suppl. Figure 4.3: Results for the linear fit between T1w/T2w ratio and Age (T1w/T2w ratio Slope) in the three age groups (with and without CT ratio regressed out from T1w/T2w ratio before computing the linear fit between T1w/T2w ratio and Age); A.1) Source map of the slope values from the linear fit between T1w/T2w ratio and Age; A.2) Source maps of the slope values from the linear fit between T1w/T2w ratio and Age, with CT regressed out as a confound.; A.3) Source map of the difference between A.1 and A.2: the difference is computed only between the values that are significant in both original contrasts; B.1) T1w/T2w ratio slope values distribution for each group in each brain sector of interest (mean in black, median in grey); B.2) T1w/T2w ratio slope values distribution with CT regressed out as a confound for each group in each brain sector of interest (mean in black, median in grey); significance asterisks summarize the results of a t-test between the three age groups for each brain sector separately (*** for p< 0.0001; ** for p < 0.001; * for p< 0.05). Grey asterisks refer to the comparison between the first and the third group.

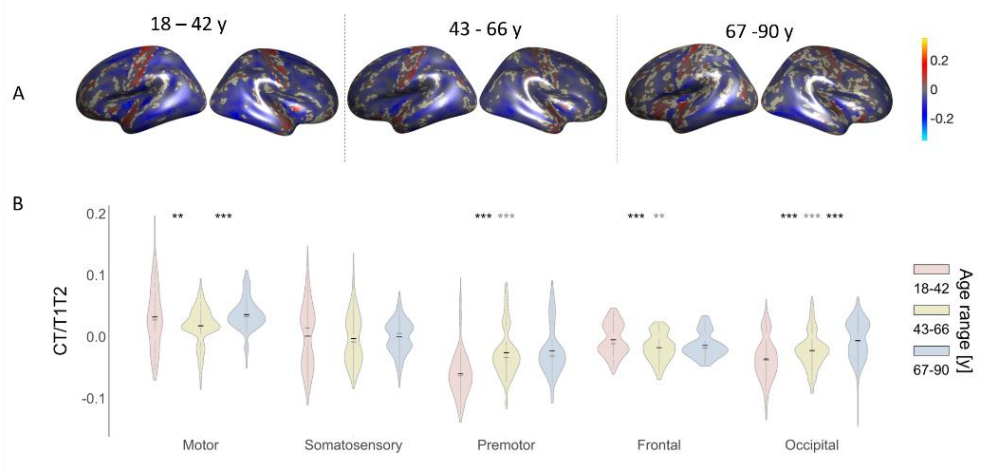

Suppl. Figure 4.4: Results for the linear fit between CT and T1w/T2w ratio in the three age groups; A) Source map of slope values from the linear fit between CT and T1w/T2w ratio; B) Slope distribution from the linear fit between CT and T1w/T2w ratio for each group in each brain sector of interest (mean in black, median in grey); significance asterisks summarize the results of a t-test between the three age groups for each brain sector separately (*** for p< 0.0001; ** for p < 0.001; * for p< 0.05). Gray asterisks refer to the comparison between the first and the third group.

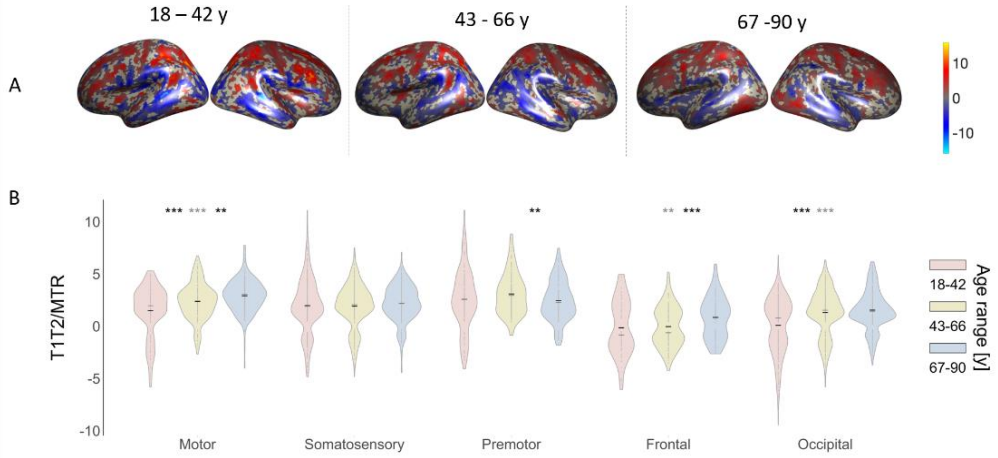

Suppl. Figure 4.5: Results for the linear fit between T1w/T2w ratio and MTR in the three age groups; A) Source map of slope values from the linear fit between T1w/T2w ratio and MTR; B) Slope distribution from the linear fit between T1w/T2w ratio and MTR for each group in each brain sector of interest (mean in black, median in grey); significance asterisks summarize the results of a t-test between the three age groups for each brain sector separately (*** for p< 0.0001; ** for p < 0.001; * for p< 0.05). Gray asterisks refer to the comparison between the first and the third group.

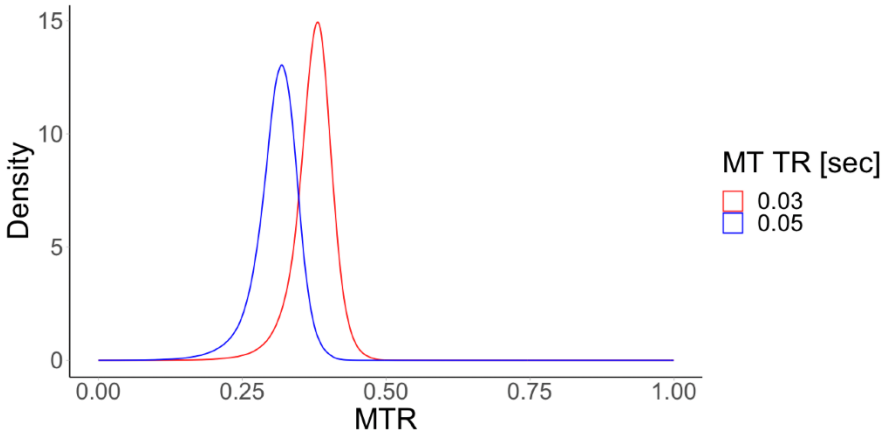

Suppl. Figure 4.6: Density plot for the distribution of MTR values with respect to the MT sequence repetition times for all subjects and all vertices in the selected sectors.

Conclusions

This Ph.D. dissertation examines previously overlooked factors which have possibly contributed to the mixed results in stroke literature. In our opinion, these factors need to be taken into account to understand the plastic brain changes following a stroke. Specifically, these factors are: the individual structural and functional characteristics (structural reserve of the callosum, cortical myelin concentration, connectivity patterns), the dynamic nature of diaschisis mechanisms, the influence of the local brain-state in the affected/unaffected hemisphere in the response to TMS over the motor cortex. These factors, we propose, should be evaluated in the individual patient to understand the plastic changes following stroke. We hope that the findings presented in this thesis will contribute to develop new and more complete theoretical accounts that integrate both functional and structural characteristics of the individual patient.

In Chapter 1, we reported an overview of recent findings investigating different aspects of the stroke brain. In particular, we described how current models of post-stroke brain reorganization are not consistent and do not account for results of recent meta-analyses and that, therefore, they need revision. In particular, the current models of post-stroke brain reorganization inspiring the stimulation rehabilitation protocols used so far were conceptualized on the basis of contradicting pieces of evidence. For this reason, they laid the basis to stimulation protocols which are different, sometimes opposite from each other and most importantly, not efficient. Moreover, these models further lack in the integration of recent evidence suggesting new factors to be included in stroke patients' assessment. Specifically, we support a new account that considers the inhibitory mechanisms in the interhemispheric interplay as another expression of integrative processes. In fact, previous frameworks which see the two hemispheres as bound by rivalry cannot explain why greater structural reserve at the level of the callosum is predictive of a better prognosis: in this sense, if the callosum

were mediating interhemispheric inhibition sustaining competition, this finding should be opposite. Therefore, since we embrace the new account of interhemispheric integration, the callosal structural reserve is suggested here as a further factor in stroke assessment. In fact, we report recent evidence that, depending on patient impairment level, the structural integrity of different sections of the callosum correlate with recovery. This suggests that different connectivity pathways are available to the individual patient depending on which callosal sections are spared and therefore still able to support interhemispheric integration. Importantly, we propose that structural integrity should not be assessed only right after the stroke. In fact, new evidence has been found on the dynamic nature of the structural damage, which needs to be assessed at multiple time points from stroke. Specifically, diaschisis, which refers to the degeneration of sub-/cortical sites and white matter tracts connected to the lesioned area, has been recently proven to be a process involving the stroke brain for years following the stroke event. Therefore, we propose structural assessment of stroke patients to be implemented also in late post-stroke stages. This would help explain the post-stroke changes in the connectivity patterns and how these are associated with recovery. In this regard, we report different works showing that connectivity patterns tend to change depending on individual impairment level in the patient. To conclude, the review presented in Chapter 1 highlights how current models of the stroke brain are simplistic in explaining plastic brain changes following a stroke. To do so, we report recent evidence from meta-analyses and studies investigating the relationship between structural/functional connectivity and impairment levels in stroke patients. Finally, we developed a potential to-be-validated framework of stroke brain plasticity which takes into account the aforementioned previously overlooked factors.

In Chapter 2, we investigated the influence of the local brain-state on the response to TMS stimulation over M1 in both affected and unaffected hemispheres of stroke patients. We provide for the first time evidence of instantaneous local excitability state of the motor cortex, as defined by the phase of the

mu-alpha oscillation, differently influencing the response to TMS in the two hemispheres. In particular, the affected hemisphere shows a low differentiation between the different excitability states compared to the unaffected one and healthy controls. Differently, we found that this differentiation between the local excitability states is preserved in the unaffected hemisphere. Therefore, the exaggerated TMS evoked potentials from the affected hemisphere mainly seen in severe stroke patients is here ascribed to the low differentiation found between the high- and low-excitability states. Importantly, if this low differentiation between excitability states in the affected hemisphere will be confirmed in further studies, we propose that the assessment of the degree of differentiation between the high and low excitability states should be used in clinical practice at different stages post-stroke.

In Chapter 3, we provided a compound approach for studying connectivity in the alpha frequency band. The reason behind the choice of investigating alpha connectivity lays in the need of assessing connectivity patterns' changes in stroke patients, in which alpha connectivity has been linked with improvement in both cognitive and motor domains. To this aim, using MEG resting state recording from a big healthy subjects' cohort (N = 223), we investigated alpha connectivity patterns exploiting the partial complementarity of two connectivity metrics: the WPPC and the WPLI. WPPC is characterized by a higher sensitivity in the alpha band, while WPLI, unlike WPPC, is not sensitive to zero-lag spurious correlations as it is computed from the sign of the imaginary part of the coherence. We found the strongest connectivity in the fronto-parietal connections, followed by fronto-occipital and parieto-occipital connectivity. Furthermore, we showed that, when assessing connectivity in alpha, WPPC is more suited for finding patterns of stronger/weaker connections between regions compared to WPLI (this is because WPPC has a greater sensitivity compared to WPLI). Differently, WPLI can be used to confirm which of the correlations found with the WPPC are non-spurious. This compound approach could be useful to understand the effects of rTMS stimulation protocols, by

comparing connectivity patterns assessed with both metrics, between pre- and post- application of rehabilitation protocols.

In Chapter 4, we focused on age-dependent brain structural changes, both in terms of cortical thinning and myelin loss. The rationale behind this chapter finds its roots in the fact that stroke studies investigating corticospinal excitability often include healthy participants relevantly younger than patients in the control group. This represents an issue since corticospinal excitability has been found to be affected by the levels of cortical myelin concentration. Therefore, the age-related changes in this quantity need to be controlled for when patients are compared with controls. In fact, stroke patients are often in their elderly and for this reason, beside the stroke, they might also suffer from normal age-related brain degeneration. In this light, if controls are not chosen according to the age-matched criterion, differences in corticospinal excitability due to age-related myelin loss might be overlooked. Therefore, we wanted to assess whether significant changes not only in cortical thickness, but also in cortical myelin concentration could be found in a big cohort (N = 610) of healthy participants aged between 18 and 89 years old. Importantly, from a methodological point of view, we assessed cortical myelin content with two different metrics, namely the T1w/T2w ratio and the Magnetization Transfer Ratio (MTR). The main findings in this study concern both anatomical and methodological aspects. First of all, we found significant age-related changes in cortical myelin content, with myelin content changes showing different trajectories depending on the sector of the brain under investigation. The changes found at the level of the parietal lobule in the cortical myelin content suggest that our concerns regarding the need of choosing only age-matched controls in studies investigating corticospinal excitability differences in stroke vs controls were meaningful. Moreover, we found that motor and sensory areas of the parietal lobe, involved in corticospinal excitability processes, show different trajectories of age-dependent cortical myelin content loss, suggesting a dissociation between these neighbour regions. Furthermore, we provide evidence that the T1w/T2w

ratio is a metric that suffers of a stronger co-dependency with cortical thickness when compared to the MTR. Therefore, we suggest MTR as a MR based neuroimaging technique specifically aimed at assessing cortical myelin content. Our results presented in Chapter 4 led to two conclusions: 1) controls need to be chosen according to the age-matched criterion in order to control for age-related structural changes; 2) the MTR is a more suitable sequence to assess cortical myelin content compared to the T1w/T2w and should be included in stroke patients' assessment.

List of Figures

Chapter 1

Chapter 2

Chapter 3

Chapter 4

List of Tables

Chapter 2

Chapter 3

Chapter 4

Outcomes and Activities

Papers published in peer-reviewed journals

1. **Brancaccio, A.**, Tabarelli, D., Bigica, M., & Baldauf, D. (2020). *Cortical source localization of sleep-stage specific oscillatory activity*. *Scientific reports*, 10(1), 1-15.

2. **Brancaccio, A.**, Tabarelli, D., & Belardinelli, P. (2022). *A new framework to interpret individual interhemispheric compensatory communication after stroke*. Journal of Personalized Medicine, 12(1), 59.

3. Tabarelli, D.*, **Brancaccio, A.***, Zrenner, C., & Belardinelli, P. (2022). *Functional Connectivity States of Alpha Rhythm Sources in the Human Cortex at Rest: Implications for Real-Time Brain State Dependent EEG-TMS*. Brain Sciences, 12(3), 348.

Conferences and Poster presentations

1. **Brancaccio, A.**, Tabarelli D., Belardinelli, P. (2022). "*Functional connectivity states of alpha rhythm sources in the human cortex at rest: implications for real-time brain state dependent EEG-TMS*" at BIOMAG 2022, Birmingham [Poster presentation]

2. **Brancaccio, A.**, Tabarelli D., Belardinelli, P. (2022). "*Myeloarchitectonic properties of sensorimotor areas influence thinning in aging*" at OHBM 2022, Glasow [Poster presentation]

3. **Brancaccio, A.**, Tabarelli D., Belardinelli, P. (2022). "*A new framework to interpret individual interhemispheric compensatory communication after stroke*", E.W.C.N - European Workshop on Cognitive Neuropsychology, International Online Meeting [Poster presentation]

4. **Brancaccio, A.,** Baldauf, D. (2019). "Implicit chunking of information in a working memory task", RAW, Rovereto Attention Workshop [Poster presentation]

5. **Brancaccio, A.,** Baldauf, D. (2019). "Behavioural Sequences and Chunking Mechanisms", CAOs 2019 - Rovereto Workshop on Concepts, Actions and Objects [Poster presentation]

Teaching

1. Teaching assistant for "Advanced Hands on M/EEG Analysis", MSc Cognitive Sciences [Professor Paolo Belardinelli, PhD]

2. Teaching assistant for "Multimodal Electrophysiological Recording and Stimulation", MSc Cognitive Sciences [Professor Paolo Belardinelli, PhD]

Authorship Statement

(according to CRediT (Contributor Roles Taxonomy) - Elsevier)

Introduction

A. Brancaccio: Conceptualization, Resources, Writing – *original draft*, Writing – *review and editing*; **P. Belardinelli**: Supervision, Writing – *review and editing*;

Chapter 1

This Chapter is adapted from "Brancaccio, A., Tabarelli, D., & Belardinelli, P. (2022). A new framework to interpret individual interhemispheric compensatory communication after stroke. *Journal of Personalized Medicine*, 12(1), 59" licensed under an open access Creative Commons CC BY 4.0 license. The copyright of this work is retained by the authors. All authors agreed on redistributing the following material for the purpose of this doctoral thesis.

A. Brancaccio: Conceptualization, Methodology, Investigation, Resources, Visualization, Writing – *original draft*, Writing – *review and editing*; **D. Tabarelli**: Visualization, Writing – *review and editing*; **P. Belardinelli**: Supervision, Writing – *review and editing*;

Chapter 2

A. Brancaccio: Conceptualization, Methodology, Resources, Software, Formal Analysis, Data Curation, Writing – *original draft*, Writing – *review and editing*; **D. Tabarelli**: Writing – *review and editing*; **P. Belardinelli**: Supervision, Writing – *review and editing*; **Ziemann Lab**: Investigation;

Chapter 3

This Chapter is adapted from "Tabarelli, D.*, Brancaccio, A.*, Zrenner, C., & Belardinelli, P. (2022). Functional Connectivity States of Alpha Rhythm Sources in the Human Cortex at Rest: Implications for Real-Time Brain State Dependent EEG-TMS. Brain Sciences, 12(3), 348" licensed under an open access Creative Commons CC BY 4.0 license. The copyright of this work is retained by the authors. All authors agreed on redistributing the following material for the purpose of this doctoral thesis.

A. Brancaccio: Conceptualization, Methodology, Resources, Software, Writing – *original draft*, Writing – *review and editing*; **D. Tabarelli**: Conceptualization, Software, Formal Analysis, Data Curation, Writing – *review and editing*; **C. Zrenner**: Writing – *review and editing*; **P. Belardinelli**: Supervision, Writing – *review and editing*;

Chapter 4

A. Brancaccio: Conceptualization, Methodology, Resources, Software, Formal Analysis, Data Curation, Writing – *original draft*, Writing – *review and editing*; **D. Tabarelli**: Methodology, Software, Data Curation, Writing – *review and editing*; **P. Belardinelli**: Supervision, Writing – *review and editing*;